The Hydrologic Evolution of Glacial Meltwater: Insights and Implications from Alpine and Arctic Glaciers

by

Carli Anne Arendt

A dissertation submitted in partial fulfillment
of the requirements for the degree of
Doctor of Philosophy
(Earth and Environmental Sciences)
in the University of Michigan
2015

Doctoral Committee:

Assistant Professor Sarah M. Aciego, Chair
Assistant Professor Jeremy N. Bassis
Professor M. Clara Castro
Associate Professor Eric A. Hetland
Professor Kyger C. Lohmann

ACKNOWLEDGMENTS

I would like to thank the University of Michigan and the Department of Earth and Environmental Sciences (Geology) for assisting me in my journey to obtain the skills necessary to build my career as a scientist. The majority of my graduate school accomplishments have stemmed from my acquaintance with and mentorship from my thesis adviser, Dr. Sarah Aciego who graciously welcomed me into her lab, convinced me to invest in obtaining a doctorate, and provided me with an abundance of opportunities for which I am incredibly grateful. More importantly, Sarah has been an exemplary role model of what it means to be a successful, young, strong female scientist and has shown me how to gracefully approach countless scenarios that beginning female scientists typically encounter. I would also like to thank the other members of my dissertation committee: Dr. Jeremy Bassis, Dr. Clara Castro, Dr. Eric Hetland, and Dr. Kacey Lohmann for helping me become a better scientist through their continued support and advice, for challenging me to look at my own research critically.

I would also like to thank the numerous others who supported me on this academic journey and encouraged me when I encountered challenges along the way. It would be impossible to name everyone who has helped contribute to my success but I would like to recognize: my fiancée and primary support system Ethan Hyland, my GIGL lab members and field companions Emily Stevenson, Yi-Wei Lui, Molly Blakowski and my roommate Sarah Aarons for being supportive of me for my entire journey here at the University of Michigan, the official and unofficial

members of GEOFRAT who helped me grow along the way Rohit Warrier, Jen Cotton, Rich Fiorella, Tara Smiley, Petr Yakolvev, Clay Tabor, Say Yun Kwon, Katie Loughney, Lydia Staish, Laura Waters and many more, the UMich EARTH office staff especially Anne Hudon for all of their guidance and assistance over the years, my completely loving and supporting parental unit and sister, my undergraduate advisers Dr. Tim Flood and Dr. Nelson Ham for encouraging me to pursue higher education and believe in myself, Dr. Henry Pollack for being a continued inspiration and role model, and the faculty, researchers, postdocs, and students in this department who have helped make the University of Michigan feel like home.

SPECIFIC CHAPTERS

Chapter 2

This research was funded by the University of Michigan Rackham Graduate School and the Turner Award from the Department of Earth and Environmental Sciences to CAA. I would like to thank Sarah Aarons for her assistance in the collection of samples used for the Athabasca Glacier case study. Datasets supporting this manuscript are available in Supporting Online Material Table S1 and Table S2. I would also like to thank Dr. Sarah Das, Dr. Maya Bhatia, and Dr. Oliver Chadwick for their cooperation and assistance in obtaining the isotopic values and fractional contribution estimations from the original studies of the data used in case studies two and three.

Chapter 3

The University of Michigan's Rackham Graduate School and Department of Earth and Environmental Science provided funding for this project through grants to C.A.A. I thank Parks

Canada for assistance in permitting and field logistics. The University of Wyoming High Precision Isotope Laboratory personnel are acknowledged for providing support. I would like to wholeheartedly thank Dr. Don Porcelli for his insightful and extremely helpful insights regarding the derivation of the age-relationship equation used in this chapter.

Chapter 4

Funding for this project was provided by the University of Michigan's Rackham Graduate School and Department of Earth and Environmental Science through research grants awarded to C.A.A. and through Packard funding awarded to S.M.A.; and by the Woods Hole Oceanographic Institution's Ocean and Climate Change Institute Arctic Research Initiative research grant to S.B.D. I thank Air Greenland for assistance with field logistics and the WHOI field team for aiding in sample collection in Ilulissat. I thank Dr. Gideon Henderson for his generosity in allowing us access to the original box-model used in Henderson, 2002.

Many thanks to all those who contributed to my success in this thesis!

TABLE OF CONTENTS

LIST OF FIGURES

Figure

LIST OF TABLES

Table

LIST OF APPENDICES

ABSTRACT

Glaciers are of critical importance in the global hydrological cycle and the implications of their recent rapid decline are still poorly understood. Subglacial processes impact glacial hydrology through nutrient production, water chemistry, and aquifer recharge, but are inaccessible to direct observation. Furthermore, understanding the impact current subglacial melt processes have on surrounding environments may provide insight to changes that likely occurred on glacial-interglacial timescales. In my work, I combine multiple elemental and isotopic systems to understand glacial hydrology, including the subglacial environment. First, I have developed a Bayesian Monte Carlo isotope-mixing model that incorporates stable isotope, $\delta^{18}O$ and δD, measurements to extrapolate relative contributions of ice and snowmelt to the glacial system. This model can also be applied to other earth surface systems with distinct end member isotopic compositions. Second, I have combined the melt fractions from my isotope-mixing model with a radioactive uranium-series (U-series) isotope age model to quantify the average residence time and storage length of subglacial melt. By combining these two isotopic systems, I provide unique insights on the size of the subglacial meltwater reservoir and its potential impacts on glacial sliding and meltwater nutrients. Third, I investigate the influence of the U chemistry of current glacial meltwater from the Greenland Ice Sheet on adjacent seawater as a proxy to reconstruct the potential influence of glacial melt on global seawater U chemistry over glacial-interglacial

timescales using a simple seawater U budget box model. The models presented here are applied to a broad geographic range to investigate the universality of climate-melt relationships and the impact of glacial melt on the chemistry of both freshwater and seawater reservoirs.

CHAPTER I

Introduction: Glacial Hydrology

Approximately seventy-five percent of all the freshwater in the world is stored in glaciers and ice sheets, making them the largest freshwater reservoir on the planet. Glaciers have been shrinking significantly as a result of climate change (Dyurgerov, 2003; Lemke and Ren, 2007; Shea and Marshall, 2007). Consequently, freshwater reservoirs created and moderated by glaciers are also shrinking (Barnett *et al.,* 2005; Coudrain *et al.,* 2005; Bradley *et al.,* 2006; Kehrwald and Thompson, 2008). The importance of glaciers in the global hydrological cycle and the implications of their rapid decline in modern years has only recently been studied. Undoubtedly river systems will suffer from lower water levels in late summer and early fall, and additional important water quality and productivity factors may also be affected; such as changes in the sediment load, nutrient production from glacial weathering, and aquifer recharge for human utilization (Smith *et al.*, 2001; Brown, 2002; Milner *et al.*, 2009). A key aspect to making predictions on the effects of the decline in ice mass is *quantifying* the interaction between climate and subsequent meltwater, which can be assessed through geochemical analyses. The primary objective of my thesis is to develop and use new geochemical and computational proxies to place constraints on the evolution of source fraction contributions to glacial discharge, the length of time meltwater is stored within/beneath the glacial system, and how glacial meltwater chemistry impacts river and ocean uranium chemistry over anthropogenic timescales and periods of glacial-interglacial climate change.

1.1. GLACIERS AND ICESHEETS

Glaciers and ice sheets are defined as perennial ice masses that flow under their own weight and are characteristically divided into zones of accumulation, where mass is gained by snow accrual, and zones of ablation, where mass is lost primarily through melting and iceberg calving. The balance between mass loss and mass gain results in either glacier advance or retreat for both high elevation alpine glaciers and polar ice sheets. Mass loss via melting has increased with increasing global temperatures, resulting in the retreat of the majority of ice masses in the world (Shea and Marshal, 2007). Glacial meltwater is a product of ablation (Braithwaite, 1995; Hock, 1999), and can lead to accelerated mass loss via positive feedbacks such as increased ice velocity associated with increased pressure from meltwater in the subglacial system (Anderson *et al.*, 2004). Glacial meltwater also transports glacially derived nutrients (Aizen *et al.*, 1996), which can significantly impact downstream productivity and ecosystems depending on total glacial flux. The scale of each of these processes depends on the magnitude of melt and the evolution of the glacial hydrological system. Meltwater is generated at the surface of the glacier (supraglacial), within the glacier (englacial) and at the base of the glacier (subglacial); the majority of meltwater is then transported to the base where it interacts with the bedrock and sediment located in the subglacial environment before exiting the system (Figure 1.1).

1.1.1. The Subglacial System

Ice sheets and glaciers can be defined by their relationship to the bed: warm-based glaciers are lubricated at the bed by a layer of meltwater, whereas cold-based glaciers are frozen to the bed. Most valley glaciers in mid-latitudes are warm based, while those at higher latitudes have warm based centers and cold margins (Wadham *et al*., 2000; Cuffey and Paterson, 2010). Warming

temperatures with climate change and large seasonal temperature fluctuations may induce a change in the ice sheet or glacier from cold to warm based. Ice sheets and ice caps are complex systems that may contain both cold and warm based regions (Siegert, 2001), with the majority of meltwater generated by surface melting within ~10 km of the ice margin (Zwally *et al*., 2002). The glacier bed in this region is likely warm and allows water to penetrate to the bed through water-driven fracture propagation (Das *et al*., 2008). Therefore both glacier and ice sheet/ice cap systems show similar hydrologic networks that may evolve seasonally or, over longer timescales, as a result of climate change.

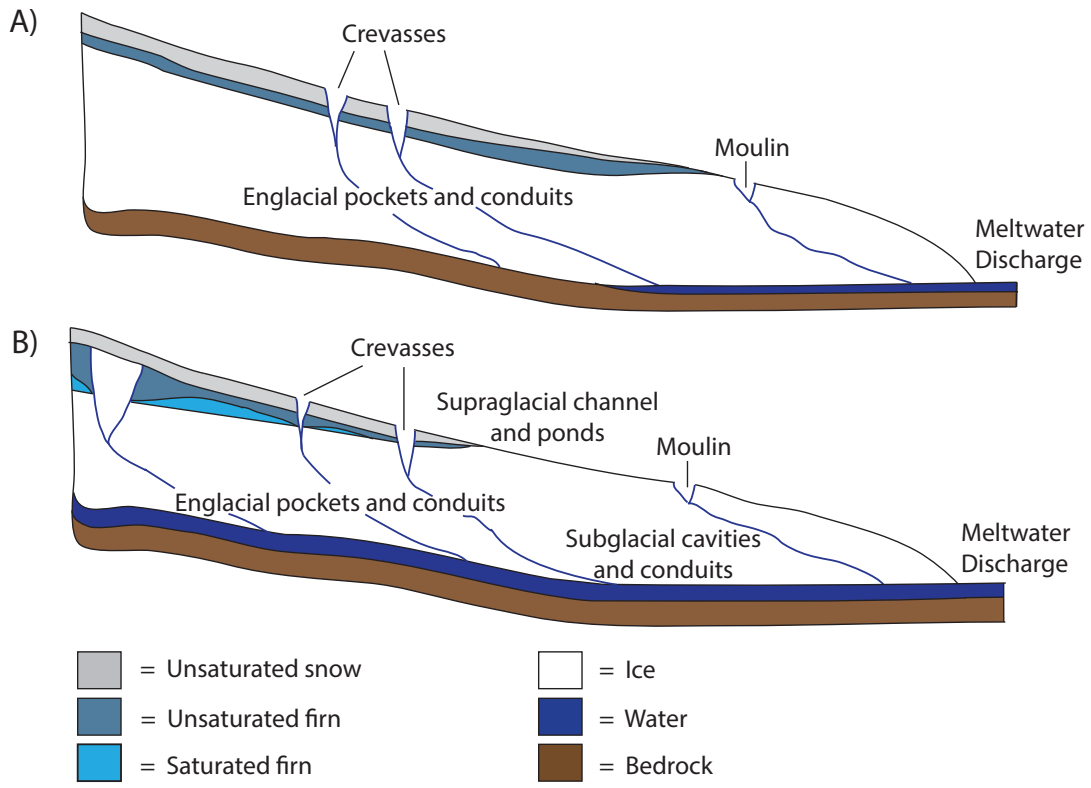

Figure 1.1: Transport pathways of glacial hydrology. These pathways evolve with changing temperature: a) Depicts pathways for glacial meltwater during minimal melt due to the presence of cold temperatures, where the subglacial system is primarily located toward the terminus, englacial pathways are still developing and snow covers the majority of the supraglacial system; and b) Depicts pathways for glacial meltwater during high melt due to the presence of above-freezing temperatures, where the subglacial system has expanded up-glacier, englacial pathways are well-developed, and the snowline has retreated up-glacier. The colored boxes indicate the nature of the corresponding material in the diagram.

The evolution of warm based glaciers and ice margins is extreme and seasonal, as depicted in the simplified illustration of a glacial cross-section presented in Figure 1.1. During the winter most of the ice mass is likely to be frozen to the bed; cold temperatures penetrate through the snow and ice to the bed and inhibit the transportation of surface melt to the basal region. The combination of a polythermal base and low surface melt results in a barrier to water flow early in the melt season (Figure 1.1a), which enhances the residence time of water, promoting chemical weathering at the bed. Subglacial water that was stored in isolation before connecting to the larger subglacial hydrologic drainage network is therefore more enriched in solutes than waters with similar discharge later in the season, because the water was exposed to the substrate longer and had more time to interact with the underlying bedrock (Skidmore *et al.*, 2005). As the melt season progresses, water will be stored in firn, englacial pockets, and surface ponds and then transported via crevasses, englacial conduits and supraglacial channels to the subglacial hydrologic network, which develops into a combination of delayed flow, with small channels, and fast flow, with large channels (Fountain and Walder, 1998) (Figure 1.1b). Finally, late in the season, the subglacial hydrology may develop into a system dominated by fast pathways with few areas of delayed flow. The residence time of subglacial water, and associated basal lubrication and sliding via basal water pressure, depends on the morphology of the subglacial drainage system throughout the melt season (Collins, 1979; Walder, 1982; Raymond, 1995; Hubbard and Nienow, 1997; Fountain and Walder, 1998; Hubbard, 2000; Creyts and Schoof, 2009; Schoof, 2010; Colgan *et al*., 2011). Multiple pathways and cavities combined with a widespread thin film of water will reduce the drainage speed and increase subglacial residence time (Fountain and Walder, 1998; Tranter, 2005; Sundal *et al*., 2011).

A well-developed supraglacial, englacial and conduit system with large, direct pathways will increase the flow-through speed and decrease subglacial residence time (Fountain and Walder, 1998; Nienow *et al*., 1998; Tranter, 2005; Sundal *et al*., 2011). The residence time of subglacial water can be influenced by processes external to the subglacial system and has countless implications for the ablation rate of glacier and ice sheets. Thus, subglacial water residence times can be used to assess the sustainability of freshwater aquifers that are dependent on meltwater recharge. The presence and extent of all of these processes mentioned above can be examined via the chemical proxies outlined in my thesis.

1.2. APPROACH

The inaccessibility of the subglacial environment under several hundred meters of ice has limited the ability to directly observe how the hydrologic networks develop and their relationship to local (and global) climate. Thus, measurements directly from the subglacial system are either impossible or extremely expensive and tedious; however, geochemical measurements of glacial meltwater collected in the main discharge channel located directly at the terminus of a glacier are good indicators of subglacial processes that the meltwater was exposed to.

In order to investigate the universality of the temporal and spatial melt relationships that exist in subglacial systems, I apply new chemical techniques to water samples collected from different glacial environments. Specifically, I investigate the isotopic composition of glacial meltwater and proximal seawater including: stable isotopes $\delta^{18}O$ and δD, and radiogenic isotopes within the uranium-series (U-series), which have been measured in glacial water samples I collected from the alpine Athabasca Glacier in the Canadian Rockies and four outlet

glaciers of the southern Greenland Ice Sheet (GrIS) (Figure 1.2). Additionally, proximal seawater samples to the GrIS outlet glaciers were collected and I analyze them for uranium concentrations and compositions. I assess these isotopic compositions to determine melt fractional contributions, subglacial meltwater residence times, and the impact of glacial melt on seawater U chemistry over glacial-interglacial timescales.

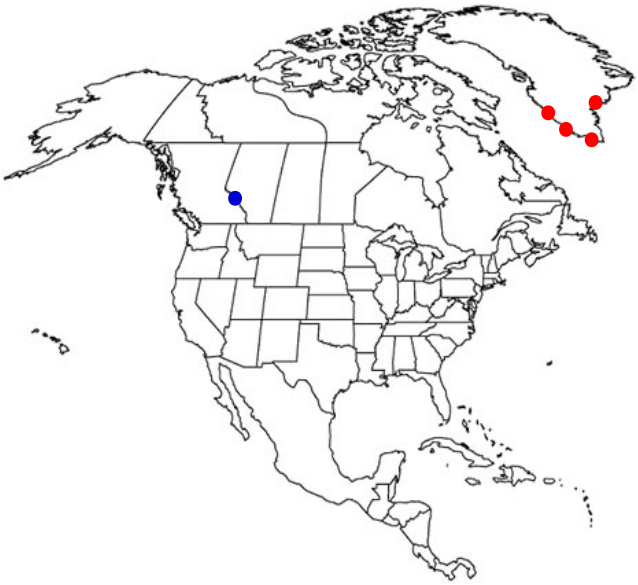

Figure 1.2: Generalized map of North America, indicating relevant field sampling locations in this thesis. The solid blue circle represents the Athabasca Glacier in Jasper National Park, Alberta, Canada. The solid red circles represent the four outlet glaciers of the southern Greenland Ice Sheet investigated in this thesis.

1.2.1. Fraction Contributions to Meltwater

The first segment of my thesis is focused on extrapolating the relative contributions of meltwater sources – snowmelt, ice melt, and summer precipitation – using a coupled statistical-chemical model (Arendt *et al.*, 2015). The isotopic composition of oxygen and hydrogen ($\delta^{18}O$ and δD) vary due to differences in air mass precipitation associated with distance from the ocean, elevation, and temperature present at the time of deposition (Dansgaard, 1964). $\delta^{18}O$ and δD

measurements have been widely used as hydrologic tracers to interpret current and past trends and variations in climate, precipitation patterns, and to constrain estimated volumes and water sources to rivers and lakes. In glacial environments, the stable water isotope compositions derived from snowmelt, ice melt, and summer precipitation have unique compositions that provide a mechanism for determining where glacial discharge is generated (Craig, 1961; Gat, 1996; Bhatia *et al.*, 2011; Cable *et al.*, 2011).

I apply $\delta^{18}O$ and δD measurements of Athabasca Glacier subglacial water samples to a Bayesian Monte Carlo (BMC) estimation scheme, a linear mass-mixing model to determine the fractional contributions of water sources from bulk meltwater samples. Importantly, this BMC model also assesses the uncertainties associated with these meltwater fractional contribution estimations, which provides an assessment of how well the system is constrained. By defining the proportion of overall melt that is coming from snow versus ice using stable isotopes, the volume of water generated by ablation can be calculated. This water volume has two important implications. First, communities that depend on glacial water for aquifer recharge can start assessing future water resources, as glacial decline will make snowmelt the dominant water reservoir. Second, the calculated source fraction water volumes are a starting point for additional geochemical models to investigate water storage within the subglacial hydrological network.

Further applications of my BMC model are highlighted in this chapter of my thesis, as the model is relevant to a variety of earth surface systems and applicable to numerous isotopic systems, including: $\delta^{18}O$, δD, and ^{222}Rn to determine melt sources of Greenland Ice Sheet bulk discharge, and $^{87}Sr/^{86}Sr$ and ε_{Nd} to determine source contributions to Hawaiian soils.

1.2.2. Subglacial Meltwater Residence Time

Current quantitative calculations of glacial residence time are largely based on reservoir models, which assume a linear relationship between water volume stored and discharged (Hannah and Gurnell, 2001; Cuffey and Paterson, 2010). These models and their subsequent residence time calculations have been aimed at predicting runoff (Hannah and Gurnell, 2001), yet differences between the supraglacial, englacial, and subglacial reservoir ages have not been explicitly calculated. Model-calculated residence times for combined englacial-subglacial reservoirs vary from hours to days in alpine glaciers (Hubbard and Nienow, 1997; Creyts and Schoof, 2009). Similarly, dye-tracing studies (Baker, 1982; Verbunt *et al*., 2003; Schaefli *et al.,* 2005) indicate that the transport time between a draining moulin and exit at the glacier terminus can be less than an hour. Constraining the maximum or average residence time from dye-tracers is complicated because complete dye loss, partial recovery and transit time do not distinguish between englacial and subglacial reservoirs: e.g., englacial transport distance is only well-defined in scenarios where boreholes drain completely (Kamb, 1985; Hooke, 1994; Hubbard and Nienow, 1997; Chandler, 2013).

Complex geophysical models can accurately simulate glacial hydrology and hydrological response (Arnold *et al*., 1998; Flowers and Clarke, 2002a, b) but require extensive calibration of physical parameters that are glacier-specific. Furthermore, as the study conducted by Bell *et al.* [2008] demonstrated, the residence time of ice sheet subglacial water is even more uncertain – early studies indicated long residence times (4 – 100 ka) beneath large ice sheets, while more recent studies of the Greenland Ice Sheet (GrIS) margin indicate short residence times (e.g.,

weeks) due to increased seasonal surface melt (Shepherd *et al*., 2009; Bartholomew *et al*., 2010). Studies located at ice sheet margins have largely focused on the transit time for surface melt to reach the bed and exit the ice margin (McMillan *et al*., 2007; Das *et al*., 2008; Bhatia *et al*., 2011)**,** rather than the residence time of water within the distributed network. Thus, it is important to note that in the studies mentioned, the process being measured is actually the minimum transit time and not the length of time the water is actually *stored* in the subglacial reservoir.

Motivated by the lack of information on subglacial meltwater storage time, the second segment of my thesis investigates a new method for quantifying the storage time of meltwater in subglacial systems (Arendt *et al.*, *Submitted*). The combination of this information pertaining to storage time with the isotope-mixing model from my second chapter provides unique insights on the size of subglacial meltwater reservoirs and potential impacts on glacier sliding via lubrication and meltwater nutrient chemistry. Previous work on the residence time or storage of subglacial water has proven to be either inconclusive or inconsistent (Bell *et al.*, 2002; Mitchell and Brown, 2008) because there are few chronometers appropriate for glacial water. However, U-series dating methods based on the ratio of parent isotopes to the decay product isotopes (^{238}U /^{234}U and ^{234}U/^{230}Th) have been used to study the residence time of aquifer systems (Innocent *et al.*, 2008). Recent advances in high resolution – low concentration U-series geochemistry (Sims *et al.*, 2008; Aciego *et al.*, 2009; Arendt *et al.*, 2014) have opened up the possibility of using these methods on subglacial water.

The U decay series has distinct advantages over other isotopic systems for determining timescales of processes due to the variable decay rates with half-lives comparable to the timescale of geologic processes and chemical behavior of daughter nuclides within the chains (Ivanovich, 1991; Chabaux, 2003; Porcelli and Swarzenski, 2003). Taking advantage of this unique isotope system, I have implemented an age-based relationship equation using a radioactive parent isotope, ^{238}U, and radiogenic daughter isotopes, ^{234}U and ^{222}Rn, in measurements of subglacial waters to determine average residence time values of meltwater in the subglacial system. Through the application of U-series isotopic analysis combined with subglacial models, I have directly measured the average time that water is stored in the subglacial system. My results indicate that the length of subglacial storage is several orders of magnitude longer than commonly accepted by the glaciology community (Arendt, *Submitted*), due to this direct measurement of average storage time rather than transit time. Hence, these findings significantly contribute to a more complete understanding of hydrologic processes in glacier systems.

1.2.3. Impact of Glacial Meltwater U Chemistry on Seawater U Chemistry

The third research segment of my thesis assesses the implications and global relevance of the subglacial meltwater residence time technique I have developed. Expanding the geographic application of my research gauges the accuracy and the applicability of my method and allows me to place more comprehensive constraints on the storage time of subglacial water and associated subglacial chemistry worldwide. Applying my research to quantify melting processes and subglacial relationships in large ice sheets provides insight on the implications of widespread melting for global climate change by constraining the impact of glacial meltwater chemistry on

the surrounding environment. To test the scaling of my subglacial water residence time technique, I investigate several outlet glaciers of the GrIS. Additional implications of melting ice sheets are assessed through the collection and chemical analysis of proximal seawater to the GrIS outlet glaciers. These samples are used to explore the potential impact that glacial melt contributions have on seawater U chemistry. Through the chemical analysis of $\delta^{234}U$ in both the GrIS outlet glacier glacial melt and proximal seawater samples, a clear relationship in which the seawater U chemistry is influenced by glacial melt U chemistry is highlighted. With this knowledge, I expand on the seawater U chemistry box model of Henderson (2002), incorporating glacial melt U fluxes from my GrIS study and previous studies. Using this box model, I assess the resulting $\delta^{234}U$ seawater chemistry from various scenarios of glacial meltwater compositions, glacial melt volume, and sources of glacial meltwater on glacial-interglacial timescales (Arendt *et al.*, *Submitted*).

Identifying potential fluctuations in the $\delta^{234}U$ chemistry of seawater has a direct impact on paleoclimate reconstructions obtained through U/Th dating of corals, which is dependent on the assumption that $\delta^{234}U$ seawater chemistry has remained constant over time. By incorporating the GrIS subglacial U chemistry values as representative compositions of glacial and interglacial meltwater runoff in a simple box model, I assess the impact glacial melt may have on seawater $\delta^{234}U$ over glacial-interglacial timescales.

1.3. SUMMARY

Gaining insight on meltwater fraction contributions, meltwater storage timescales, glacial meltwater chemistry and the impact glacial meltwater may have on the chemistry and nutrient

supply of surrounding environments are all critical in placing further constraints on climate change. The synthesis of these findings has important implications for the prediction of the anticipated rate of climate change and the magnitude of the associated hydrological consequences of this change. Broader impacts of the research presented in my thesis include new geochemical analysis techniques to be used in glacial and hydrologic systems worldwide, contributions to resolving sociopolitical issues such as water rights in meltwater-dependent regions, an increased knowledge of the pace and impacts of global climate change, and the placement of constraints on how well we understand the impact of glacial meltwater on surrounding marine environments. Thus, the combined application of the glacial hydrology chemical proxies presented in this thesis provides further clarity of subglacial system processes and the implications of these processes global scales.

1.4. PUBLICATIONS RESULTING FROM THIS DISSERTATION

1) Arendt, C.A., Aciego, S.M., and Hetland, E.A., 2015. An open source multiple isotope Bayesian Monte Carlo mixing model with applications in Earth surface processes. Geochemistry, Geophysics, Geosystems. DOI: 10.1002/2014GC005683 **(Chapter 2).**
2) Arendt, C.A., Aciego, S.M., Sims, K.W.W., and Aarons, S.M., *In review*. Models underestimate glacial meltwater storage time. Geochimica et Cosmochimica Acta, **(Chapter 3).**
3) Arendt, C.A., Aciego, S.M., Stevenson, E.I., Das, S.B., and Sims, K.W.W., *In Review.* Greenland outlet glacier subglacial water residence times and proximal seawater U chemistry: Implications for seawater $(^{234}U/^{238}U)_{ACT}$ on glacial-interglacial timescales. **(Chapter 4).**

1.5. REFERENCES CITED

Aciego, S.M., *et al*., A new procedure for separating and measuring radiogenic isotopes (U, Th, Pa, Ra, Sr, Nd, Hf) in ice cores, Chemical Geology (2009), doi:10.1016/j.chemgeo.2009.06.003

Aizen, V.B., *et al.*, Precipitation, melt and runoff in the northern Tien Shan, Journal of Hydrology (1996), 186: 229-251.

Anderson, R.S., *et al*., Strong feedbacks between hydrology and sliding of a small alpine glacier, Journal of Geophysical Research-Earth Surface (2004), 109(F3): F03005.

Arendt, C.A., *et al*., Sequential separation of radioactive U, and radiogenic Nd and Hf Concentrated from natural waters, Geostandards and Geoanalytical Research (2014), doi:10.1111/j.1751-908X.2014.00322.x

Arendt, C.A., *et al*., An open source Bayesian Monte Carlo isotope mixing model with applications in Earth surface systems, Geochemistry, Geophysics, Geosystems (2015), doi:10.1002/2014GC005683

Arendt, C.A., *et al*., Models underestimate glacial meltwater storage time, evidence from U-series, Geochimica et Cosmochimica Acta, *In Review.*

Arendt, C. A., *et al.*, Greenland outlet glacier subglacial water residence times and proximal seawater U chemistry: Implications for seawater $(^{234}U/^{238}U)_{ACT}$ on glacial-interglacial timescales, Earth and Planetary Science Letters, *In Review*.

Arnold, N., *et al*., Initial results from a distributed, physically based model of glacier hydrology, Hydrological Processes (1998), 12(2): 191-219.

Baker, D., A glacier discharge model based on results from field studies of energy-balance, water storage and flow, Hydrological Sciences Journal (1982), 27: 257.

Barnett, T. P., Adam, J. C. *et al*., Potential impacts of a warming climate on water availability in snow-dominated regions, Nature (2005), 438(7066): 303-309.

Bartholomew, I., *et al.*, Seasonal evolution of subglacial drainage and acceleration in a Greenland outlet glacier, Nature Geoscience (2010), 3(6): 408-411.

Bhatia, *et al*., Seasonal evolution of water contributions to discharge from a Greenland outlet glacier: insight from a new isotope-mixing model, Journal of Glaciology (2011), 57(205).

Bell, E.B., *et al*., Origin and fate of Lake Vostok water frozen to the base of the East Antarctic ice sheet. Nature (2002), 416: 307-313.

Bradley *et al*., Threats to water supplies in the tropical Andes, Science (2006), 312: 1755-1756.

Braithwaite, R., Positive degree-day factors for ablation on the Greenland ice-sheet studied by energy-balance modeling, Journal of Glaciology (1995), 41: 153-160.

Brown, G.H., Glacier meltwater hydrochemistry, Applied Geochemistry (2002), 17: 855-883.

Cable, *et al*., Contribution of glacier meltwater to streamflow in the Wind River Range, Wyoming, inferred via a Bayesian mixing model applied to isotopic measurements, Hydrological Processes (2011), 25(14): 2228-2236.

Chabaux, F., *et al*., U-Th-Ra fractionation during weathering and river transport, Uranium-Series Geochemistry (2003), 52: 533-576.

Chandler, D. M., *et al.*, Evolution of the subglacial drainage system beneath the Greenland Ice Sheet revealed by tracers, Nature Geoscience (2013), 6(3): 195-198

Colgan, A., *et al*., The annual glaciohydrology cycle in the ablation zone of the Greenland ice sheet: Part 1. Hydrology model, Journal of Glaciology (2011), 57(204): 697-709.

Collins, D. N., Quantitative determination of the subglacial hydrology of two Alpine glaciers, Journal of Glaciology (1979), 23(89): 347-369.

Coudrain, *et al.,* Glacier shrinkage in the Andes and consequences for water resources, Hydrological Sciences Journal (2005), 50: 925-932.
Craig, H., Isotopic Variations in Meteoric Waters, Science (1961), 133(3465): 1702-1703.
Creyts, T.T. and Schoof, C.G., Drainage through subglacial water sheets, Journal of Geophysical Research (2009),114: 1-18.
Cuffey, K. M., and W. B. Paterson (2010). Physics of Glaciers. Academic Press.
Dansgaard, W., Stable isotopes in precipitation, Tellus (1964), 16: 436-468.
Das, S. B., *et al*., Fracture propagation to the base of the Greenland Ice Sheet during supraglacial lake drainage, Science (2008), 320(5877): 778-781.
Dyurgerov, M., Mountain and subpolar glaciers show an increase in sensitivity to climate warming and intensification of the water cycle, Journal of Hydrology (2003), 282: 164-176.
Flowers, G. E. and G. K. C. Clark, A multicomponent coupled model of glacier hydrology - 2. Application to Trapridge Glacier, Yukon, Canada, Journal of Geophysical Research-Solid Earth and Planets (2002a), 107(B11): 2287-2288.
Flowers, G. E. and G. K. C. Clark, A multicomponent coupled model of glacier hydrology - 1. Theory and synthetic examples, Journal of Geophysical Research-Solid Earth and Planets (2002b), 107(B11): 2288-2294.
Fountain, A. G., and J. S. Walder, Water flow through temperate glaciers, Reviews of Geophysics (1998), 36(3): 299-328.
Gat, J. R., Oxygen and hydrogen isotopes in the hydrologic Cycle, Annual Review of Earth and Planetary Sciences (1996), 24(1): 225-262.
Hannah, D. M., and A. M., Gurnell, A conceptual, linear reservoir runoff model to investigate melt season changes in cirque glacier hydrology, Journal of Hydrology (2001), 246(1-4): 123-141.
Henderson, G. M., Control on ($^{234}U/^{238}U$) during the last 800 thousand years, Earth and Planetary Science Letters (2002), 199: 97-110.
Hock, R., A distributed temperature-index ice- and snowmelt model including potential direct solar radiation. Journal of Glaciology (1999), 45: 101-111.
Hooke, R. L., and V. A. Pohjola, Hydrology of a segment of a glacier situated in an overdeening, Storglaciaren, Sweden, Journal of Glaciology (1994), 40(134): 140-148.
Hubbard, B. and Nienow, P., Alpine subglacial hydrology, Quaternary Science Reviews (1997), 16: 939-955.
Hubbard, B., *et al*., Spectral roughness of glaciated bedrock geomorphic surfaces: Implications for glacier sliding, Journal of Geophysical Research (2000), 105(21): 295-303.
Innocent, C., *et al.,* U-series constraints on aquifer groundwater residence time; the Adour-Garonne district case (southwest France), Mineralogical Magazine (2008), 72(1): 321-324.
Ivanovich, M., *et al.*, Uranium-Series Radionuclides in Fluids and Solids, Milk River Aquifer, Alberta, Canada, Applied Geochemistry (1991), 6(4): 405-418.
Kamb, B., *et al.*, Glacier surge mechanism - 1982-1983 Surge of Variegated Glacier, Alaska, Science (1985), 227(4686): 460-479.
Kehrwald, N. M., *et al*., Mass loss on Himalayan glacier endangers water resources, Geophysical Research Letters (2008), 35(22).
Lemke, P. and J. W. Ren (2007). Observations: Changes in Snow, Ice and Frozen Ground. New York, Cambridge University Press.

McMillan, M., *et al*., Seasonal evolution of supra-glacial lakes on the Greenland Ice Sheet, Earth and Planetary Science Letters (2007), 262(3-4): 484-492.
Milner, A.M., *et al*., Hydroecological response of river systems to shrinking glaciers, Hydrological Processes (2009), 23: 62-77.
Mitchell, A.C., and Brown, G.H., Modeling geochemical and biochemical reactions in subglacial environments. Institute of Arctic and Alpine Research (2008), 40(3): 531-547.
Nienow, P., *et al.*, Seasonal changes in the morphology of the subglacial drainage system, Haut Glacier d'Arolla, Switzerland, Earth and Surface Processes and Landforms (1998), 23(9): 825-843.
Porcelli, D. and P. W. Swarzenski, The behavior of U- and Th-series nuclides in groundwater, Uranium-Series Geochemistry (2003), 52, 317-361.
Raymond, C. F., *et al*., Hydrological discharges and motion of Fels and Black Rapids Glaciers, Alaska, U.S.A.: implications for the structure of their drainage systems, Journal of Glaciology (1995), 41(148), 290-304.
Schaefli, B., *et al.*, A conceptual glacio-hydrological model for high mountainous catchments, Hydrology and Earth Science Systems (2005), 9: 95-109.
Schoof, C. G., Ice sheet acceleration driven by melt supply variability, Nature (2010), 468: 803-806.
Shea, J. M. and S. J. Marshall, Atmospheric flow indices, regional climate, and Glacier mass balance in the Canadian Rocky Mountains, International Journal of Climatology (2007), 27(2): 233-247.
Shepherd, A., *et al.*, Greenland ice sheet motion coupled with daily melting in late summer, Geophysical Research Letters (2009), 36: L01501.
Siegert, M. J. (2001). Ice sheets and Quaternary environmental change. New York, Wiley.
Sims, K.W.W., *et al.*, 238U-(230)Th-(226)Ra-(210)Pb-(210)Po, (232)Th-(228)Ra, and (235)U-(231)Pa constraints on the ages and petrogenesis of Vailulu'u and Malumalu Lavas, Samoa, Geochemistry Geophysics Geosystems (2008), doi: 10.1029/2007GC001651
Skidmore, M., *et al.,* Comparison of microbial community compositions of two subglacial environments reveals a possible role for microbes in chemical weathering processes, Applied and Environmental Biology (2005), 71(11): 6986-6997.
Smith, B.P.G., *et al*., A hydro-geomorphological context for ecological research on alpine glacial rivers, Freshwater Biology (2001), 46: 1579-1596.
Sundal, A. V., *et al.*, Melt-induced speed-up of Greenland Ice Sheet offset by efficient subglacial drainage, Nature (2011), 469(7331): 522-538.
Tranter, M., *et al*., Geochemical weathering in glacial and proglacial environments, Surface and Groundwater, Weathering and Soils (2005), 5: 189-205.
Wadham, J.L., *et al.*, Hydrochemistry of meltwaters draining a polythermal-based, high-Arctic glacier, south Svalbard: II. Winter and early Spring, Hydrological Processes (2000), 14(10): 1767-1786.
Walder, J., Stability of sheet flow of water beneath temperate glaciers and implications for glacier sliding, Journal of Glaciology (1982), 28: 273-293.
Verbunt, M., *et al.*, The hydrological role of snow and glaciers in alpine river basins and their distributed modeling, Journal of Hydrology (2003), 282: 36-55.
Zwally, H. J., *et al.*, Surface melt-induced acceleration of Greenland Ice Sheet flow, Science (2002), 297(5579): 218-222.

CHAPTER II

An open source Bayesian Monte Carlo isotope mixing model with applications in Earth surface processes

Official citation:

Arendt, C.A., Aciego, S. M., and Hetland, E.A., 2015. An open source Bayesian Monte Carlo isotope mixing model with applications in Earth surface processes.
Geochemistry, Geophysics, Geosystems. DOI: 10.1002/2014GC005683
Reproduced within author's rights.

ABSTRACT

The implementation of isotopic tracers as constraints on source contributions has become increasingly relevant to understanding Earth surface processes. Interpretation of these isotopic tracers has become more accessible with the development of Bayesian Monte Carlo (BMC) mixing models, which allow uncertainty in mixing end-members and provide methodology for systems with multi-component mixing. This study presents an open source multiple isotope BMC mixing model that is applicable to Earth surface environments with sources exhibiting distinct end-member isotopic signatures. Our model is first applied to new $\delta^{18}O$ and δD measurements from the Athabasca Glacier, which showed expected seasonal melt evolution trends and vigorously assessed the statistical relevance of the resulting fraction estimations. To highlight the broad applicability of our model to a variety of Earth surface environments and relevant isotopic systems we expand our model to two additional case studies: deriving melt sources from $\delta^{18}O$, δD and ^{222}Rn measurements of Greenland Ice Sheet bulk water samples and assessing nutrient sources from ε_{Nd} and $^{87}Sr/^{86}Sr$ measurements of Hawaiian soil cores.

The model produces results for the Greenland Ice Sheet and Hawaiian soil datasets that are consistent with the originally published fractional contribution estimates. The advantage of this method is that it quantifies the error induced by variability in the end-member compositions, unrealized by the models previously applied to the above case studies. Results from all three case studies demonstrate the broad applicability of this statistical BMC isotopic mixing model for estimating source contribution fractions in a variety of Earth surface systems.

2.1 INTRODUCTION

Both stable and radiogenic isotopes provide insight to the provenance of source material in Earth surface systems. Coupled with a Bayesian Monte Carlo (BMC) mixing model, isotopic tracers can be used to determine fractional contributions of multiple end-members to a bulk sample (i.e., water, soil, etc...). This information is crucial in understanding processes such as glacier melt evolution [*Bhatia et al.,* 2011; *Cable et al*., 2011], the nutrient sources for soil development and sustainability [*Chadwick et al.,* 1999], the impact of pollution on a natural system [*Barber and Wearing,* 2001], stable and radiogenic isotopes in seawater [*Pichler,* 2005; *Rickli et al.,* 2010] and water usage within ecosystems [*McCluney and Sabo*, 2010; *Grupe*, 2014].

Implementing Bayesian estimation techniques allows for the representation of spatio-temporal processes, incorporation of uncertainties, and extrapolation of input source magnitudes, and accounts for prior information and assumptions [*Soulsby et al.,* 2003; *Wikle*, 2003; *Singh and Bengtsson*, 2005; *Moore and Semmens*, 2008]. The goal of this study is to develop and provide the Earth science community with an open source, statistically robust, BMC isotope mixing model that can be applied to both stable and radiogenic isotopic systems in a variety of Earth

surface processes. The model is executed in a straightforward Matlab script, which is easy to implement and modify by researchers with minimal programming experience.

The advantage of the isotope statistical model presented in this study is that model inputs are straightforward, requiring only an Earth system with unique end-member isotopic signatures [*Theakstone*, 2003] and measurements of a sample's isotopic composition. Another benefit of this model is that it incorporates uncertainty in end-member isotopic compositions and provides an uncertainty estimation of the fractional contributions. Stable isotopes $\delta^{18}O$ and δD have commonly been used to determine contributing water sources and relative proportions of these sources to a system. Radiogenic isotopes ε_{Nd}, $^{87}Sr/^{86}Sr$, and ε_{Hf} have frequently been applied to terrestrial and oceanic settings to identify the provenance of and inputs to regolith, soils, and water masses.

Earth surface $\delta^{18}O$ and δD samples are easy to collect, require no special sampling equipment or need for low-blank, metal free cleanliness, and are time insensitive if the collection vials are sealed properly. Radiogenic Earth surface ε_{Nd}, $^{87}Sr/^{86}Sr$, and ε_{Hf} samples require additional precaution in their collection and analyses, but are gaining accessibility as the application of these isotopes is expanding. Both stable and radiogenic isotope systems in these Earth surface environments can be addressed by the model presented in this study.

For this work, we developed a BMC mixing model and applied it to a new set of $\delta^{18}O$ and δD measurements of bulk meltwater collected from the Athabasca Glacier during the summer of 2011. The aim of this study was not to expose an unknown seasonal progression, but to

corroborate the effectiveness of our model by comparing our resulting fractional contribution estimations to expected seasonal melt source contribution trends. The application of the model to this dataset allowed us to quantify the actual proportion and volume of water coming from each end-member source, which holds importance for relative contributions of snowmelt versus ice melt in the context of water storage and hydrologic use. We include a thorough description of the field site, sampling methods, analytical techniques, seasonal trend analysis, and statistical relevance of the calculated end-member fractional contributions for the Athabasca Glacier.

We apply the same type of multi-component linear mixing model to two additional case studies, one in Greenland and the other in Hawaii, which have already been subjected to simple isotope mixing models, to test the applicability and accuracy of our model. Lengthy descriptions of sampling, analysis and discussion of implications of results are not included for the Greenland Ice Sheet nor the Hawaiian soil case studies, as the implications from these datasets and estimated fractional contributions have already been addressed in previous publications [*Kennedy et al.*, 1998; *Chadwick et al*., 1999; *Kurtz et al*., 2001; *Chadwick et al*., 2009; *Bhatia et al*., 2011], and are used only to assess the applicability to additional isotopic and Earth surface systems.

2.1.1. Bayesian Mixing Model

Initially motivated by *Ogle et al.* [2004] and *Cable et al.* [2011], we developed a Bayesian Monte Carlo (BMC) estimation strategy, to solve for fractional contributions of end-member compositions from isotopic measurements. The BMC strategy is such that samples of a prior probability density function (PDF) are retained or rejected in proportion to data likelihood,

resulting in samples of a posterior PDF [e.g. *Mosegaard and Tarantola*, 1995]. Bayes' Theorem as applied to our estimation of fractional contributions is

$$p(f_i) \propto p'(f_i \& I_i)\, L(o_j | f_i \& I_i), \tag{1}$$

where f_i are the fractional contributions (i.e., the unknown model), o_j are the isotopic measurements, I_i are the isotopic composition of the end-member components, $p(f_i)$ and $p'(f_i \& I_i)$ are the prior and posterior PDFs, respectively, and $L(o_j | f_i \& I_i)$ is a data likelihood function. Bayesian estimation narrows the given prior PDF to a posterior PDF by testing the statistical likelihood of predicted isotopic values against the observations [e.g. *Mosegaard and Tarantola*, 1995].

The prior PDF includes both the isotopic compositions of the end-member components and constraints on the fractional contributions of the end-member components. Rather than assuming that the isotopic composition of the end-members are precisely known, we include variances of the end-member compositions in the prior PDF, where the variances can account for either uncertainty in the compositions or natural variability in the end-member components. *Cable et al.* [2011] and *Parnell et al.* [2013] assumed a specialized covariance model of the uncertainties assuming that the isotopic compositions of each end-member directly influence the mass fractionation of the other end-members. We have no evidence to support this complexity of the end-member covariance in the case studies presented here. Hence we follow a simpler approach in which we assume that the uncertainties of the isotopic compositions of the end-members are uncorrelated and that the end-member compositions are normally distributed with standard deviation given by the measurement uncertainties: although use of other PDFs, either analytic or

empirical, can be included.

The priors of the fractional contributions can include detailed prior knowledge and assumptions of the fractional contributions or, can consist of more simple priors in which the sum of all fractional contributions is equal to one. The applications presented here use the latter. Specifically, all the applications presented here assume that there are only three possible contribution sources (see below for discussion of additional sources), and in this case the constraint is

$$f_a + f_b + f_c = 1, \tag{2}$$

where f_a, f_b, and f_c are the fractional contributions of the three sources. Additional end-members may be added so long as there are an equal number of constraints and/or system equations, which are given by the number of isotopic species considered. Other than the constraints in equation (2), we assume all combination of $0 \geq f_i \leq 1$ are equally likely.

Additional constraints may be added to the prior without the addition of end-members to increase the certainty of the fraction predictions. Constraints may be incorporated to narrow the possible range of values within which a mass fraction must lie. For time series datasets, a potential constraint could be the expected likelihood of certain estimations at diff t time periods. Likewise, expected temporal variations of the end-member isotopic composition could also be incorporated into the prior. For example, temporal constraints could account for variation of fractionation of $\delta^{18}O$ during snowmelt, where the variance on the end-member $\delta^{18}O$ may be smaller during time periods with minimal snowmelt (e.g. late summer, fall) and larger during time periods with maximum snowmelt (e.g. spring, early summer). In the applications we present, we make no

assumption about how the fractional contributions vary through time and estimate the posterior PDFs independently at each time for which the data are available.

We assume purely Gaussian (normal) and uncorrelated uncertainties on the measured isotopic compositions. The data likelihood function is then given as

$$L(o_j|f_i\&I_i) \propto \prod_j \exp\left[\frac{(o_j^p - o_j)^2}{2\sigma_j^2}\right], \tag{3}$$

where σ_j are the uncertainties on the isotopic measurements and o^p_j are the isotopic values predicted by a test model of f_i and the realization of I_i. To compute the predicted isotopic values, we use a standard linear mixing model [*Sharp et al.,* 1995; *Ogle et al.,* 2004; *Moore and Semmens*, 2008; *Bhatia et al.*, 2011; *Cable et al.*, 2011; *Parnell et al.*, 2013], which is discussed in detail for each case study below. An additional complication in the mixing relationship arises when the values of the isotopic complications of the three source end-members are not precisely known, and the degree to which they are known is not explicitly characterized [*Theakstone*, 2003; *Moore and Semmens*, 2008; *Parnell et al*., 2010]. We deal with this complication by including variability of the end-member compositions in the prior, as discussed above. The consideration of more isotopic tracers with distinct end-member compositions would in general result in lower final uncertainties in the final posteriors, which is discussed explicitly in Case Study 2 below.

We use a straightforward Monte Carlo sampling scheme, where randomly chosen samples of the prior are retained as samples of the posterior proportional to the likelihood based on the misfit between predictions and data. The samples of the prior represent random realizations of end-member contributions and fractions of contributing components. The retained samples are then samples of the posterior PDF, and represent fractional contributions of the end-members.

Rejection and acceptance of the prior samples is relative to the most likely model. For example, prior samples are always accepted if the relative likelihood is one (i.e., the most likely estimate), accepted half of the time with 50% probability if the relative likelihood is 0.5, and never accepted if the relative likelihood is zero.

The Monte Carlo sampling strategy we use is equivalent to a uniform random walk in which no transitional properties are needed [e.g. *Mosegaard and Tarantola*, 1995]. Our approach is in contrast to the Markov Chain Monte Carlo (MCMC) Bayesian approach used by *Cable et al.* [2011] where the selection of prior samples is based on the likelihood of a proposed sample relative to the likelihood of the previous sample tested [e.g. *Mosegaard and Tarantola*, 1995]. While our uniform BMC is less computationally efficient than a MCMC approach, the linear mixing system is computationally trivial and sufficient posterior samples can be determined on an average desktop computer in a tractable time frame (roughly twenty minutes to several hours on a standard desktop computer, depending on sample size).

For each stock measurement, we tested approximately 10^7 prior samples, and accepted those as posterior samples in proportion to the relative likelihood of their associated prediction. In each run we present here, $1–8 \times 10^4$ samples were found to be statistically likely relative to the most likely estimate for each stock sample. The density in the fractional contribution space of the accepted posterior samples reflects the statistics of the estimated fractional contributions and is statistically consistent with the measurements. We calculate mean values, standard deviations, and covariance of the posterior samples (i.e., fractions of the source contributions) for each stock sample. The normal statistical moments characterize the posteriors well, although it is important

to bear in mind that the posteriors are bound by the constraints of the solutions (i.e. all fractional contributions are ≥ 0 and must sum to 1), and thus are non-Gaussian. Covariance values reflect how dependent the fractional contribution of each individual end-member is on the projected fractional contribution of the other end-members.

2.2 CASE STUDIES

2.2.1 Case Study One: Glacial meltwater fractions based on $\delta^{18}O$ and δD from the Athabasca Glacier

The Athabasca Glacier is one of eight outlet glaciers draining the Columbia Icefield, a 325 km^2 ice plateau (Figure 2.1). The Columbia Icefield straddles the continental divide in the Canadian Rocky Mountains, lying at the north end of Banff National Park and the south end of Jasper National Park in Alberta, Canada. The Columbia Icefield is approximately 1900 m at the lowest elevation and 3400 m at the highest point, Snow Dome. The Athabasca Glacier connects to the Columbia Icefield at approximately 2700 m and extends down to 2030 m at its terminus. Melt from the Columbia Icefield drains into three major oceans, including the Arctic, Pacific, and Atlantic oceans, but is located over 2000 km from the nearest ocean [*Butler,* 1980; *Brugmann*, 1994; *Hart,* 2006].

Local climate in the Columbia Icefield region has remained relatively consistent throughout the past half century [*Letreguilly,* 1988; *Canada National Climate Archive*, 2013] with no abrupt changes, although the local mean annual temperature has been gradually increasing [*Canada National Climate Archive*, 2013]. In the past decade, average local winter temperatures ranged from -15 to -19˚C, summer temperatures ranged from +16 to +20˚C, and annual temperatures

averaged +1˚C [*Shea and Marshall*, 2007; *Canada National Climate Archive*, 2013]. Total annual precipitation for the region has ranged from 395 mm to 475 mm in the past decade, with the majority coming from snowfall (~65-90%) [*Shea and Marshall,* 2007; *Canada National Climate Archive*, 2013]. The balance between mass gain through annual precipitation and mass loss through ablation, primarily melting, has trended toward mass loss since the Little Ice Age, and the Athabasca Glacier retreats several meters annually [*Hart,* 2006].

Meltwater from the Columbia Icefield recharges the local confined aquifer, and subglacial melting is responsible for the development of a karst system between the Castleguard and Saskatchewan glaciers [*Ford et al.,* 1983; *Smart,* 1983], which are outlet glaciers to the south of the Athabasca Glacier. The lithology beneath the Athabasca Glacier consists of Middle Cambrian limestone and carbonic shale, which allow for karst formation [*Hart*, 2006]. Discharge from the aquifer occurs via large springs between 1500 m and 1900 m in elevation throughout the region [*Ford et al*., 1983], and there is a proximal spring to the Athabasca Glacier approximately 130 m lower in elevation than the terminus (Figure 2.1). There is an absence of groundwater input to the subglacial environment because the aquifer is confined and located at lower elevation than the terminus of the Athabasca Glacier. Thus, snowmelt, ice melt, and summer precipitation are the primary contributions to the water discharge from the Athabasca Glacier terminus.

Because the Athabasca Glacier is an outlet glacier of a larger ice body, the mass balance of the Columbia Icefield directly impacts the mass balance of the Athabasca Glacier. The accumulation area, the Columbia Icefield plateau, accumulates summer and winter snow, has little surface melt

and produces the blue ice that is ultimately exposed in the ablation zones of its outlet glaciers, including the Athabasca Glacier. Summer ablation from the outlet glaciers will include both winter snow pack deposited on the glacier surface and blue ice from the Columbia Icefield that is a combination of both summer and winter deposition.

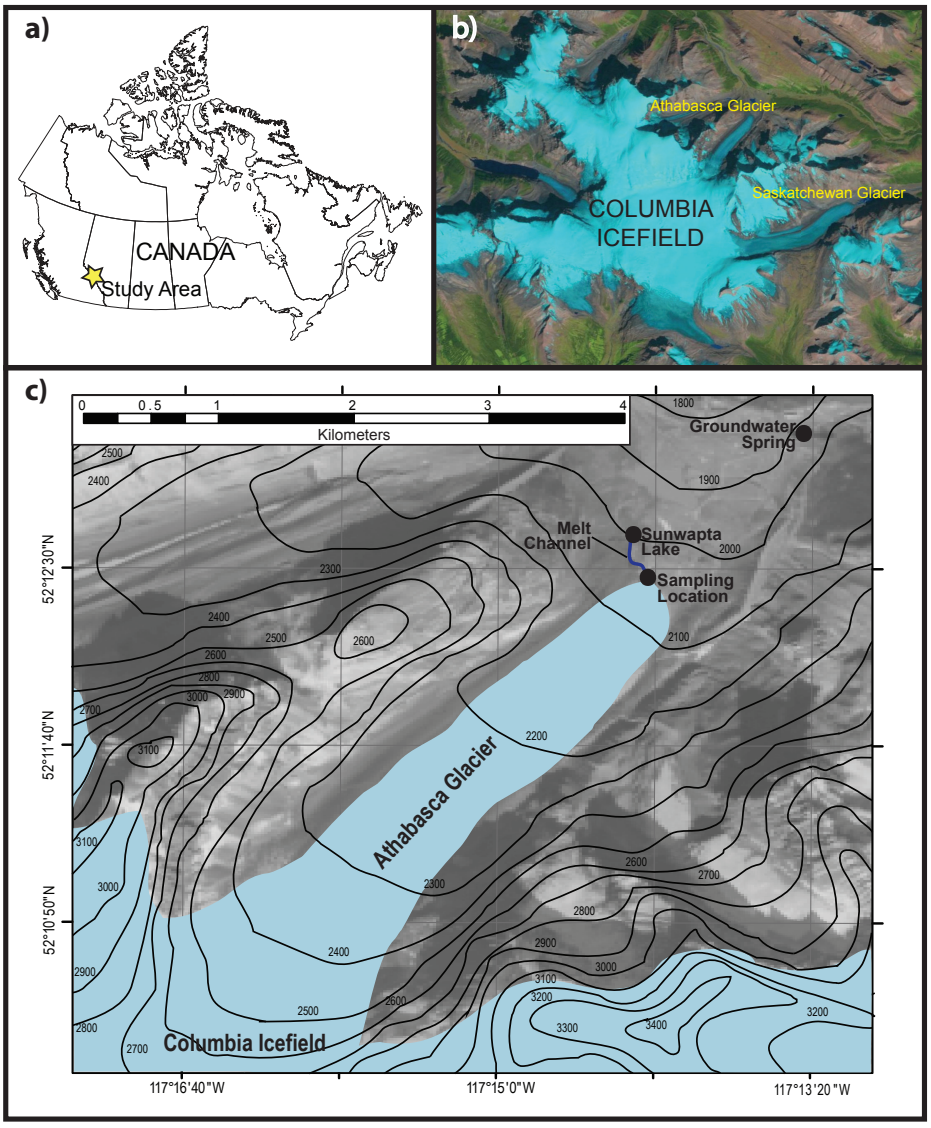

Figure 2.1: Detailed location map for the Athabasca Glacier. a) Athabasca Glacier (yellow star) is located in Jasper National Park, Alberta, Canada. b) The Athabasca Glacier is a prominent lobe coming off of the Columbia Icefield, situated in the Canadian Rockies. c) Sampling site at the terminus of the Athabasca Glacier is indicated by a black circle, at N52°12.54, W117°14.29. Sampling took place at the main meltwater channel, within 20 m of the ice terminus of the Athabasca Glacier. A melt channel connects our sampling site to Lake Sunwapta (black circle), located approximately 0.25 km from the terminus of the Athabasca Glacier. A black circle approximately 1.5 km from the terminus of the Athabasca Glacier and over 150 m lower in elevation than our sampling location, denotes a local groundwater spring. Map is composed of a Digital Elevation Model, DEM, which shows elevation contour lines at 100 m, ranging from lowest elevation of 1800 m to the highest elevation of 3400 m, overlain onto 12 Systeme Pour l'Observation de la Terre, SPOT.

2.2.1.1 Sample collection and in situ measurements

Water samples were collected from the main outlet channel 10 m downstream from the Athabasca Glacier terminus (located 2030 m above sea level at N52°12.54 and W117°14.29). In situ measurements took place every morning in May and July of 2011 alongside samples that were being collected for a corresponding study of Athabasca Glacier subglacial water residence time [*Arendt et al*., In Review]. Samples were collected at the same time daily (in the morning) for consistency and to avoid variations in bulk melt sample composition due to daily fluctuations. The dataset consisted of samples collected in May and July, but not June because of the time and resource intensiveness required for obtaining a suite of time series samples. Thus, the collection season was scheduled to align with the important hydrological time periods, including onset and peak of melt. Similar strategies have been employed in previous studies, e.g. *Bhatia et al.* [2011]. Samples collected for oxygen and hydrogen isotopes were collected onsite directly into Kimble™ 20 ml glass screw-thread scintillation vials (No. 74516 20) with cone caps. Vials were filled to the top to minimize atmospheric headspace and sealed tightly until measurement.

Daily discharge measurements were taken concurrently, at the same location and time that the water samples were collected. Manual measurements of discharge were acquired using an Acoustic Doppler Velocimeter, or ADV, Flow-tracker. A measuring tape was set across the width of the channel, perpendicular to water flow. The ADV Flowtracker's sensor was submerged at the edge of the channel parallel to water flow and calibrated prior to measurement. Following calibration, the ADV Flowtracker measured velocity and water depth at one-foot increments spanning the width of the main discharge channel at the terminus of the glacier.

Velocity and water depth measurements across the channel allowed the calculation of discharge, using the standard 0.6 rule [*Morlock et al*., 2002] (Table 2.1), and subsequently converted from cubic feet per second to cubic meters per second.

Table 2.1: Time series discharge and bulk meltwater $\delta^{18}O$ and δD measurements. Includes associated standard deviations and *in field* weather notes for Case Study 1, the Athabasca Glacier.

DOY	Discharge (m^3/s)	$\delta^{18}O$	2σ	δD	2σ	Field Notes
125	0.01	-20.8	0.1	-160.8	1.3	sleet
126	0.01	-20.9	0.1	-161.8	1.3	–
127	0.01	-21.3	0.1	-164.4	1.3	sleet
128	0.01	-21.7	0.1	-167.5	1.3	sleet
129	0.04	-22.0	0.1	-169.5	1.3	–
130	0.02	-22.7	0.1	-175.5	1.3	–
131	0.05	-23.6	0.1	-181.2	1.3	–
132	0.06	-25.1	0.1	-193.5	1.3	sleet/rain
133	0.07	-25.0	0.1	-192.7	1.3	–
134	0.07	-24.2	0.1	-186.5	1.3	–
135	0.07	-24.3	0.1	-186.0	1.3	–
136	0.07	-24.5	0.1	-186.2	1.3	–
137	0.10	-24.5	0.1	-186.7	1.3	sleet
138	0.11	-24.5	0.1	-186.3	1.3	–
139	0.07	-24.2	0.1	-184.4	1.3	sleet/rain
140	0.11	-24.0	0.1	-181.2	1.3	–
141	0.22	-24.6	0.1	-185.0	1.3	–
142	0.19	-24.3	0.1	-185.8	1.3	–
143	0.35	-24.1	0.1	-184.1	1.3	–
144	0.51	-23.5	0.1	-176.6	1.3	–
145	0.44	-23.5	0.1	-176.4	1.3	–
146	1.17	-23.3	0.1	-174.9	1.3	rain
147	0.54	-23.8	0.1	-174.8	1.3	sleet/rain
148	0.43	-23.3	0.1	-173.6	1.3	sleet/rain
149	0.41	-23.2	0.1	-175.0	1.3	–
183	2.10	-21.3	0.1	-159.5	1.3	–
184	2.42	-19.9	0.1	-148.0	1.3	rain
185	1.60	-21.1	0.1	-155.5	1.3	–
186	1.52	-21.5	0.1	-156.7	1.3	–
187	2.32	-20.9	0.1	-155.9	1.3	–
188	3.28	-21.0	0.1	-156.3	1.3	–
189	1.55	-20.9	0.1	-156.7	1.3	sleet/rain
190	1.55	-21.7	0.1	-157.2	1.3	rain
191	1.22	-21.3	0.1	-158.8	1.3	–
192	1.24	-21.2	0.1	-158.3	1.3	–
193	2.14	-20.6	0.1	-153.2	1.3	rain
196	2.90	-20.7	0.1	-152.3	1.3	rain
197	2.79	-20.8	0.1	-153.2	1.3	–
198	2.85	-20.8	0.1	-152.0	1.3	–
199	3.40	-20.5	0.1	-156.5	1.3	rain
200	2.10	-20.6	0.1	-154.9	1.3	–

Continued on next page

Table 2.1 – continued from previous page

DOY	Discharge (m^3/s)	$\delta^{18}O$	2σ	δD	2σ	Field Notes
201	2.22	-20.8	0.1	-154.5	1.3	rain
202	4.11	-21.5	0.1	-158.3	1.3	rain
203	1.44	-21.2	0.1	-154.8	1.3	sleet/rain
204	1.34	-20.5	0.1	-150.5	1.3	–
205	1.53	-21.2	0.1	-151.6	1.3	–
206	3.21	-21.0	0.1	-151.2	1.3	–
207	3.32	-20.4	0.1	-146.9	1.3	rain
208	1.98	-20.8	0.1	-151.2	1.3	rain

The stable isotope compositions of ice and snow samples were collected from the terminus (~2030-2050 m ASL) of the Athabasca Glacier (Table 2.2). End-member samples of snow were collected at the beginning and end of the fi season and averaged. End-member samples of ice were collected across a horizontal transect of the glacier to encompass a range of ice ages and averaged. Precipitation values were not directly collected as the directionality and timing of precipitation events made the collection of an adequate sample volume impossible. Thus, 2011 summer precipitation $\delta^{18}O$ and δD values were compiled from three regional weather stations for the years 2010-2011 including *Athabasca 1* (N54°43.20, W113°17.17), *Athabasca AGCM* (N54°38.05, W113°22.55) and *Athabasca LO* (N52°25.00, W117°47.00) [*Shea and Marshall,* 2007; *Canada National Climate Archive*, 2013]. Precipitation isotopic values were averaged and used as the representative precipitation end-member. These three distinct isotopic signatures for contributing water masses to the Athabasca Glacier subglacial discharge are defined in Table 2.2. The ranges in end-member isotopic measurements, both directly measured and taken from literature, are accounted for as the standard deviation of each end-member value given (Table 2.2).

Table 2.2: Athabasca Glacier end member isotopic compositions. Isotopic end-member values and number of samples (n) collected for the Athabasca Glacier case study that were either directly measured or referenced from regional data bases [*Canada National Climate Archive*, 2013].

End-member	$\delta^{18}O$	$\sigma\delta^{18}O$	δD	$\sigma\delta D$
Ice melt	-20.0	0.5	-140.0	2.0
Snowmelt	-25.5	0.7	-205.0	4.0
Summer Precipitation	-13.0	2.0	-104.0	10.0

2.2.1.2 Mass spectrometry

Water stable isotope measurements were performed at the University of Michigan Stable Isotope Laboratory. Deuterium measurements were made using a Finnigan H-Device coupled to a dual inlet gas source Thermo Finnigan Delta V Plus mass spectrometer. The analysis process entailed use of an A CTC Analytics Pal Autosampler to inject 1 ml of water per sample into a chromium reactor set at 800˚C, where the sample reacts for approximately 2 minutes. Next, the samples were equilibrated in the dual inlet for 1 minute (allowing the H_2O and CO_2 in the system to reach isotopic equilibrium) and run at 8V against a reference gas of known composition [*Socki et al.,* 1992]. The samples were run in duplicate to account for memory effects and bracketed against known standards (VSMOW/VSLAP, in-house standards) to ensure accuracy in the machine's measurements. Sample measurements were then normalized relative to the VSMOW/VSLAP scale and expressed relative to VSMOW. Accuracy and precision is better than ± 1 ‰ on replicate analyses, and analytical error on standards over time is better than ± 1.3 ‰.

Oxygen isotopes ($^{18}O/^{16}O$) were measured by continuous flow on a Thermo Finnigan Gas Bench II coupled to the inlet of a Thermo Finnigan Delta V Plus mass spectrometer. The analysis process entailed use of an A CTC Analytics Pal Autosampler to inject 0.5 ml of water per sample into a pre-evacuated Labco exetainer. Next, the samples were loaded into the Finnigan Gas Bench II sample tray. The A CTC Analytics Pal Autosampler was used to flush the samples with 0.3% CO_2 in a helium (He) mixture for 8 minutes. The samples were then allowed to equilibrate over a two-day period at 30˚C. Pure He (UHP grade) was then used to flush each sample for 8 minutes. The sample gas was then transported via helium flow, cleaned of any remaining water with the Gas Bench water traps, and pushed through a GC column set at 70˚C. The CO_2 was then

admitted through a capillary to the inlet of the mass spectrometer where multiple sample peaks were measured against the CO_2 reference gas peaks. The data were normalized and reported relative to the VSMOW/VSLAP scale. Accuracy and precision for these samples is ± 0.1 ‰.

The oxygen and hydrogen isotopic composition of water samples and corresponding discharge measurements from the Athabasca Glacier are summarized in Table 2.3.

2.2.1.3 Oxygen and hydrogen isotopic composition of glacial meltwater

The stable isotopes of the bulk discharge water samples from the primary discharge channel at the Athabasca Glacier show distinct changes through the onset of summer melting in May and peak melt in July (Table 2.1). At the initial onset of melt our $\delta^{18}O$ and δD data become increasingly depleted only to show a reversal in trend in the second week of May, where $\delta^{18}O$ and δD become increasingly enriched in lighter isotopes for the remainder of the month. Samples from July show less enriched $\delta^{18}O$ and δD values, comparable to those samples from the very beginning of May, with no obvious temporal trends and little variation.

Results are presented in dual isotope space along with the Local Meteoric Water Line (LMWL) [*Clark and Fritz,* 1997] for Canada, (Figure 2.2). When plotted in this manner, our $\delta^{18}O$ and δD measurements follow the expected relationship of waters in dual isotope space [*Craig,* 1961]. All meltwater samples exhibit positive deuterium excess values (d-excess = δD - 7.75 x $\delta^{18}O$, where 7.75 is the slope of the LMWL). Samples from early May show the smallest deuterium excess (less than 1.0 ‰), with values trending toward more positive values through May and into July (between 3 and 12 ‰).

Table 2.3: Athabasca Glacier raw fraction contribution estimations. Fraction contribution predictions and associated standard deviations for ice melt (fi), snowmelt (fs) and summer precipitation (fr) from our Bayesian Monte Carlo isotope mixing-model using the data presented in Table S1 for Case Study 1.

DOY_2011	fi_mean	fi_std	fs_mean	fs_std	fr_mean	fr_std
125	0.3325	0.1696	0.441	0.0752	0.2265	0.1032
126	0.3262	0.1674	0.4528	0.0742	0.221	0.1021
127	0.3302	0.1629	0.4785	0.0721	0.1912	0.0993
128	0.3204	0.1549	0.5139	0.0695	0.1657	0.0934
129	0.3172	0.1488	0.536	0.067	0.1468	0.0897
130	0.2654	0.1291	0.6159	0.0611	0.1187	0.0773
131	0.2162	0.1038	0.6969	0.0545	0.0869	0.0606
132	0.0934	0.0561	0.8627	0.0428	0.044	0.032
133	0.0989	0.0583	0.8548	0.0427	0.0464	0.0335
134	0.1581	0.0827	0.7711	0.0488	0.0708	0.0478
135	0.1638	0.0844	0.7671	0.0495	0.069	0.0487
136	0.1583	0.0815	0.7762	0.0497	0.0655	0.0466
137	0.1541	0.0798	0.7819	0.049	0.064	0.045
138	0.1556	0.0809	0.7776	0.048	0.0668	0.0473
139	0.1829	0.0887	0.7467	0.0503	0.0704	0.0513
140	0.2154	0.1012	0.7058	0.0533	0.0788	0.0596
141	0.1699	0.0841	0.7652	0.0491	0.0649	0.0484
142	0.1631	0.0847	0.767	0.0491	0.0699	0.0497
143	0.1833	0.092	0.7415	0.0511	0.0752	0.0535
144	0.2701	0.1185	0.6401	0.0582	0.0898	0.0694
145	0.2724	0.1205	0.6366	0.0588	0.0909	0.071
146	0.2932	0.126	0.6112	0.0611	0.0956	0.0733
147	0.2752	0.1292	0.6317	0.0613	0.0931	0.0769
148	0.306	0.1309	0.5993	0.0628	0.0946	0.0763
149	0.2913	0.1258	0.6125	0.0613	0.0962	0.0734
183	0.4497	0.1803	0.3941	0.0781	0.1562	0.1085
184	0.5149	0.2188	0.2534	0.0932	0.2317	0.1324
185	0.5203	0.1907	0.331	0.0818	0.1487	0.1142
186	0.5241	0.1888	0.3463	0.0811	0.1296	0.1131
187	0.4813	0.1923	0.3465	0.0825	0.1721	0.1158
188	0.4888	0.1899	0.3484	0.0817	0.1628	0.114
189	0.4612	0.1902	0.3603	0.0817	0.1785	0.1149
190	0.526	0.1875	0.3521	0.0805	0.1219	0.1123
191	0.4679	0.1834	0.3815	0.0793	0.1506	0.1097
192	0.4676	0.1832	0.376	0.0787	0.1564	0.1105
193	0.504	0.2012	0.3108	0.0857	0.1853	0.1216
196	0.5437	0.2026	0.2899	0.0861	0.1664	0.1219
197	0.5347	0.2001	0.3021	0.0849	0.1631	0.1208
198	0.5633	0.203	0.2815	0.0867	0.1552	0.1216
199	0.3873	0.1863	0.3805	0.0809	0.2322	0.1135
200	0.4573	0.1956	0.3426	0.0841	0.2	0.1182
201	0.5037	0.1964	0.3245	0.0834	0.1718	0.119
202	0.4966	0.1825	0.3698	0.0786	0.1336	0.1094
203	0.5441	0.1918	0.3178	0.082	0.1381	0.1151
204	0.559	0.2093	0.2663	0.0889	0.1746	0.1261
205	0.6014	0.204	0.2691	0.0859	0.1294	0.123
206	0.5963	0.2058	0.2648	0.0874	0.1388	0.1233
207	0.6322	0.2168	0.2069	0.0915	0.161	0.1303

The combination of low mean annual temperatures, high elevation and distance from precipitation source drives depletion in the stable isotopes of water, $\delta^{18}O$ and δD, via Rayleigh fractionation [*Dansgaard,* 1964; *Aizen et al.,* 2005; *Cooper,* 1998; *Petit et al.,* 1999; *Moore and Semmens*, 2008; *Singh*, 2013]. In addition, there is a significant seasonality to the depletion, with winter snow producing the most negative isotopic compositions. Thus, $\delta^{18}O$ and δD values of ice are medians between summer and winter snowpack $\delta^{18}O$ and δD values [*Aizen et al*., 2005; *Canada National Climate Archive*, 2013].

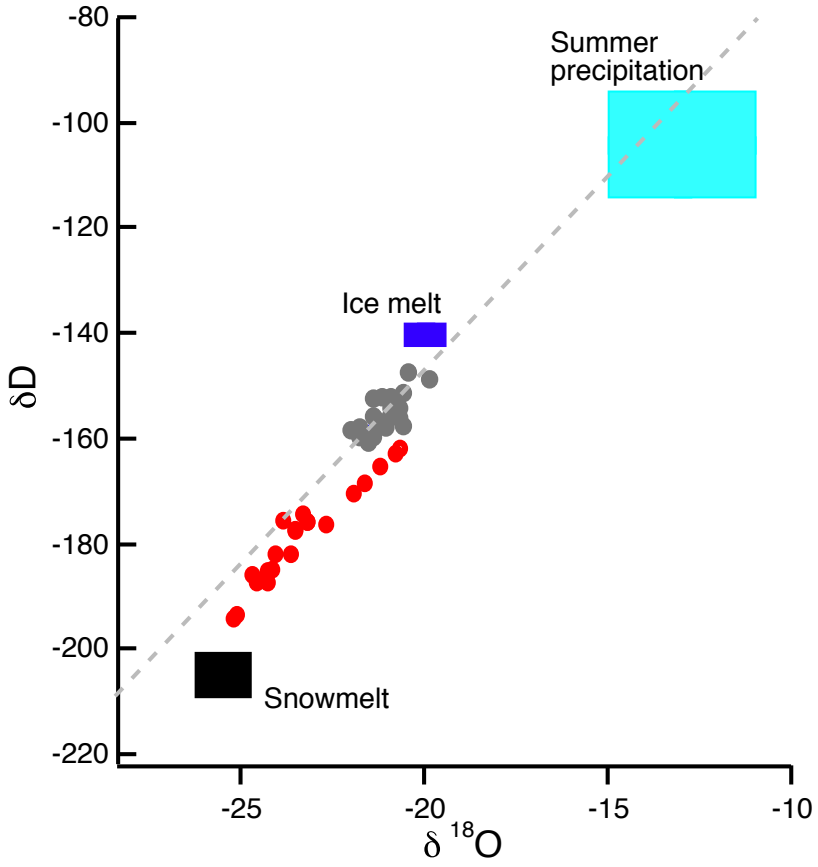

Figure 2.2: Dual isotope plot of $\delta^{18}O$ and δD values of Athabasca Glacier bulk water samples. Samples for May (grey) and July (red) 2011 in comparison to the Local Meteoric Water Line for Canada (Clark and Fritz, 1997). Rectangles represent the mean isotopic end-member values and variation in end-member values for snowmelt, ice melt, and summer precipitation as described in the text and in Table 2.1.

2.2.1.4 Fractional contributions to meltwater discharge

We assume that the Athabasca Glacier system has three possible contribution sources: snowmelt, ice melt, and summer precipitation. Thus, the sum of the fraction from snowmelt (f_s), fraction of ice melt, (f_i), and fraction from summer precipitation/rain (f_r) is constrained to equal one:

$$f_s + f_i + f_r = 1, \tag{4}$$

The likelihood of a model prediction was calculated using

$$L \propto \exp\left[\frac{(\delta^{18}\mathrm{O}_p - \delta^{18}\mathrm{O}_o)^2}{2\sigma^2_{\delta^{18}\mathrm{O}}}\right] \cdot \exp\left[\frac{(\delta\mathrm{D}_p - \delta\mathrm{D}_o)^2}{2\sigma^2_{\delta\mathrm{D}}}\right], \tag{5}$$

where $\delta^{18}\mathrm{O}_p$ and $\delta^{18}\mathrm{O}_o$ are the predicted and observed measurements of $\delta^{18}\mathrm{O}$, respectively, $\sigma_{\delta^{18}\mathrm{O}}$ is the measurement uncertainty, and likewise for δD.

Fractional contributions f_i, f_s and f_r were estimated from the bulk water for each day that a sample was collected and the isotopic composition measured. These sample day fractional contributions at the Athabasca Glacier are summarized in the Table 2.3. As described above, we characterize the posteriors (or uncertainty of PDFs after incorporating additional constraints) by the averages, variance, and covariance values calculated. In Figure 2.3 we show the average estimated fractional contributions for each DOY and in Figure 2.4 we show the 67% credible ellipses of multivariate Gaussian PDFs describing the posteriors. We chose to 67% (mean value $\pm 2\sigma$) instead of 95% (mean value $\pm 1\sigma$) credible intervals to optimize the clarity of the plots. In Figure 2.5 we compare the 67% ellipse to the full posterior corresponding to the 200th day of 2011, which is a representative posterior of all of the days.

Model results show that in May the dominant contributor to the water volume at the main

discharge outlet varied temporally. Initially, the base flow comprised approximately equal parts f_i, f_s and f_r, but shifted within several days to primarily f_s (Figure 2.3). The range of fractional contributions for the end-members in May was 0.44-0.86 (f_s), 0.09-0.33 (f_i), and 0.04-0.23 (f_r). In July the contribution fractions had evolved so that f_i was the main contributor, followed by f_s and f_r. The range of fractional contributions for the end-members in July was 0.44-0.63 (f_i), 0.08-39 (f_s), and 0.12-0.23 (f_r). Throughout the duration of our field season, f_r was always the smallest mass contributor, ranging consistently between 0.04 and 0.23 in both May and July.

The estimated fractional contributions are more uncertain in July than in May, in particular the uncertainty in f_i is larger in July than in May (Figure 2.4). f_i is negatively correlated to both f_s and f_r, with the correlations slightly stronger in July than in May (Figure 2.4). In contrast, covariances between f_s and f_r generally indicate moderate positive correlations (Figure 2.4b).

For all end-member relationships, the errors in the covariance of fractional contribution in July are significantly larger than the errors in the covariance of fractional contribution in May (Figure 2.4). The smaller errors in May are likely due to the fact that snow dominated as the most available melt source and that precipitation was limited, thus the system was primarily two-component mixing and the isotopic composition was clearly closer to an end-member composition. In July, f_i became the dominant contributor and the composition of the bulk mixture had almost equivalent source components, thus small variations in the relative contributions have large uncertainty in our BMC model. Not surprisingly, there is significant covariance between f_s and f_i because they are the two most abundant end-members, are dominantly driven by air temperature and provide the largest volumetric input to the main outlet channel.

2.2.1.5 Snowmelt versus ice melt discharge

The prominent seasonal shift in the dominant source of the discharged water at the terminus of the Athabasca Glacier signifies a change in the volume of snow and ice available for melt contributions. In May the length of the Athabasca Glacier was blanketed by snow cover, which insulated the underlying surface ice. Thus, the primary ice melt in May is derived from basal ice. In July the snow extent had retreated up-glacier by approximately 1 km, exhausting the available snow supply and exposing glacial ice to the atmosphere and solar radiation.

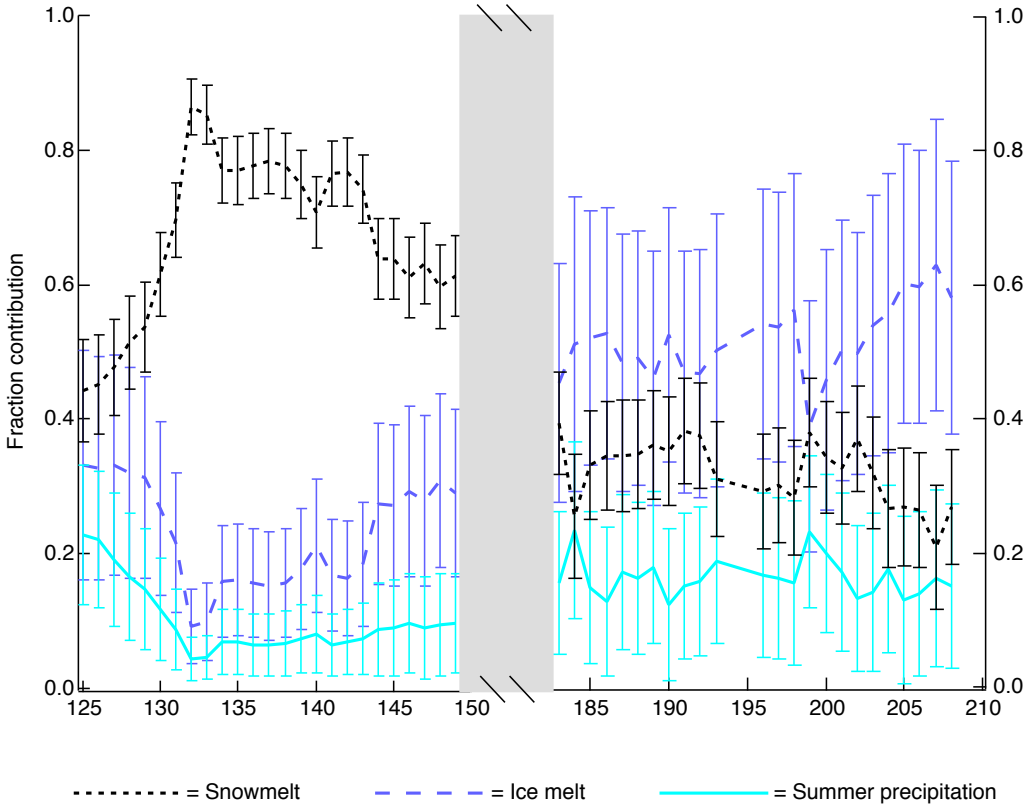

Figure 2.3: Athabasca Glacier meltwater source fraction contribution estimations. Time series graph of the best fi calculated f_S, f_I, and f_R to the main discharge channel of the Athabasca Glacier in May and July 2011. Sampling days where precipitation was observed in the field are presented in Table 2.1.

We calculated the glacial discharge originating from each source using daily *in situ* discharge measurements and the model calculated fractional contributions. While the fraction input from

each melt source shifts drastically from May to July, in the context of the water volume initiating from f_i, f_s and f_r, the difference between melt generated, or water volume being discharged from the Athabasca Glacier, shows that melt contribution volumes were far more significant in July than in May (Table 2.1). Although we assume the fractional contributions were approximately constant throughout the day, we note that discharge measurements were taken in the morning and discharge volumes likely increased with increasing temperature throughout the course of a day. Observations of precipitation at our sampling site (Table 2.1) are in agreement with the major f_r spikes produced by our model (Figure 2.3), confirming that our model is consistent with the physical system. DOY 199 in (Figure 2.3) stands out in that the f_i decreases significantly while the f_s and f_r increase. The spike in f_r is corroborated by our in fi observations of precipitation on that day (Table 2.1) and an increase in f_s is likely due to increased surface melt caused by precipitation. Hence, the ice melt volume may not have decreased but the overall f_i must decrease to encompass the sudden increase in precipitation and f_s.

The prominence of f_i in July indicates that the Athabasca Glacier drainage basin would have a high base flow water discharge available even in the absence of snowmelt. Our calculations are in agreement with the general observation that glacial watersheds are tremendous natural reservoirs that can store and produce freshwater over millennial timescales [*Verbunt et al.,* 2003; *Barnett et al.,* 2005; *Singh and Bengtsson*, 2005; *Thayyen et al*., 2007; *Kehrwald et al.*, 2008; *Fortner et al.,* 2009] whereas snow-only watersheds are typically depleted annually [*Verbunt et al.,* 2003; *Singh and Bengtsson*, 2005; *Thayyen et al.,* 2007; *Liu et al*., 2008; *Stewart,* 2009]. Glacial melt from the Columbia Icefield and the Athabasca Glacier has helped maintain the water balance of many rivers and lakes in Alberta [*Ford et al.,* 1983; *Smart*, 1983; *Falcone*,

2007]. However, if the Athabasca Glacier continues to retreat, it has the potential to become a snow-dominated watershed, which could reduce the water supply by a half and negatively impact the human and biotic communities that rely on a certain base flow water discharge [*Barnett et al.,* 2005].

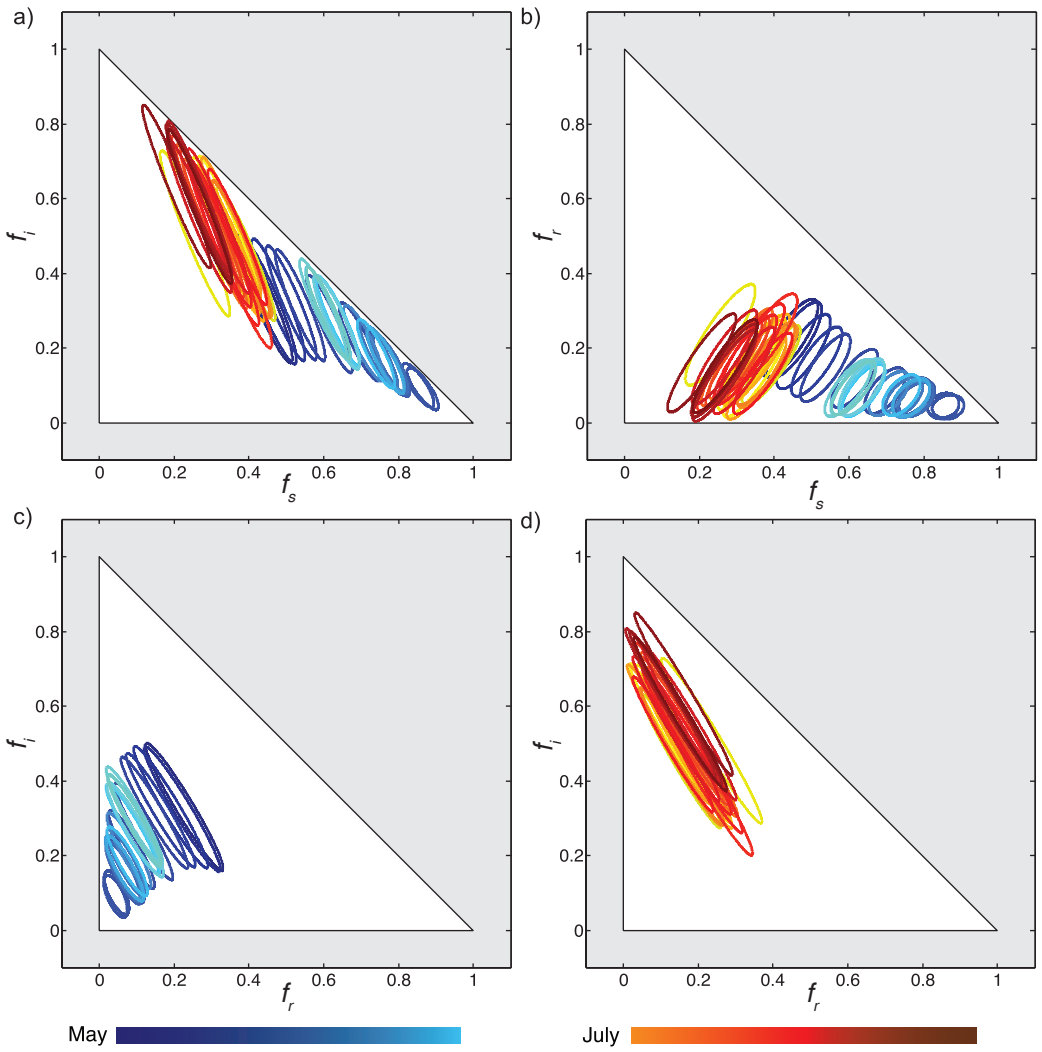

Figure 2.4: Covariance plots of Athabasca Glacier end-member source fraction estimations. The 67% credible ellipses (mean ± 2σ) of multivariate Gaussian PDFs fi to the posteriors of estimated fractional contributions for May and July of 2011. Credible ellipses depict the mean, standard deviations, and covariance of the posteriors (see Figure 2.5 for a graphical comparison of the 67% ellipse and the full posterior corresponding to the 200th day of 2011). Color of the ellipses corresponds to the sample day, with blue to cyan corresponding to days in May and yellow to red corresponding to days in July, depicting early to late in each respective month.

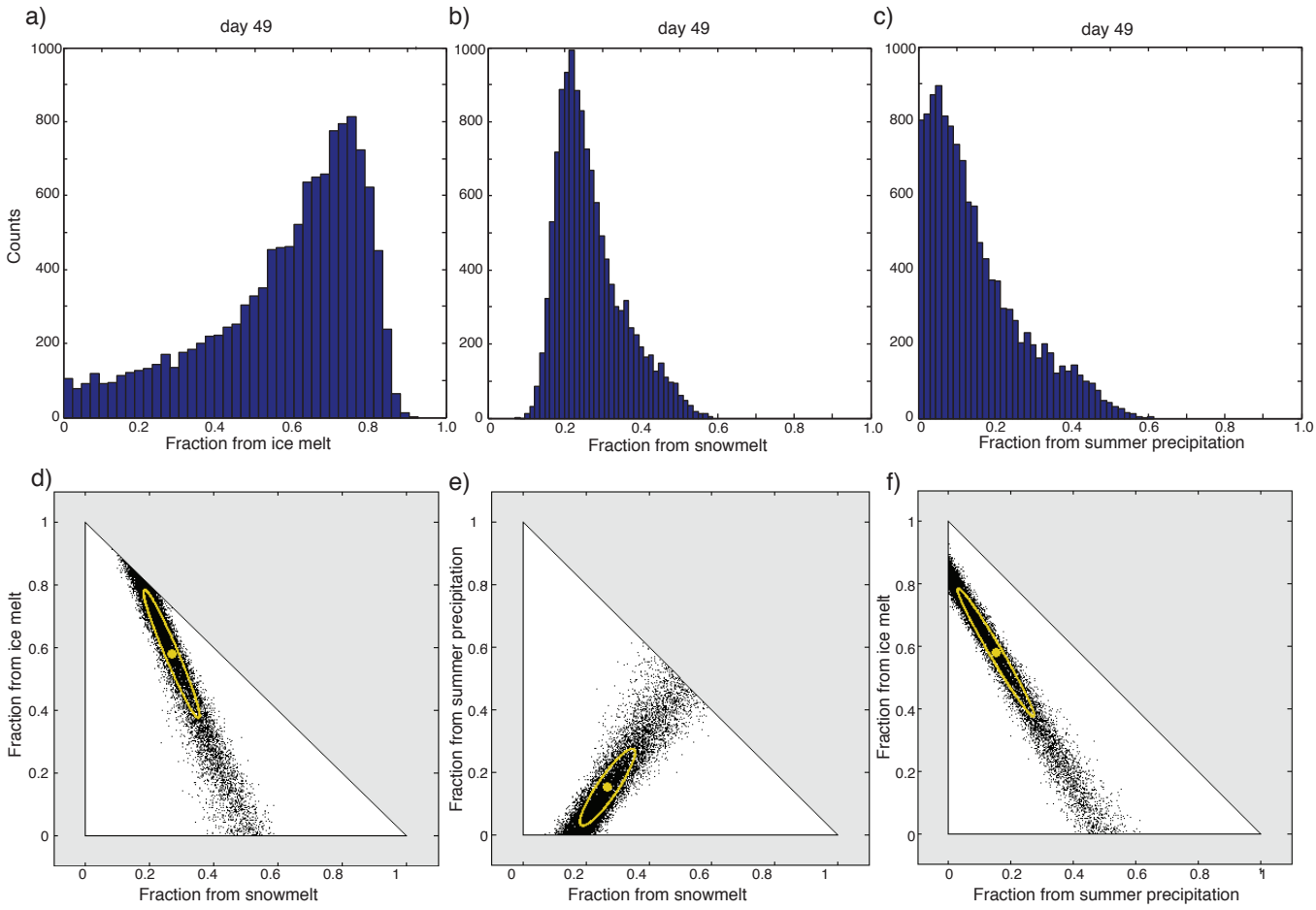

Figure 2.5: Statistical histogram and covariance scatter plots for Athabasca Glacier sample 49. Histogram and covariance plots depicting all solutions generated for sample 49 collected on the 200th day of the year 2011. a-c) Histograms depicting number of generated solutions for different fraction contributions of ice melt, snowmelt and summer precipitation d) Covariance relationship solutions generated for fraction contribution of ice melt and fraction contribution of snowmelt. e) Covariance relationship solutions generated for estimated fraction contribution of snowmelt and fraction contribution of summer precipitation. f) Covariance relationship solutions generated for fraction contribution of summer precipitation and fraction contribution of ice melt. d-f)Yellow dots depict the best mean covariance value of the two end members and the yellow ellipses depict the mean covariance relationship of the two end members at 67% confidence for May and July 2011.

2.2.1.6 Potential caveats

Previous studies have suggested that the $\delta^{18}O$ and δD composition of snowpack can fractionate through time due to equilibrium isotopic exchange between the snowmelt and residual snowpack; observations from the Sierra Nevada snowpack indicate a 3-40 ‰ shift in the $\delta^{18}O$ of

snowmelt per year [*Taylor et al.,* 2001; *Unnikrishna*, 2002]. However, the assigned standard deviations (Table 2.2) encompass a significant portion of this shift and the increase to $\delta^{18}O$ values of – 230 ‰ is likely not due to complete melting of the snowpack given that we observed more than one meter of snow on top of the glacier at the end of May. The difference between the minimum $\delta^{18}O$ values in May and the $\delta^{18}O$ values in the beginning of July is ~40 ‰, which lies within the range of expected fractionation [*Cooper*, 1998] (Table 2.1). Therefore, to the fi order, our model is an accurate representation of source partitioning fluxes from a glacial watershed.

Our model also does not differentiate between contributions of $\delta^{18}O$ and δD at the surface, exposed to evaporation to the atmosphere, and those in the basal environment, exposed to winter refreezing. These processes generally only change the deuterium excess [*Craig*, 1961; *Hooper and Shoemaker,* 1986; *Gat,* 1996], whereas changes in the primary isotopic compositions are within the uncertainties of the end-member values we assumed. Variations in deuterium excess in this glacial environment are likely driven by refreezing of subglacial ice [*Souchez et al.,* 1983, 1984; *Hubbard et al.,* 1995; *Souchez,* 2000], but modeling this process is beyond the scope of the work presented in this paper.

2.2.2 Case Study Two: Quantifying surface versus basal glacial melt using $\delta^{18}O$ and ^{222}Rn from the Greenland Ice Sheet

The Greenland Ice Sheet (GrIS) is the largest ice mass in the Northern Hemisphere, and represents a potentially massive source of meltwater to the world's oceans. Placing constraints on the proportion of different water sources and how they evolve seasonally, would further our understanding of melt dynamics, and thus the GrIS's likely response to global warming. In a

study published in 2011, *Bhatia et al.* collected bulk meltwater from a small land-terminating outlet glacier on the Southwest margin of the GrIS, approximately 125 km south of the well-studied Jakobshavn Isbrae. Samples representing bulk subglacial discharge were collected during the peak melt of 2008 from the primary outflow directly at the margin of the outlet glacier. End-member samples of surface snow, glacial ice, and delayed flow (described below) were collected from surface snow and surface melt ponds, glacial ice samples, and a proglacial stream, respectively. The samples were analyzed for $\delta^{18}O$ and δD in a laboratory and ^{222}Rn was measured *in situ*. These isotopes were ultimately incorporated into a simple linear mixing model based on invariant end-member composition [*Bhatia et al.,* 2011].

The distinct isotopic $\delta^{18}O$ and δD signatures of the end-members in this case study allow for the assessment of bulk water isotopic composition to ascertain fractional contributions from end-members of snow and ice, similar to the methods used in the Athabasca Glacier case study. However, the third isotope used in this case study, ^{222}Rn, is applied primarily to constrain the fractional contribution from the delayed flow component, derived from water melting in the subglacial environment, as both surface snow and glacial ice melted in contact with the atmosphere do not contain detectable amounts of ^{222}Rn. End-member $\delta^{18}O$, δD and ^{222}Rn values can be found in Table 2.4. The bulk composition water $\delta^{18}O$ and ^{222}Rn measurements are plotted with the source end-member $\delta^{18}O$ and ^{222}Rn measurements in Figure 2.6. In this case study we assess the uncertainties associated with fractional contribution estimates using both a two isotope system model and a three isotope system model.

2.2.2.1 Fractional contributions to Greenland Ice Sheet bulk meltwater

In the original study, *Bhatia et al.* [2011] found that the main source contributor to the bulk meltwater samples collected from the GrIS during the onset of melt in the summer of 2008 was delayed flow waters, which composed 0.10–0.70 fractional contribution in May and decreased to 0.04–0.18 in July. In contrast, the glacial ice fractional contributions increased from 0.02–0.70 in May to 0.80 and 0.95 in July, and the surface snow contribution stayed consistently between 0.15 and 0.35 in May, and decreased to less than 0.08 in July.

Bhatia et al. [2011] employed a linear isotope mixing model with invariant end-member compositions, using $\delta^{18}O$, δD and ^{222}Rn, to estimate fractional contributions of surface snow, glacial ice and delayed flow waters to the GrIS melt water. To evaluate these estimates, and associated uncertainties, we input their $\delta^{18}O$, δD and ^{222}Rn into our BMC model. We also explicitly test the decrease in uncertainty associated with increasing the number of constraints by comparing the model with two isotope systems ($\delta^{18}O$ - ^{222}Rn) and three isotope systems ($\delta^{18}O$ - δD - ^{222}Rn). We compare the resulting fractional contribution estimates to the results of *Bhatia et al.* [2011].

Table 2.4: Isotopic end-member values from *Bhatia et al.* [2011] GrIS samples. Uncertainties were assigned at 10% for $\delta^{18}O$ and δD and 25% for ^{222}Rn for this case study.

End-member	$\delta^{18}O$	$\sigma\delta^{18}O$	δD	$\sigma\delta D$	^{222}Rn	$\sigma^{222}Rn$
Surface snow	-12.3	1.2	-89.9	9.0	0.0	0.0
Glacial ice	-28.2	2.8	-216.1	21.6	0.0	0.0
Delayed flow waters	-29.6	3.0	-222.7	22.3	209.5	52.4

In the application of our model to this case study, we assume that these GrIS samples have three possible contribution sources: surface snow, glacial ice, and delayed flow waters. Thus, the sum of the fraction from surface snow (f_{ss}), fraction from glacial ice, (f_g), and fraction from delayed

flow waters (f_d) is constrained to equal one:

$$f_{ss} + f_g + f_d = 1, \tag{6}$$

The likelihood of a model prediction was calculated using

$$L \propto \exp\left[\frac{(\delta^{18}O_p - \delta^{18}O_o)^2}{2\sigma^2_{\delta^{18}O}}\right] \cdot \exp\left[\frac{(^{222}Rn_p - ^{222}Rn_o)^2}{2\sigma^2_{^{222}Rn}}\right], \tag{7}$$

for the two isotope system and

$$L \propto \exp\left[\frac{(\delta^{18}O_p - \delta^{18}O_o)^2}{2\sigma^2_{\delta^{18}O}}\right] \cdot \exp\left[\frac{(\delta D_p - \delta D_o)^2}{2\sigma^2_{\delta D}}\right] \cdot \exp\left[\frac{(^{222}Rn_p - ^{222}Rn_o)^2}{2\sigma^2_{^{222}Rn}}\right], \tag{8}$$

for the three isotope system. Here $\delta^{18}O_p$ and $\delta^{18}O_o$ are the predicted and observed measurements of $\delta^{18}O$, respectively, $\sigma_{\delta^{18}O}$ is the measurement uncertainty, and likewise for δD and ^{222}Rn.

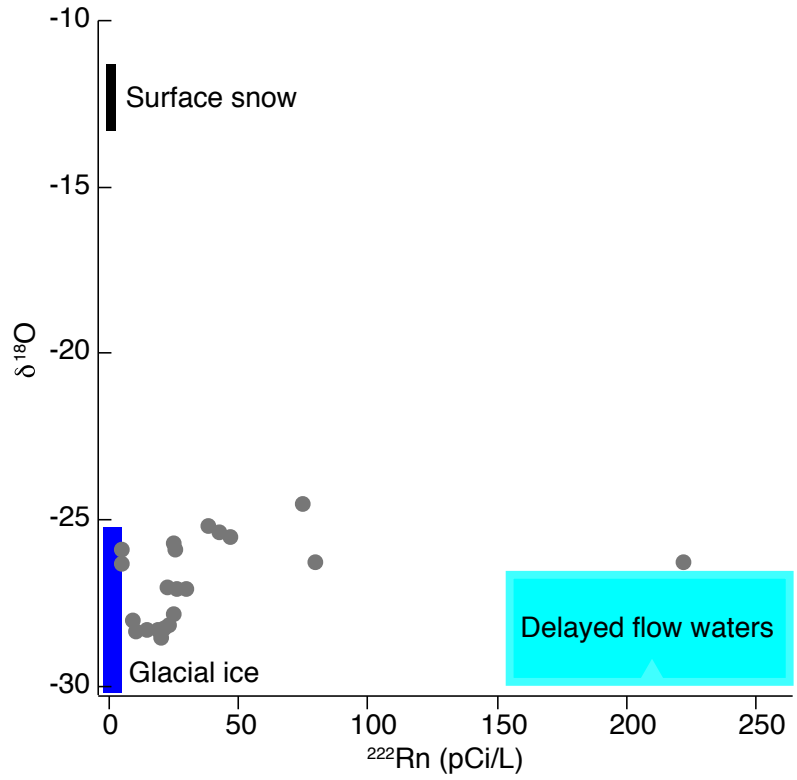

Figure 2.6: Dual isotope plot of end-members and GrIS bulk meltwater samples. $\delta^{18}O$ and ^{222}Rn values of Greenland Ice Sheet bulk water samples for May and July of 2008. Rectangles represent the mean isotopic end-member values and variation in end-member values for surface snow, glacier ice, and delayed flow waters, taken from *Bhatia et al.* [2011]. End-member isotopic compositions and uncertainties can be found in Table 2.4.

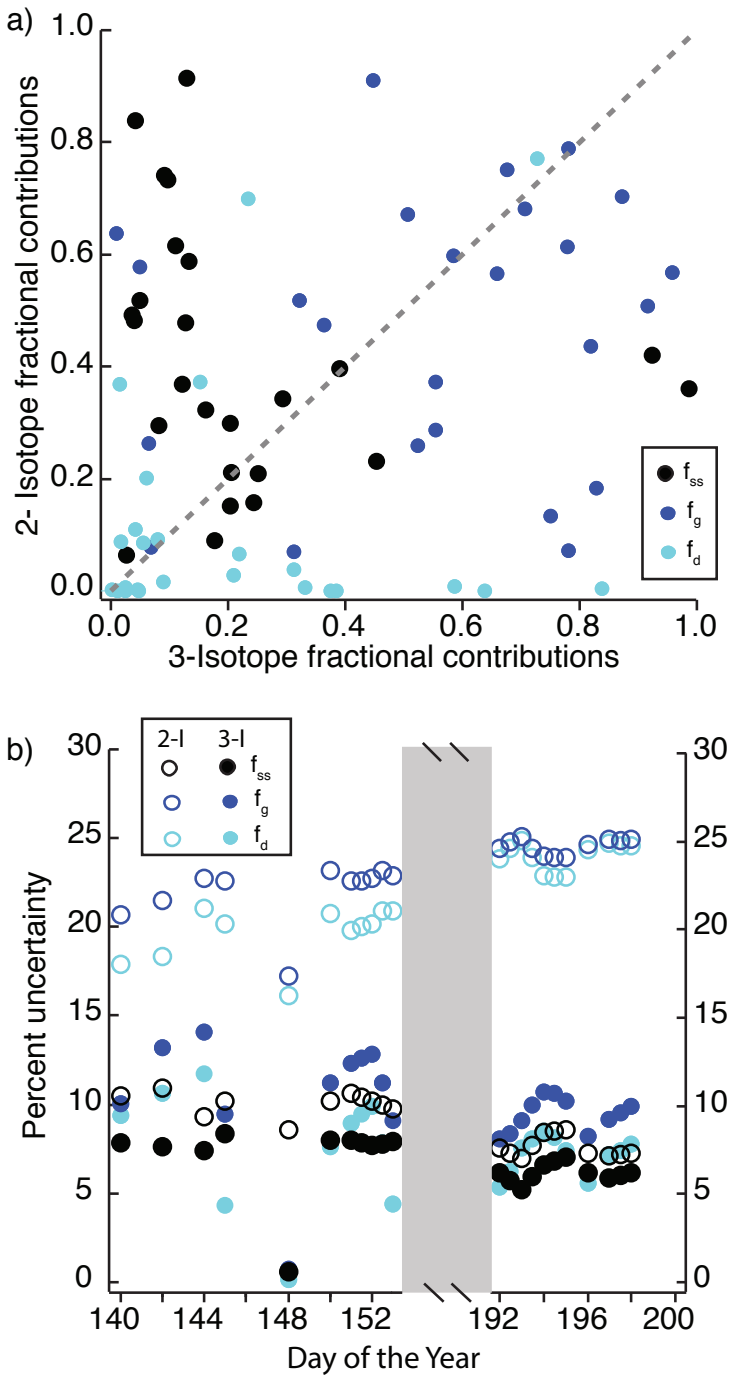

Figure 2.7: GrIS fraction contribution estimations with 2-isotope versus 3-isotope comparison. a) Estimated fraction contributions f_{SS}, f_g and f_d calculated from a two-isotope constrained model (δ^{18}O and ^{222}Rn) plotted against those calculated from a three-isotope model (δ^{18}O, δD and ^{222}Rn). Greenland Ice Sheet bulk water isotopic measurements taken from *Bhatia et al.* [2011]. Dashed grey line represents a one:one ratio of fractional contributions from the two isotope model and three isotope model. b) Calculated uncertainties for the estimated fraction contributions from f_{SS}, f_g and f_d. Open circles denote uncertainties from a model run using only two isotopes, δ^{18}O and ^{222}Rn (2-I). Filled circles denote uncertainties calculated from a model run using all three isotopes (δ^{18}O, δD and ^{222}Rn) (3-I).

Fractional contribution estimations from the application of the BMC model to a two isotope system ($\delta^{18}O$ and ^{222}Rn) are compared to the application of the BMC model to a three isotope system ($\delta^{18}O$, δD and ^{222}Rn) in Figure 2.7a. The applications of the BMC model with different constraints show a systematic bias in the magnitude of contributions coming from each end-member source (Figure 2.7a); in particular, the contribution from surface snow is larger and more variable in the two isotope model than the three isotope model. This difference is likely due to the similarity of the snow and glacial melt samples in ^{222}Rn isotopic space (Figure 2.6). The additional isotope system (δD) separates the snow and glacial contributions in a third dimension. These data suggests that the inclusion of a third isotope increases the accuracy of the model. The introduction of a third isotope system as an additional constraint also increases the precision of the model; uncertainties are lower in all sample calculations for the three isotope model than the two isotope model (Figure 2.7b).

The estimated source fractional contributions from the model in this study, using $\delta^{18}O$, δD and ^{222}Rn to calculate the relative contributions of the end-member sources, are within error of the linear mixing model utilized by *Bhatia et al.* [2011]. A direct comparison of the f_{ss}, f_g and f_d estimations from our BMC model to the fractional contribution predictions from *Bhatia et al.* [2011], with both models utilizing the three isotope system ($\delta^{18}O$, δD and ^{222}Rn), are found in Figure 2.8. The BMC model consistently produced f_{ss} estimations between 0.01 and 0.38, f_g estimations primarily between 0.4 and 0.95 (with a few lower fractional estimations between 0.17 and 0.26), and f_d estimations primarily between 0.07 and 0.37 (with a few estimations between 0.42 and 0.78). Thus, the fractional contributions resulting from our BMC model are in clear agreement with the fractional contributions predicted by *Bhatia et al.* [2011] (Figure 2.8).

The *Bhatia et al.* [2011] model had no explicit calculations of uncertainties for the estimated fractional contributions; the BMC model takes the *Bhatia et al.* [2011] a step further by incorporating the uncertainties of the end-member isotopic compositions, which provides a range for the most likely fractional contributions from each end-member for each sample.

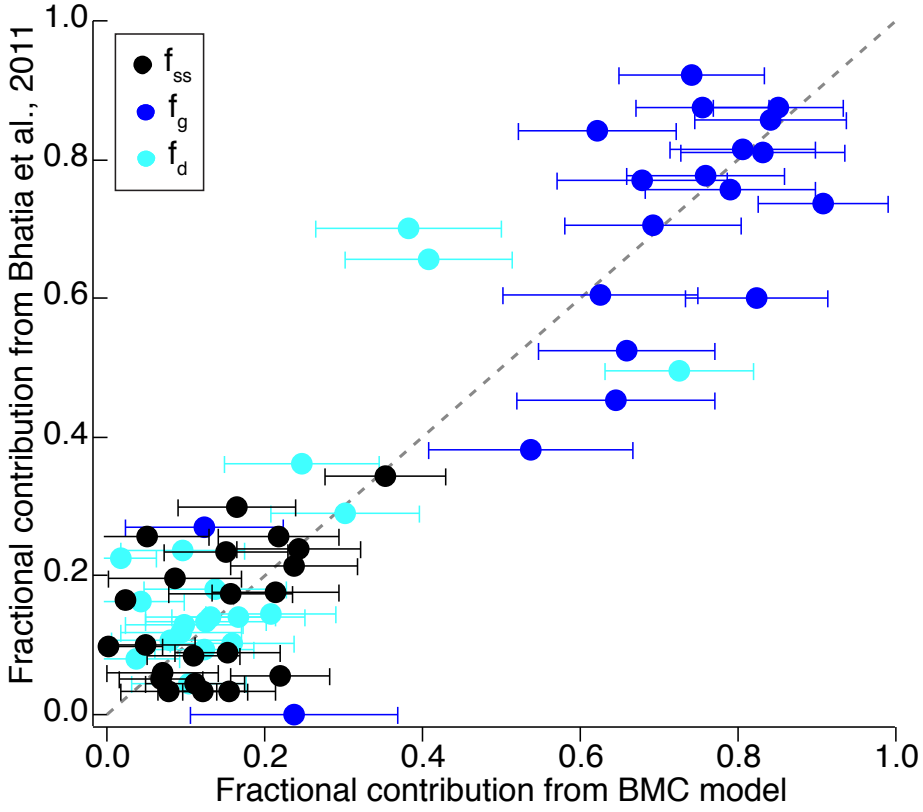

Figure 2.8: Comparison of GrIS contribution estimations from original study and this study: for f_{ss}, f_g and f_d calculated from $\delta^{18}O$, δD and ^{222}Rn values of Greenland Ice Sheet bulk water samples by *Bhatia et al.* [2011] and the three isotope system Bayesian Monte Carlo mixing model from this study. The dashed grey line represents a one to one ratio of fractional contributions from model runs from *Bhatia et al.* [2011] and the BMC model. No error bars are available for the y-axis, but x-axis errors are the uncertainties produced in the BMC model.

2.2.3 Case Study Three: Nutrient sources to Hawaiian soils using ε_{Nd} and $^{87}Sr/^{86}Sr$

In addition to its applications for hydrological and glacial systems, this BMC model can also be applied to radiogenic isotopes as tracers. As an example we examine tropical soils in Hawaii

using radiogenic isotopes ε_{Nd} and $^{87}Sr/^{86}Sr$ to assess the fractional contribution of bedrock, dust and seaspray to this environment. Four depth transect soil samples from Long Substrate Age Gradient (LSAG) cores were analyzed for ε_{Nd} and $^{87}Sr/^{86}Sr$ and quartz abundance by *Kurtz et al.* [2001]. Relative contributions from the Asian dust end-member source were determined for these same samples in *Chadwick et al., (1999)* using a simple model that incorporated major cation measurements. The four cores analyzed by *Kurtz et al.* [2001] were collected from four locations in the Hawaiian Islands with distinct ages: Laupahoehoe, Big Island (20 ka), Kohala, Big Island (150 ka), Molokai (1400 ka) and Kauai (4100 ka).

Measurements of ε_{Nd} and $^{87}Sr/^{86}Sr$ provide isotopic fingerprints for sediment sourced from regions with contrasting lithologic and weathering histories. The three end-members for the isotope system used to describe these Hawaiian soil cores include Asian dust, Hawaiian basalt, and Pacific seawater. The ε_{Nd} and $^{87}Sr/^{86}Sr$ of surface Pacific seawater is known with confidence [*Tanaka et al.,* 2012]. The basalt and dust ε_{Nd} end-member values incorporated into the original model [*Chadwick et al.,* 1999] did not include uncertainties in the end-member compositions: to get more accurate fractional contribution estimates we have incorporated known uncertainties for the ε_{Nd} values of Hawaiian basalt [*Hanano et al.,* 2010] and Asian dust [*Biscaye et al*., 1997]. Thus, we use the same end-member composition values as the original model but have also included a seawater ε_{Nd} value [*Tanaka et al*., 2012; *Kennedy et al*., 1998] and assess the relative errors of the estimations by incorporating uncertainties in the basalt and dust radiogenic compositions.

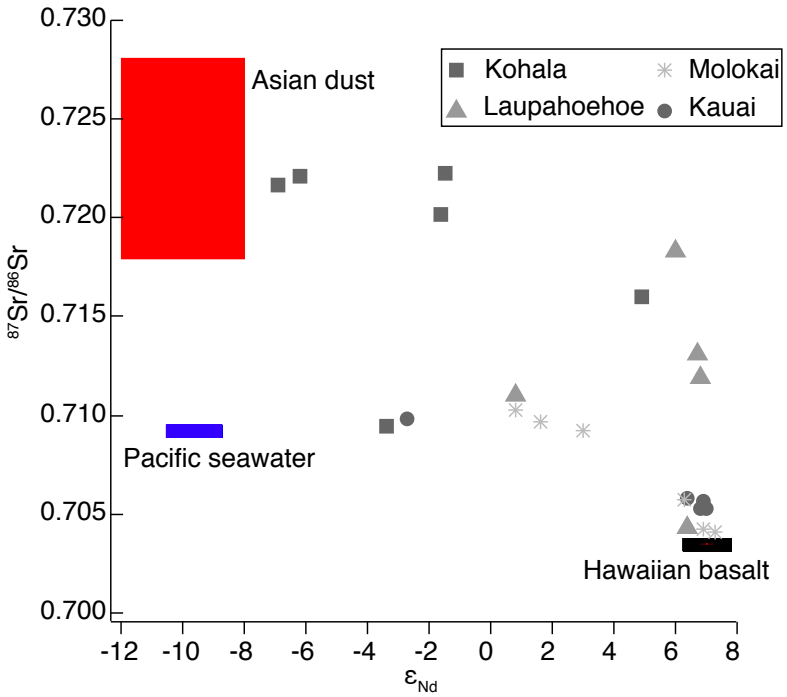

Figure 2.9: Dual isotope plot of end members and Hawaiian soil samples. Plot of ε_{Nd} and $^{87}Sr/^{86}Sr$ values of Hawaiian soil samples taken from *Chadwick et al.* [1999] and *Kurtz et al.* [2001]. Rectangles represent the mean isotopic end member values and variation in end member values for Hawaiian basalt, Asian dust, and Pacific seawater, measurements taken from *Chadwick et al.* [1999], *Kurtz et al.* [2001], and *Tanaka et al.* [2000]. End member isotopic compositions and uncertainties can be found in Table 2.5.

The distinct isotopic compositions of each end-member enable the model to derive source fractional contributions at varying soil depths. End-member ε_{Nd} and $^{87}Sr/^{86}Sr$ values can be found in (Table 2.5). The bulk composition soil ε_{Nd} and $^{87}Sr/^{86}Sr$ measurements are plotted with the source end-member ε_{Nd} and $^{87}Sr/^{86}Sr$ measurements in Figure 2.9.

Table 2.5: Isotopic end-member values from *Chadwick et al.* [1999]. The ε_{Nd} and $\sigma\varepsilon_{Nd}$ of Pacific seawater values are from *Tanaka et al.* [2000]. The $\sigma\varepsilon_{Nd}$ values for Asian dust and Hawaiian basalt have been incorporated from previous publications [*Biscaye*, et al., 1997; *Hanano*, et al., 2010].

End-member	ε_{Nd}	$\sigma\varepsilon_{Nd}$	$^{87}Sr/^{86}Sr$	$\sigma^{87}Sr/^{86}Sr$
Basalt	7	0.7	0.7035	0.0002
Dust	-10	1.2	0.7210	0.0035
Seawater	-9.6	0.9	0.7092	0.0001

2.2.3.1. Fractional contribution to Hawaiian soils

The fractional contributions of Asian dust to the Hawaiian soil core samples estimated by *Chadwick et al.* [1999] were determined using measurements of Th, Er, quartz, and Nd, and ranged between 0.01 to 0.87 fractional contribution estimations for all samples collected. *Chadwick et al.* [1999] did not break up the dust fractional contribution estimates based on location or depth, but rather combined all dust fractional contribution estimations into one plot. The original study investigated major cations compared to the age of the samples to find evidence that these end-member sources were present amongst all samples collected, but did not explicitly calculate Pacific seawater contributions. Our model was applied to the ε_{Nd} and $^{87}Sr/^{86}Sr$ measurements from the same Hawaiian soil core samples investigated in *Chadwick et al.* [1999] with the ε_{Nd} and $^{87}Sr/^{86}Sr$ of these samples published in *Kurtz et al.* [2001]. In this study, we estimate the fractional contribution of all three source end-members within each of the four sample locations independently, and compare the Asian dust fractional contributions calculated from our model to the ranges found in *Chadwick et al.* [1999].

In the application of our model to this case study, we assume that the Hawaiian soil samples have three possible contribution sources: Hawaiian basalt, Asian dust, and Pacific seawater. Thus, the sum of the fraction from basalt (f_b), fraction from dust, (f_{du}), and fraction from seawater (f_{sw}) is constrained to equal one:

$$f_b + f_{du} + f_{sw} = 1, \tag{9}$$

The likelihood of a model prediction was calculated using

$$L \propto \exp\left[\frac{(\epsilon\mathrm{Nd}_p - \epsilon\mathrm{Nd}_o)^2}{2\sigma^2_{\epsilon\mathrm{Nd}}}\right] \cdot \exp\left[\frac{\left({}^{87}\mathrm{Sr}/{}^{86}\mathrm{Sr}_p - {}^{87}\mathrm{Sr}/{}^{86}\mathrm{Sr}_o\right)^2}{2\sigma^2_{{}^{87}\mathrm{Sr}/{}^{86}\mathrm{Sr}}}\right], \tag{10}$$

where εNd_p and εNd_o are the predicted and observed measurements of $\varepsilon_{Nd,}$ respectively, $\sigma\varepsilon_{Nd}$ is the measurement uncertainty for $^{87}Sr/^{86}Sr$. The calculated soil source fractional contributions from our BMC model are presented in Figure 2.10. Estimated fractional contributions and uncertainties from the application of our model to the ε_{Nd} and $^{87}Sr/^{86}Sr$ measurements from these HI soil cores can be found in Table 2.5. The Laupahoehoe and Molokai soil depth transects followed similar trends with basalt as the dominant source contributor, consistently ranging from 0.60 - 0.97. Asian dust was the next largest contributor with a strong presence in the initial surface depths of 0.30 - 0.40, decreasing to fractional contributions of less than 0.15 as the depth of the transect increased. Pacific seawater composed the smallest source contributor, remaining less than 0.06 throughout both the Lapahoehoe and Molokai transects.

The Kohala core estimations produced the only fractional contribution trends in which the Asian dust was the dominant source contribution for the majority of the transect, and where the Pacific seawater component was the strongest signal at the surface. Surface measurements indicated a basalt fractional contribution of 0.34, a dust fractional contribution of 0.02, and a high seawater contribution of 0.64. With increasing depth, the Pacific seawater component became the smallest source contributor remaining at fractional contribution values of less than 0.04 throughout the rest of the transect. With increasing depth, the Asian dust component became the dominant source contributor throughout the middle depths of the transect with fractional contribution values of 0.61 - 0.94 before decreasing to 0.18 at 60 cm depth. The basalt component initially decreased with depth, with fractional contribution values of less than 0.06 for the middle segment of the transect before increasing with depth to become the dominant fractional contribution of 0.81 at 60 cm depth.

The Kauai core estimations placed the basalt and seawater components at roughly equal fractional contributions at the surface of 0.41. With increasing depth, the seawater component decreased to fractional contribution values of less than 0.07 while the basalt component increased to fractional contribution values of more than 0.9 for the remaining depth of the transect. The dust component in the Kauai core composed a fractional contribution of 0.18 at the surface and remained between values of 0.05 and 0.09 through the final depth measured. A potential reason that the Kohala and Kauai samples display notable amounts of Pacific seawater contributions near the surface is that these two locations are situated in the northwest of their respective islands, which corresponds to the wind trajectory and may be cause for an elevated seawater component.

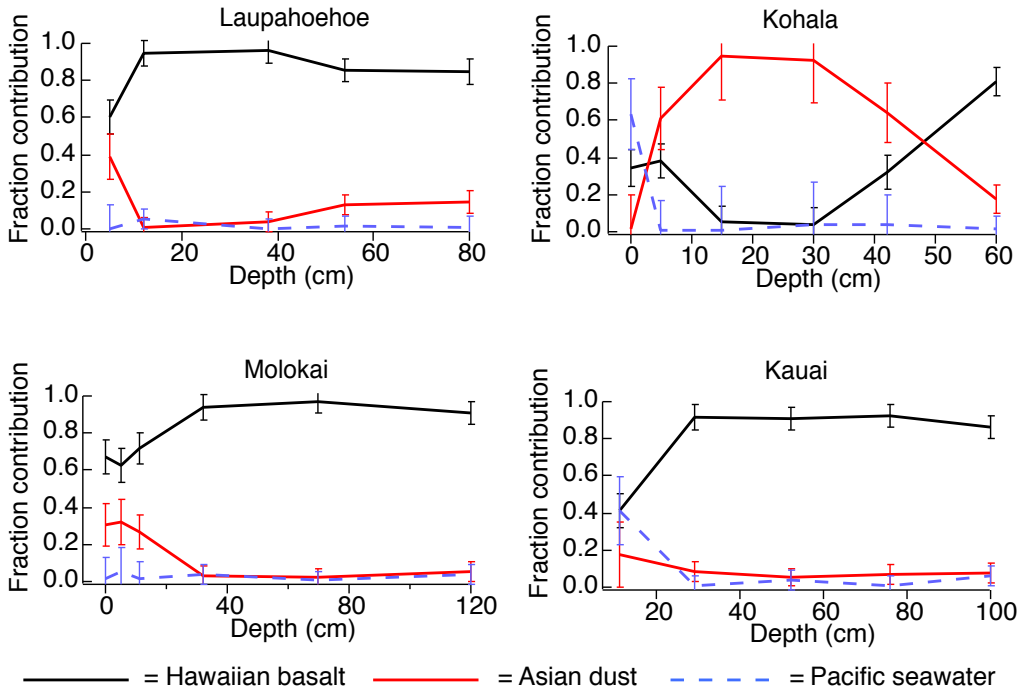

Figure 2.10: Source fraction contribution estimations for Hawaiian soil samples. Fractional contributions, f_b, f_{du} and f_{sw}, to Hawaiian soil transects using the BMC model, end-member compositions as indicated in Figure 2.9, and ε_{Nd} and $^{87}Sr/^{86}Sr$ measurements of samples described in *Chadwick et al.* [1999] and *Kurtz et al.* [2001].

Even with error bars (encompassing all uncertainties in these Hawaiian soil fractional contribution estimations of Hawaiian basalt, Asian dust, and Pacific seawater) the transect fractional contribution trends are distinct between sources and locations (Figure 2.10). The estimated Asian dust fractional contributions from the model in this study, using only ε_{Nd} and $^{87}Sr/^{86}Sr$ to calculate the relative contributions of the end-member sources, are within error of the original Asian dust fractional contribution estimations from the mixing model utilized in *Chadwick et al.* [1999]. The BMC implementation provides two additions: (1) a calculation of the fractional contribution of seaspray to the soil budget and (2) uncertainty in the calculated fractions.

2.2.4 MODEL LIMITATIONS

In assuming that the bulk samples are derived from only three possible sources in all three case studies, we limit the complexity of the system. Possible sources of error in our BMC model may arise from our assumption that the end-member values do not covary, as compared to end-members in *Cable et al.,* [2011]. We observed no physical evidence to suggest a covariance between isotopic compositions from the three different melt sources at the Athabasca Glacier, and the original GrIS melt and Hawaiian soil publications did not indicate the existence of such processes. Thus, we chose not to represent such relationships in our case studies.

For the Athabasca Glacier and GrIS case studies, the end-member uncertainties do not incorporate temporal changes in end-member values. Specifically, in the case of the GrIS case study, ^{222}Rn values for delayed flow waters likely exhibit temporal variations, due to variations in the residence time of subglacial water [*Arendt et al*., In Review, EPSL] that are not accounted

for in the initial model. The division of the delayed flow end-member into two separate end-members (fast-flow and slow-flow) would place constraints on variations in ^{222}Rn values that originated from temporal disparities and provide a more detailed quantification of relative contributions. A potential additional uncertainty constraint that could be incorporated into both the Athabasca Glacier and GrIS case studies would be to utilize the deuterium excess.

Using the linear multi-component Bayesian Monte Carlo mixing model presented in this study, estimations of fractional contributions from sources are more precise if end-member compositions are distinct from one another. In analyzing the end-member compositions from the Greenland Ice Sheet case study (Figure 2.6), it is apparent that the surface snow, glacial ice and delayed flow water isotopic compositions overlap with one another. This overlap is likely the main source of uncertainty observed in our fractional contribution estimates (Figure 2.8). The uncertainties associated with the estimated fractional contributions decrease with the degree to which the end-member isotopic compositions are distinguishable from one another. The end-member isotopic compositions for the Athabasca Glacier and Hawaiian soil case studies are notably distinct (Table 2.2 and Table 2.5; Figures 2.2 and 2.8), causing the degree of uncertainty in the fractional contribution estimates to be low (Figures 2.3 and 2.9).

2.2.5 BROADER IMPLICATIONS

The multi-component linear BMC mixing model presented in this study is shown to be widely applicable to numerous Earth surface systems and can be extended to systems beyond soil nutrients and melt contributions in glacial environments (i.e. dust provenance records, water mass mixing, and ecological systems). The model is capable of accounting for both prior

information and assumptions of a given system. This open source linear isotopic mixing BMC model is applicable to many environments because it allows for the addition of end-members, further constraints and isotopic systems, and the incorporation of large uncertainties in end-member values. End-member isotopic compositions can encapsulate both spatial and temporal variation in their assigned standard deviation values, which can be critical in certain types of case studies (i.e. alpine glacier, time series samples, etc...). Furthermore, understanding how well these estimated fractional contribution values are known (estimation of uncertainty) allows for a more complete representation of a system. Because the coding for this multi-component linear BMC mixing model is supplied in the Appendix, it can be readily adapted to both new and existing datasets to infer source contributions in Earth surface systems.

2.3 CONCLUSIONS

This study has validated the relevance and applicability of our linear multi-component BMC mixing model to derive contribution fractions in Earth surface systems with source end-members that have distinct isotopic signatures. The application of our model to a new dataset from the Athabasca Glacier resulted in statistically significant fractional contribution estimates that followed expected seasonal trends for alpine glacier melt evolution [*Cable et al*., 2011; *Hindshaw et al*., 2011]. The application of our model to two additional case studies in differing locations using diverse isotope systems resulted in fractional contributions comparable to those calculated in their initial publications [*Kennedy et al*., 1998; *Chadwick et al*., 1999; *Kurtz et al*., 2001; *Chadwick et al*., 2009; *Bhatia et al*., 2011]. The addition of a third isotopic system in the Greenland Ice Sheet case study resulted in decreased uncertainty of the fractional contribution estimations by placing additional constraints on the most likely fractional contributions that are unaccounted for in a two isotope system. The Matlab script presented here is straightforward for

users to modify the priors of the end-member isotopic compositions. For instance, inclusions of different analytic or empirical PDFs, correlations in compositions, or more complex variability in the isotopic compositions can be modified into the script. However, these modifications should be done on a case-by-case basis based on physical observations of the Earth surface system of interest. Thus, the BMC estimation strategy supplied here can be used to effectively generate solutions and associated uncertainties for mass partitioning of distinct input end-members from bulk samples in a variety of Earth surface systems and is easily accessible to a diverse range of scientific applications.

Appendix A: Matlab BMC Coding

2.4. REFERENCES

Aizen, V. B., *et al*., (2005), Stable-isotope time series and precipitation origin from fi and snow samples, Altai glaciers, Siberia, *Journal of Glaciology*, *51* (175), 637–654.

Arendt, C. A., *et al*., (In Review), Uranium-series isotopes confirm prolonged residence time of subglacial water, *Geochimica et Cosmochimica Acta*.

Barber, R. W., and M. J. Wearing (2001), *Water Resource Management*, vol. 4, chap. A mathematical model for estimating the pollution exchange coefficient of small tidal embayments, pp. 331–340, WIT Press.

Barnett, T. P., *et al*., (2005), Potential impacts of a warming climate on water availability in snow-dominated regions, *Nature*, *438* (7066), 303–309, doi: 10.1038/nature04, 141.

Bhatia, M. P., *et al*., (2011), Seasonal evolution of water contributions to discharge from a Greenland outlet glacier: insight from a new isotope-mixing model, *Journal of Glaciology*, *57* (205), doi: 10.3189/002214311798043,861.

Biscaye, P. E., *et al*., (1997), Asian provenance of glacial dust (stage 2) in the Greenland Ice Sheet Project 2 Ice Core, Summit, Greenland, *Journal of Geophysical Research*, *102* (C12), 26,765–26,781, doi: 10.1029/97JC01,249.

Brugmann, M. N., and Demuth, M., (1994), Surface and basal topography of the Athabasca Glacier: a glaciological interpretation and recommendation for the location of near-ice interpretive facilities., *National Hydrology Research Institute Contract Report, Jasper National Park.*, National Hydrology Research Institute, Saskatoon.

Butler, D. (1980), Shallow core snow chemistry of Athabasca Glacier, Alberta., *Journal of Earth Sciences*, *17*, 278–281, doi: 10.1139/e80–024.

Cable, J., *et a*l., (2011), Contribution of glacier meltwater to streamflow in the Wind River Range, Wyoming, inferred via a Bayesian mixing model applied to isotopic measurements, *Hydrological Processes*, *25* (14), 2228–2236, doi: 10.1002/hyp.7982.

Canada National Climate Archive (2013), National climate data and information archive, *Technical report*, National Climatic Data Center.

Chadwick, O. A., *et al.,* (1999), Changing sources of nutrients during four million years of ecosystem development, *Nature*, *397*, 491–497, doi: 10.1038/17,276.

Chadwick, O. A., *et al*., (2009), Changing sources of strontium to soils and ecosystems across the Hawaiian Islands, *Chemical Geology*, *267*, 64–76, doi: 10.1016/j.chemgeo.2009.01.009.

Clark, I., and P. Fritz (1997), *Environmental isotopes in hydrogeology*, 1-331 pp., CRC Press LLC, Boca Raton, ISBN 9781566702492.

Cooper (1998), *Isotope fractionation in snowcover*, chap. 4, 1, Elsevier Science.

Craig, H. (1961), Isotopic variations in meteoric waters, *Science*, *133* (3465), 1702–1703, doi: 10.1126/science.133.3465.1702.

Dansgaard, W. (1964), Stable isotopes in precipitation, *Tellus*, *16* (4), 436–468, doi: 10.1111/j.2153–3490.1964.tb00,181.x.

Falcone, M. D. (2007), Assessing hydrological processes controlling the water balance of lakes in the Peace-Athabasca Delta, Alberta, Canada using water isotope tracers, Ph.D. thesis, University of Waterloo.

Ford, D. C., *et al*., (1983), The physiography and speleogenesis of Castleguard Cave, Columbia Icefields, Alberta, Canada, *Arctic and Alpine Research*, *15* (4), 437–450, doi:

10.2307/1551,231.
Fortner, S. K., *et al*., (2009), Trace element and major ion concentrations and dynamics in glacier snow and melt: Eliot Glacier, Oregon Cascades, *Hydrological Processes*, *23*, 2987–2996, doi: 10.1002/hyp.7418.
Gat, J. R. (1996), Oxygen and hydrogen isotopes in the hydrologic cycle, *Annual Reviews in Earth and Planetary Sciences*, *24* (1), 225–262, doi: 10.1146/annurev.earth.24.1.225.
Grupe, G. (2014), Application of isotopic mixing models for palaeodietary and paleoecological studies, *Anthropology Anzeiger*, *71*, 21–39, doi: 10.1127/0003–5548/2014/0375.
Hanano, D. W., *et al*., (2010), Horizontal and vertical zoning of heterogeneities in the Hawaiian mantle plume from the geochemistry of consecutive postshield volcano pairs: Kohala-Mahukona and Mauna Kea–Hualalai, *Geochemistry, Geophysics, Geosystems*, *11*, Q01,004, doi: 10.1029/2009GC002,782.
Hart, J. K. (2006), Athabasca Glacier, Canada - a field example of subglacial ice and till erosion?, *Earth Surface Processes*, *31*, 65–80, doi: 10.1002/esp.1233.
Hindshaw, R. S., *et al*., (2011), Hydrological control of stream water chemistry in a glacial catchment (Damma Glacier, Switzerland), *Chemical Geology*, *285*, 215–230, doi: 10.1016/j.chemgeo.2011.04.012.
Hooper, R. P., and C. A. Shoemaker (1986), A comparison of chemical and isotopic hydrograph separation, *Water Resources Research*, *22* (10), 1444–1454, doi: 10.1029/WR022i010p01,444.
Hubbard, B. P., *et al*., (1995), Borehole water level variations and the structure of the subglacial hydrological system of Haut Glacier d'Arolla, Valais, Switzerland., *Journal of Glaciology*, *41*, 572–583.
Kehrwald, N., *et al*., (2008), Mass loss on Himalayan glacier endangers water resources, *Geophysical Research Letters*, *35* (22), 1–6, doi: 10.1029/2008GL035,556.
Kennedy, M. J., *et al*., (1998), Changing sources of base cations during ecosystem development, Hawaiian Islands, *Geology*, *26* (11), 1015–1018, doi: 10.1130/0091–7613(1998)026¡1015:CSOBCD¿2.3.CO;2.
Kurtz, A. C., *et al*., (2001), Accretion of Asian dust to Hawaiian soils: Isotopic, elemental, and mineral mass balances, *Geochimica et Cosmochimica Acta.*, *65* (12), 1971–1983, doi: 10.1016/S0016–7037(01)00,575–0.
Letreguilly, A. (1988), Relation between the mass balance of western Canadian mountain glaciers and meteorological data, *Journal of Glaciology*, *34* (116), 11–18, doi: 10.1029/ 2007GL030,780.
Liu, F. J., I., (2008), Streamflow generation from snowmelt in semi-arid, seasonally snow-covered, forested catchments, Valles Caldera, New Mexico, *Water Resources Research*, *44* (12), doi: 10.1029/2007WR006,728.
McCluney, K. E., and J. L. Sabo (2010), Tracing water sources of terrestrial animal populations with stable isotopes: laboratory tests with crickets and spiders, *Plos One*, *5* (12), doi: 10.1371/journal.pone.0015,696.
Moore, J. W., and B. X. Semmens (2008), Incorporating uncertainty and prior information into stable isotope mixing models, *Ecology Letters*, *11* (5), 470–480, doi: 10.1111/j.1461– 0248.2008.01,163.x.
Morlock, S. E., *et al.,* (2002), Feasibility of acoustic doppler velocity meters for the production of discharge records from U.S. Geological Survey streamflow-gaging

stations, *Water-resources investigations report 01-4157*, USGS.
Mosegaard, K., and A. Tarantola (1995), Monte Carlo sampling of solutions to inverse problems, *Journal of Geophysical Research*, *100*, 12,431–12,447, doi: 10.1029/94JB03,097.
Ogle, K., *et al*., (2004), Reconstructing plant root area and water uptake profiles, *Ecology*, *85* (7), 1967–1978, doi: 10.1890/03–0346.
Parnell, A., D. Phillips, S. Bearhop, B. Semmens, E. Ward, J. Moore, A. Jackson, J. Grey, D. Kelly, and R. Inger (2013), Bayesian stable isotope mixing models, *Environmetrics*, *24* (6), 387–399, doi: 10.1002/env.2221.
Parnell, A. C., *et al*., (2010), Source partitioning using stable isotopes: Coping with too much variation, *Plos One*, *5* (3), doi: 10.1371/journal.pone.0009,672.
Petit, J. R., *et al*., (1999), Climate and atmospheric history of the past 420,000 years from the Vostok ice core, Antarctica, *Nature*, *399*, 429–436, doi: 10.1038/20,859.
Pichler, T. (2005), Stable and radiogenic isotopes as tracers for the origin, mixing, and subsurface history of fluids in submarine shallow-water hydrothermal systems, *Journal of Volcanology and Geothermal Research*, *139* (3-4), 211–226, doi: 10.1016/j.jvolgeores.2004.08.007.
Rickli, J., *et al*., 2010), Hafnium and neodymium isotopes in surface waters of the eastern Atlantic Ocean: Implications for sources and inputs of trace metals to the ocean, *Geochimica et Cosmochimica Acta*, *74*, 540–557, doi: 10.1016/j.gca.2009.10.006.
Sharp, M., *et al*., (1995), Comments on the use of chemically based mixing models in glacier hydrology, *Journal of Glaciology*, *41* (138), 241–246.
Shea, J. M., and S. J. Marshall (2007), Atmospheric flow indices, regional climate, and glacier mass balance in the Canadian Rocky Mountains, *International Journal of Climatology*, *27* (2), 233–247, doi: 10.1002/joc.1398.
Singh, B. P. (2013), Isotopic composition of water in precipitation in a region or place, *Applied Radiation and Isotopes*, *75*, 22–25, doi: 10.1016/j.apradiso.2013.01.013.
Singh, P., and L. Bengtsson (2005), Impact of warmer climate on melt and evaporation for the rainfed, snowfed and glacierfed basins in the Himalayan region, *Journal of Hydrology*, *300* (1-4), 140–154, doi: 10.1016/j.jhydrol.2004.06.005.
Smart, C. C. (1983), The hydrology of Castleguard Karst, Columbia Icefields, Alberta, Canada, *Arctic and Alpine Research*, *15* (4), 471–486.
Socki, R. A., *et al.,* (1992), Extraction technique for the determination of O-18 in water using preevacuated glass vials, *Analytical Chemistry*, *64* (7), 829–831, doi: 10.1021/ac00,031a026.
Souchez, R. (1984), On the isotopic composition in delta-D and delta-O-18 of water and ice during freezing, *Journal of Glaciology*, *30* (106), 369–372.
Souchez, R. (2000), Basal ice formation and deformation in central Greenland: a review of existing and new ice core data, *Geological Society: Special Publications*, *176* (0305-8719), 13–22, doi: 10.1144/GSL.SP.2000.176.01.02.
Souchez, R., *et al.,* (1983), Reconstruction of basal boundary conditions at the Greenland Ice Sheet margin from gas composition in the ice, *Earth and Planetary Science Letters*, *118* (1-4), 327–333, doi: 10.1016/0012–821X(93)90,176–A.
Soulsby, C., *et al*., (2003), Identifying and assessing uncertainty in hydrological pathways: a novel approach to end member mixing in a Scottish agricultural catchment, *Journal of Hydrology*, *274* (1-4), 109–128, doi: 10.1016/S0022–1694(02)00,398–0.

Stewart, I. T. (2009), Changes in snowpack and snowmelt runoff for key mountain regions, *Hydrological Processes*, *23* (1), 78–94, doi: 10.1002/hyp.7128.

Tanaka, T., *et al*., (2012), JNdi-1: a neodymium isotopic reference in consistency with LaJolla neodymium, *Chemical Geology*, *168*, 279–281, doi: 10.1016/S0009–2541(00)00,198–4.

Taylor, S., *et al*., (2001), Isotopic evolution of a seasonal snowpack and its melt, *Water Resources Research*, *37* (3), 759–769, doi: 10.1029/2000WR900,341.

Thayyen, R. J. *et al.,* (2007), Role of glaciers and snow cover on headwater river hydrology in monsoon regime - Micro-scale study of Din Gad catchment, Garhwal Himalaya, India, *Current Science*, *92* (3), 376–382.

Theakstone, W. H. (2003), Oxygen isotopes in glacier-river water, Austre Okstindbreen, Norway, Master's thesis, University of Manchester.

Unnikrishna, P. (2002), Isotope variations in a Sierra Nevada snowpack and their relation to meltwater, *Journal of Hydrology*, *260*, 38–57, doi: 10.1016/S0022–1694(01)00,596–0.

Verbunt, M., *et al*., (2003), The hydrological role of snow and glaciers in alpine river basins and their distributed modeling, *Journal of Hydrology*, *282* (1-4), 36–55, doi: 10.1016/S0022– 1694(03)00,251–8.

Wikle, C. K. (2003), Hierarchical models in environmental science, *International Statistical Review*, *71* (2), 181–199, doi: 10.1111/j.1751–5823.2003.tb00,192.x.

CHAPTER III

Uranium-series isotopes confirm prolonged residence time of subglacial water

Official citation:

Arendt, C.A., Aciego, S. M., Sims, K.W.W., and Aarons, S.M., 2015. AUranium-series isotopes confirm prolonged residence time of subglacial water. Geochimica et Cosmochimica Acta. *In Review.*
Reproduced within author's rights.

ABSTRACT

Here we report radiometric dating of subglacial water using a combination of U-series isotopes in meltwater from the Athabasca Glacier, Canada. We obtained residence time values for twenty-six bulk meltwater samples collected at the glacier terminus analyzed for ^{238}U, ^{234}U, ^{222}Rn and $(^{234}U/^{238}U)_{activity}$ in addition to traditional glacial hydrochemistry parameters: conductivity, alkalinity, pH and major element composition. Subglacial meltwater varied in [^{238}U] and (^{222}Rn) from 23 to 832 ppt and 9 to 171 pCi/L, respectively. Activity ratios of ($^{234}U/^{238}U$) ranged from 1.003 to 1.040, with the highest activity in early May when delayed-flow basal meltwater composed a significant portion of the bulk melt. The calculated subglacial residence time averages range from 30 years in early May, decreasing to ~ 1 year over the course of the melt season. The decrease in residence time over the melt season is consistent with prior field studies and model-predicted channel switching from slow to fast flow. However, the radiometric residence times in this study are larger than values generated by current subglacial hydrology

models and suggest that the average residence time of subglacial water is several orders of magnitude greater than minimum residence time estimates from dye-trace studies.

3.1. INTRODUCTION

Glacial hydrology – water storage, transport and fluxes – is fundamental to ice dynamics, glacier induced floods, and the prediction of runoff chemistry from ice-covered drainage basins. While glacial hydrology research has focused extensively on temporal variations in physical and chemical parameters (Anderson et al., 2004; Behrens, 1975; Collins, 1982; Fountain and Walder, 1998; Hubbard and Nienow, 1997; Mitchell and Brown, 2007; Naftz et al., 2002; Schuler, 2002; Smith et al., 2001; Verbunt et al., 2003; Walder, 1982) there are no chemical or physical tracers that directly measure meltwater storage time at the ice-rock interface.

Current quantitative calculations of subglacial residence times are largely based on reservoir models, which assume a linear relationship between water volume stored and water discharged (Cuffey and Paterson, 2010; Hannah and Gurnell, 2001). These models and their subsequent residence time calculations have been aimed at predicting runoff, while differences between the supraglacial, englacial, and subglacial reservoir ages have not been explicitly calculated. Model-calculated minimum residence time estimates for combined englacial-subglacial reservoirs vary from hours to days in alpine glaciers (Baker, 1982; Murray and Clarke, 1995; Schuler, 2002). Similarly, dye-tracing studies indicate that the transport time between a draining moulin and exit at the glacial terminus can last less than an hour (Behrens, 1975; Collins, 1982). Dye-trace studies provide transit time and dispersion information, but gaining information on the residence time of subglacial water from these studies is complicated because complete dye loss, partial

recovery, and the mixing of water with varying transit times can lead to residence time estimates that do not account for the slow-flow component of the subglacial system (Chandler, 2013; Hooke, 1994; Hubbard and Nienow, 1997; Kamb, 1985). Hence, these results obtained from dye-tracing studies represent the absolute minimum time required for water to be discharged from input at the surface to output at a glacial terminus: partial, or incomplete, dye-recovery indicates that the dye that is unaccounted for is stored for longer periods of time in the subglacial system. However, geophysical models that combine extensive calibration of glacier specific physical parameters and information from dye-trace studies have been used to accurately simulate glacial hydrology and hydrological responses (Arnold et al., 1998; Flowers and Clarke, 2002a, b).

Given the importance of residence time of water in the subglacial environment to solute chemistry (Brown, 2002; Fairchild et al., 1998; Wadham et al., 2000), ice dynamics (Collins, 1979; Creyts and Schoof, 2009; Raymond, 1995), potentially seawater chemistry (Esat and Yokoyama, 2006), biological activity (Bottrell and Tranter, 2002; Skidmore et al., 2005; Tranter, 2005) and ice sheet stability (Hubbard and Nienow, 1997; Walder, 1982); the development of new methods to address this undetermined parameter is important.

In subglacial waters the abundance of daughter nuclides of the uranium decay series (U-series) is a dynamic function of the time water is stored in contact with the underlying substrate, the abundance of U and daughter nuclides in the exposed substrate, the surface area of the exposed substrate, and the mixing of water from subglacial channels with different starting compositions. In this contribution we present measurements of ^{222}Rn and $^{234}U/^{238}U$ in subglacial waters as indicators of the length of time meltwater has been stored in the subglacial system. These

residence time calculations provide quantitative insight to the dynamic seasonal evolution of the subglacial hydrologic network and storage. By combining two radioactive isotope tracers within the same ^{238}U decay chain we can distinguish between solute concentration, dependence on residence time, substrate surface area, and water volume.

The work presented here presents a new method for determining subglacial water residence times to complement existing techniques, such as dye-trace studies in understanding the morphology and dynamics of subglacial hydrology. The implementation of our multi-proxy method quantifies the average length of time water is stored beneath a particular glacier, providing insight on a parameter that has thus far been elusive.

3.2. BACKGROUND

3.2.1. Importance of Subglacial Meltwater Residence Time

Glacial hydrology influences two crucial factors controlling the solute flux and residence times from melting glaciers and ice sheets: (1) the rock-water contact time at the ice-rock interface (i.e., residence time), and (2) the ratio of volume of subglacial water to subglacial bedrock or sediment surface area, which influences solute flux (Raiswell, 1984). The duration of subglacial water residence time, and these glacial hydrologic controls on the residence time, has several consequences. First, long residence times imply high basal water pressures, lubrication of the bed and high glacier sliding velocities. Once the water pressures are high enough, the configuration of the subglacial pathways will change to allow fast water transit times, lower residence times, and lower sliding velocities (Anderson et al., 2004). Joughin *et al* (2008) provides remote sensing and GPS evidence for variations in the subglacial network and water pressures between

the fast-flowing outlet glaciers and bare-ice margin of the GrIS margin. One explanation for this difference between water pressure and glacial velocities in these two contrasting subglacial hydrologic environments is the potential for a continuous supply of basal meltwater beneath existing ice streams, which would provide uniform water pressure throughout the year.

Second, the residence time of subglacial water is implicitly related to water-rock interaction time, which controls the weathering fluxes from reactions at the glacier base. Subglacial weathering is dominated by carbonate hydrolysis, carbonation and sulfide oxidation; where hydrolysis and sulfide oxidation lower the pH and promote carbonate dissolution (Tranter, 2005). Even in silicate bedrock material, carbonate dissolution rates are higher than aluminosilicate mineral dissolution rates (Fairchild et al., 1998; Maher et al., 2006b). Estimates indicate that sulfide oxidation dissolves carbonate relative to silicate five times more than the global average and results in high calcium fluxes from glacial melt (Anderson, 2007; Brown, 2002; Tranter et al., 2002). Furthermore, active subglacial microbial communities that mediate sulfide oxidation can draw down dissolved oxygen (DO) concentrations to the point of anoxia (Bottrell and Tranter, 2002; Skidmore et al., 2005; Tranter et al., 2002; Wadham et al., 2004). These reactions will vary depending on the availability of silicate, carbonate and sulfide minerals, but also the dissolved gas composition (CO_2 and O_2). The hydrologic network determines the extent of dissolution or exsolution of gases and the sources that gases could be lost to or gained from; modern atmospheric, derived from gas bubbles in ice, or from bedrock interaction. Therefore, seasonal changes in the glacial hydrology and residence time have a fundamental impact on the subglacial weathering environment - redox state, pH, DO, pCO_2 - and weathering fluxes of nutrients and trace elements, and their isotopic composition from a single glacier may very well

change seasonally and with climate. Additionally, the residence time of subglacial water is associated with local climate and geographic location, which influence the extent of subglacial erosion and weathering; thus, acting as a primary control on subglacial water chemistry, impacting microbial populations present and downstream ecosystems (Bottrell and Tranter, 2002; Fairchild et al., 1998; Maher et al., 2006b; Skidmore et al., 2005; Tranter, 2005; Tranter et al., 2002; Wadham et al., 2004).

3.2.2. U-series, Mixing, and Residence Time

Uranium-series nuclides in natural aqueous systems are powerful tools for quantifying rates of chemical and physical processes occurring at the Earth's surface. The U decay series has distinct advantages over other isotopic systems for determining timescales of processes; daughter nuclides within the chains have variable decay rates with half-lives comparable to the timescale of many geologic processes. The ^{238}U decay chain includes the daughter isotopes ^{234}U with $t_{1/2}$ = 248 ka (Cheng et al., 2000) and ^{222}Rn with $t_{1/2}$ = 3.8 days (Picolo, 1996) where $t_{1/2}$ is the half-life. The combination of these daughter isotopes with drastically different half-lives allows their analyses to be applied to samples with broad age ranges (Cochran and Masque, 2003).

In undisturbed rocks and minerals older than ~1 Ma, the activity of the parents and the daughters are in secular or radioactive equilibrium and the activity ratio will be equal to one: $[^{238}U]\ \lambda_{238} = [^{234}U]\ \lambda_{234} = [^{222}Rn]\ \lambda_{222}$ where square brackets indicate isotopic concentrations and λ refers to the isotope specific decay constant, and an isotope's specific activity and activity ratios are indicated by parenthesis. Departure from equilibrium, for all ratios assuming equal dissolution rates, occurs during water-rock interaction because of the preferential release of daughter

nuclides from the solid by recoil associated with high-energy alpha decay (Aciego et al., 2011; DePaolo et al., 2006; Semkow, 1991). As these interactions occur, solids become depleted in the daughter nuclides and liquids become enriched; for example, (^{234}U /^{238}U) activity ratios of 0.5 - 0.9 are commonly measured in fine-grained solids (Dosseto et al., 2008; Maher et al., 2006a; Skwarzec et al., 2002) and activity ratios of 1.05 - 11 have been measured in natural waters and ice (Aciego et al., 2011; Dosseto et al., 2008; Henderson et al., 2006; Maher et al., 2006a; Pogge von Strandmann, 2006; Vigier, 2006). Recoil accumulation of ^{222}Rn results in high concentrations in natural waters (Porcelli and Swarzenski, 2003), but its short half-life ($t_{1/2}$ = 3.85 days (Picolo, 1996)) leads to rapid attainment of steady-state concentrations. The absolute value of this steady-state concentration will depend on the water-rock ratio of the reservoir: low surface area or high water volumes will lead to low steady-state [^{222}Rn] and conversely high surface area or low water volumes will lead to high steady-state [^{222}Rn]. For example, radon concentrations measured in glacial meltwater at the Greenland Ice Sheet margin are high early in the melt season at low melt production rates, which then decrease as the melt production increases, presumably from mixing of low [^{222}Rn] surface melt and snow with high steady-state [^{222}Rn] from basal melt (Bhatia et al., 2011). A similar relationship is also expected at smaller scale alpine glaciers.

Depending on conditions present in the subglacial system the chemical composition, and more specifically the [^{222}Rn], [^{234}U], [^{238}U] and (^{234}U /^{238}U), of subglacial water pockets in differing channel systems will vary due to:

- The length of time subglacial water is in contact with underlying bedrock; longer contact increases subglacial water chemical concentrations.

- The age and composition of the underlying bedrock; bedrock older than ~1 Ma will be in radioactive equilibrium for ^{238}U, ^{234}U and ^{222}Rn and the lithology will control the overall [^{238}U] available for recoil and dissolution.
- The surface area of bedrock exposed to subglacial water; larger surface area exposes more chemical exchange sites, which may increase chemical weathering and dissolution concentrations as well as the fraction of daughter products released due to recoil.
- The volume of water in contact with the exposed bedrock/substrate; larger volumes decrease subglacial water chemical concentrations.
- The number of stream orders present; higher stream orders implies water mass mixing with differences in surface area, bedrock composition and residence time.
- The drainage efficiency; fast-flow dominance leads to lower average residence times (and vice-versa).
- The exposure of the subglacial water to the atmosphere; exposure to atmosphere increases likelihood of radon loss due to volatile exsolution.

In summary, the [^{222}Rn], [^{234}U], [^{238}U] and (^{234}U /^{238}U) of the bulk subglacial water reflect the average values of all contributing sources (e.g., fast-flow channels, slow-flow channels and their respective relationships with the underlying substrate).

3.2.3. Seasonal Evolution of Subglacial Drainage Network

Traditional research on the hydrology of glaciers has been primarily conducted on systems that are constrained by topography - alpine and valley glaciers - and are located within temperate latitudes (Anderson et al., 2004; Behrens, 1975; Collins, 1982; Fountain and Walder, 1998; Hubbard and Nienow, 1997; Mitchell and Brown, 2007; Naftz et al., 2002; Schuler, 2002; Smith

et al., 2001; Verbunt et al., 2003; Walder, 1982). The evolution of subglacial hydrology at temperate glaciers is seasonal. As the melt season progresses meltwater is transported via crevasses, englacial conduits and supraglacial channels to the subglacial hydrologic network, which develops into a combination of delayed flow in small channels, and fast flow in large channels (Fountain and Walder, 1998; Sharp, 1995). Subglacial hydrology may seasonally develop or permanently transition with warming climate into a more efficient system where fast-flow and slow-flow channels mix on a more regular basis as the subglacial network expands, with fast-flow being the dominant contributor causing the residence time of bulk subglacial water composition to decrease (Fountain and Walder, 1998; Nienow et al., 1998; Sundal et al., 2011; Tranter, 2005).

Our multi-proxy method incorporates both fast-flow and slow-flow networks that exist in subglacial hydrologic networks; producing average residence times of all water in the subglacial system as the slow-flow and fast-flow water volumes mix together in varying proportions over the course of the melt season. Because subglacial hydrologic systems are inherently complex, we model the isotopic evolution of the system in this study by generalizing the subglacial hydrologic system into a traditional Strahler stream order (Figure 3.1a, b, c). Stream order one (SO1) represents slow flow that has been isolated from the primary drainage system and contains the oldest subglacial water. Stream order two (SO2) represents delayed flow and melt water generated within SO2 pathways. Stream order three (SO3) represents SO1 plus SO2 with the addition of melt incorporated into the subglacial system from surface melt and englacial conduits. Similarly, stream order four (SO4) represents all contributing upstream water sources – slow flow and fast flow, basal and supra glacial melt – and as the main trunk of the subglacial

tributary system is also the bulk discharge from the glacier terminus. Lower stream orders represent the slowest, oldest flow with the lowest rate of discharge, whereas higher order streams have faster flow, higher discharge rates, and mixing of water sources.

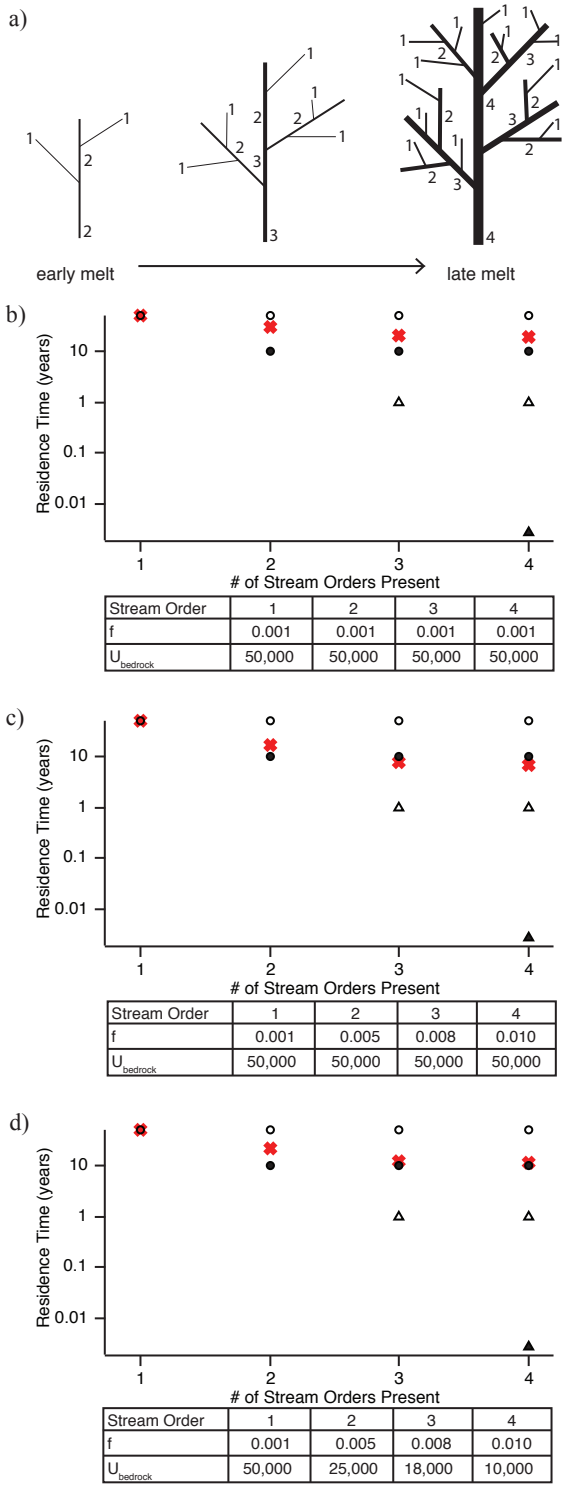

Figure 3.1: Simplified fractal depiction of the seasonal evolution of subglacial hydrology. Scenarios are for an ice sheet margin or glacier with (a) the progressing stages of melt evolution from early to late melt season: Early melt season: only first and second order channels present. Mid-melt season: third order channels develop and first and second order channels widen. Late melt season: fourth order channels develop and first, second and third order channels widen further. (b), (c) and (d) are plots of residence time versus stream orders present with initial residence times (assigned) plotted for stream order one as open black circles, stream order two as solid black circles, stream order three as open black triangles, and stream order four as solid black triangles. Variations of modeled residence times for the different number of stream orders present from equation 9 plotted as red x's: (b) the equation 9 model is used where the initial residence time varies between stream orders but f and $U_{bedrock}$ remain constant; (c) the equation 9 model is used where the initial residence time and f value varies between stream orders but $U_{bedrock}$ remain constant; and (d) equation 9 model is used where the residence time, f value, and $U_{bedrock}$ value all vary between stream orders.

3.3. U-SERIES RESIDENCE TIME EQUATION

3.3.1. Derivation of Residence Time Equation

Calculations of water-rock interaction time were derived from the following equations modified from (Goldstein et al., 2004). The original application of this U-series age constraint recoil model was to quantify the recoil age of ice from chemical interactions with dust particles trapped within the ice. In this study, the equation is used to obtain the recoil age, or residence time, of subglacial water from chemical interactions with the sediment/substrate present within the subglacial system. However, it is important to note that in this system, the concentration of dust in ice is too small (Aciego et al., 2011) relative to the U-series flux from direct interactions of meltwater with bedrock/substrate to noticeably alter the chemistry of subglacial water from ice melt alone.

The concentrations and decay constants of relevant isotopes in the following equations are:

- $[U_{234}]$ is the concentration of ^{234}U.
- λ_{234} is the ^{234}U decay constant, 2.829×10^{-6} yr^{-1} using ^{234}U $t_{1/2}$ of 2.45×10^{5} yr (Cheng et al., 2000).
- $[U_{238}]$ is the concentration of ^{238}U.
- λ_{238} is the ^{238}U decay constant, 1.554×10^{-10} yr^{-1} using ^{238}U $t_{1/2}$ of 4.46×10^{9} yr (Cheng et al., 2000).
- $[Rn_{222}]$ is the concentration of ^{222}Rn.
- λ_{222} is the ^{222}Rn decay constant, 66.27 yr^{-1} using ^{222}Rn $t_{1/2}$ of 1.046×10^{-2} yr (Picolo, 1996).

The subscripts used in the following equations denote the substance/process to which the variables refer:

- *water* refers the values measured in water samples.
- *bedrock* refers to the starting composition values of the bedrock.
- *dissolution* refers to the water composition components input through dissolution processes where ^{238}U, ^{234}U and ^{222}Rn contribute equally, respective to their concentrations in the rock.
- *recoil* refers to the water composition daughter-product excess that accumulates through recoil processes where only ^{234}U and ^{222}Rn contribute.

The geometric fraction term (f) is the fraction of recoil daughters ejected from the substrate solids related to the surface area of underlying bedrock, or till exposed at any given time. The volume of water (v) in contact with the exposed bedrock is divided through the terms to obtain concentrations in the stored water.

For the production of recoil ^{222}Rn and ^{234}U:

$$\frac{([Rn_{222}]\lambda_{222})_{water}}{v} = f\frac{([U_{238}]\lambda_{238})_{bedrock}}{v}\left(1 - e^{-\lambda_{222}t}\right) + \frac{([Rn_{222}]\lambda_{222})_{dissolution}e^{-\lambda_{222}t}}{v} + \frac{([U_{238}]\lambda_{238})_{dissolution}(1 - e^{-\lambda_{222}t})}{v} \quad (1a)$$

$$\frac{([U_{234}]\lambda_{234})_{water}}{v} = f\frac{([U_{238}]\lambda_{238})_{bedrock}}{v}\left(1 - e^{-\lambda_{234}t}\right) + \frac{([U_{234}]\lambda_{234})_{dissolution}e^{-\lambda_{234}t}}{v} + \frac{([U_{238}]\lambda_{238})_{dissolution}(1 - e^{-\lambda_{234}t})}{v} \quad (1b)$$

which expands to:

$$\frac{([Rn_{222}]\lambda_{222})_{water}}{v} = f\frac{([U_{238}]\lambda_{238})_{bedrock}}{v}\left(1 - e^{-\lambda_{222}t}\right)$$

$$+\frac{([\mathrm{Rn}_{222}]\lambda_{222})_{\mathrm{dissolution}}\mathrm{e}^{-\lambda_{222}\mathrm{t}}}{v}$$
$$+\frac{([\mathrm{U}_{238}]\lambda_{238})_{\mathrm{dissolution}}-([\mathrm{U}_{238}]\lambda_{238})_{\mathrm{dissolution}}\mathrm{e}^{-\lambda_{222}\mathrm{t}}}{v} \quad (2a)$$

$$\frac{([\mathrm{U}_{234}]\lambda_{234})_{\mathrm{water}}}{v}=\mathrm{f}\frac{([\mathrm{U}_{238}]\lambda_{238})_{\mathrm{bedrock}}}{v}\left(1-\mathrm{e}^{-\lambda_{234}\mathrm{t}}\right)$$
$$+\frac{([\mathrm{U}_{234}]\lambda_{234})_{\mathrm{dissolution}}\mathrm{e}^{-\lambda_{234}\mathrm{t}}}{v}$$
$$+\frac{([\mathrm{U}_{238}]\lambda_{238})_{\mathrm{dissolution}}-([\mathrm{U}_{238}]\lambda_{238})_{\mathrm{dissolution}}\mathrm{e}^{-\lambda_{234}\mathrm{t}}}{v} \quad (2b)$$

Expanding for multiple residence times where there is the maximum number of different channel environments, or stream orders within the system, the equations become:

$$\frac{([\mathrm{Rn}_{222}]\lambda_{222})_{\mathrm{water}}}{v}=\left(\mathrm{f}\frac{([\mathrm{U}_{238}]\lambda_{238})_{\mathrm{bedrock}}}{v}\left(1-\mathrm{e}^{-\lambda_{222}\mathrm{t}_1}\right)\right.$$
$$+\frac{([\mathrm{Rn}_{222}]\lambda_{222})_{\mathrm{dissolution}}\mathrm{e}^{-\lambda_{222}\mathrm{t}_1}}{v}$$
$$\left.+\frac{([\mathrm{U}_{238}]\lambda_{238})_{\mathrm{dissolution}}-([\mathrm{U}_{238}]\lambda_{238})_{\mathrm{dissolution}}\mathrm{e}^{-\lambda_{222}\mathrm{t}_1}}{v}\right)$$
$$+\cdots$$
$$+\left(\mathrm{f}\frac{([\mathrm{U}_{238}]\lambda_{238})_{\mathrm{bedrock}}}{v}\left(1-\mathrm{e}^{-\lambda_{222}\mathrm{t}_n}\right)\right.$$
$$+\frac{([\mathrm{Rn}_{222}]\lambda_{222})_{\mathrm{dissolution}}\mathrm{e}^{-\lambda_{222}\mathrm{t}_n}}{v}$$
$$\left.+\frac{([\mathrm{U}_{238}]\lambda_{238})_{\mathrm{dissolution}}-([\mathrm{U}_{238}]\lambda_{238})_{\mathrm{dissolution}}\mathrm{e}^{-\lambda_{222}\mathrm{t}_n}}{v}\right) \quad (3a)$$

$$\frac{([\mathrm{U}_{234}]\lambda_{234})_{\mathrm{water}}}{v}=\left(\mathrm{f}\frac{([\mathrm{U}_{238}]\lambda_{238})_{\mathrm{bedrock}}}{v}\left(1-\mathrm{e}^{-\lambda_{234}\mathrm{t}_1}\right)\right.$$
$$+\frac{([\mathrm{U}_{234}]\lambda_{234})_{\mathrm{dissolution}}\mathrm{e}^{-\lambda_{234}\mathrm{t}_1}}{v}$$
$$\left.+\frac{([\mathrm{U}_{238}]\lambda_{238})_{\mathrm{dissolution}}-([\mathrm{U}_{238}]\lambda_{238})_{\mathrm{dissolution}}\mathrm{e}^{-\lambda_{234}\mathrm{t}_1}}{v}\right)$$

$$+\cdots$$
$$+\left(\mathrm{f}\frac{([\mathrm{U}_{238}]\lambda_{238})_{\mathrm{bedrock}}}{v}\left(1-\mathrm{e}^{-\lambda_{234}\mathrm{t}_n}\right)\right.$$
$$+\frac{([\mathrm{U}_{234}]\lambda_{234})_{\mathrm{dissolution}}\mathrm{e}^{-\lambda_{234}\mathrm{t}_n}}{v}$$
$$\left.+\frac{([\mathrm{U}_{238}]\lambda_{238})_{\mathrm{dissolution}}-([\mathrm{U}_{238}]\lambda_{238})_{\mathrm{dissolution}}\mathrm{e}^{-\lambda_{234}\mathrm{t}_n}}{v}\right) \quad (3b)$$

Which are further expanded for the situation, e.g., Figure 3.1, where differing channel environments have different sediment surface area and f values, uranium concentrations, water volumes, and residence times ($f_1 \neq f_2 \neq \ldots \neq f_n$; $[U_{238}]_{bedrock\text{-}1} \neq [U_{238}]_{bedrock\text{-}2} \neq \ldots \neq [U_{238}]_{bedrock\text{-}n}$; $v_1 \neq v_2 \neq \ldots \neq v_n$; $t_1 \neq t_2 \neq \ldots \neq t_n$; *etc*…):

$$\frac{([\mathrm{Rn}_{222_1}]\lambda_{222})_{\mathrm{water}_1}}{v_1}+\cdots+\frac{([\mathrm{Rn}_{222_n}]\lambda_{222})_{\mathrm{water}_n}}{v_n}=$$
$$\left(\mathrm{f}_1\frac{([\mathrm{U}_{238_1}]\lambda_{238})_{\mathrm{bedrock}_1}}{v_1}\left(1-\mathrm{e}^{-\lambda_{222}\mathrm{t}_1}\right)\right.$$
$$+\frac{([\mathrm{Rn}_{222_1}]\lambda_{222})_{\mathrm{dissolution}_1}\mathrm{e}^{-\lambda_{222}\mathrm{t}_1}}{v_1}$$
$$\left.+\frac{([\mathrm{U}_{238_1}]\lambda_{238})_{\mathrm{dissolution}_1}-([\mathrm{U}_{238_1}]\lambda_{238})_{\mathrm{dissolution}_1}\mathrm{e}^{-\lambda_{222}\mathrm{t}_1}}{v_1}\right)$$
$$+\cdots$$
$$+\left(\mathrm{f}_n\frac{([\mathrm{U}_{238_n}]\lambda_{238})_{\mathrm{bedrock}_n}}{v_n}\left(1-\mathrm{e}^{-\lambda_{222}\mathrm{t}_n}\right)\right.$$
$$+\frac{([\mathrm{Rn}_{222_n}]\lambda_{222})_{\mathrm{dissolution}_n}\mathrm{e}^{-\lambda_{222}\mathrm{t}_n}}{v_n}$$
$$\left.+\frac{([\mathrm{U}_{238_n}]\lambda_{238})_{\mathrm{dissolution}_n}-([\mathrm{U}_{238_n}]\lambda_{238})_{\mathrm{dissolution}_n}\mathrm{e}^{-\lambda_{222}\mathrm{t}_n}}{v_n}\right) \quad (4a)$$

$$\frac{([\mathrm{U}_{234_1}]\lambda_{234})_{\mathrm{water}_1}}{v_1}+\cdots+\frac{([\mathrm{U}_{234_n}]\lambda_{234})_{\mathrm{water}_n}}{v_n}=$$

$$
\begin{aligned}
&\left(\mathrm{f}_1 \frac{([\mathrm{U}_{238_1}]\lambda_{238})_{\mathrm{bedrock}_1}}{v_1}\left(1-\mathrm{e}^{-\lambda_{234}\mathrm{t}_1}\right)\right.\\
&+\frac{([\mathrm{U}_{234_1}]\lambda_{222})_{\mathrm{dissolution}_1}\mathrm{e}^{-\lambda_{234}\mathrm{t}_1}}{v_1}\\
&\left.+\frac{([\mathrm{U}_{238_1}]\lambda_{238})_{\mathrm{dissolution}_1}-([\mathrm{U}_{238_1}]\lambda_{238})_{\mathrm{dissolution}_1}\mathrm{e}^{-\lambda_{234}\mathrm{t}_1}}{v_1}\right)\\
&+\cdots\\
&+\left(\mathrm{f}_n \frac{([\mathrm{U}_{238_n}]\lambda_{238})_{\mathrm{bedrock}_n}}{v_n}\left(1-\mathrm{e}^{-\lambda_{234}\mathrm{t}_n}\right)\right.\\
&+\frac{([\mathrm{U}_{234_n}]\lambda_{234})_{\mathrm{dissolution}_n}\mathrm{e}^{-\lambda_{234}\mathrm{t}_n}}{v_n}\\
&\left.+\frac{([\mathrm{U}_{238_n}]\lambda_{238})_{\mathrm{dissolution}_n}-([\mathrm{U}_{238_n}]\lambda_{238})_{\mathrm{dissolution}_n}\mathrm{e}^{-\lambda_{234}\mathrm{t}_n}}{v_n}\right)
\end{aligned}
\tag{4b}
$$

If we apply mean volumes, f values, concentrations and average residence time to the whole system of channels the equations simplify to:

$$
\begin{aligned}
\frac{([\mathrm{Rn}_{222_{mean}}]\lambda_{222})_{\mathrm{water}_{total}}}{v_{total}} =&\\
&\left(\mathrm{f}_{mean}\frac{([\mathrm{U}_{238_{mean}}]\lambda_{238})_{\mathrm{bedrock}_{mean}}}{v_{mean}}\left(1-\mathrm{e}^{-\lambda_{222}\mathrm{t}_{mean}}\right)\right.\\
&+\frac{([\mathrm{Rn}_{222_{mean}}]\lambda_{222})_{\mathrm{dissolution}_{mean}}\mathrm{e}^{-\lambda_{222}\mathrm{t}_{mean}}}{v_{mean}}\\
&\left.+\frac{([\mathrm{U}_{238_{mean}}]\lambda_{238})_{\mathrm{dissolution}_{mean}}-([\mathrm{U}_{238_{mean}}]\lambda_{238})_{\mathrm{dissolution}_{mean}}\mathrm{e}^{-\lambda_{222}\mathrm{t}_r}}{v_{mean}}\right.
\end{aligned}
\tag{5a}
$$

$$
\begin{aligned}
\frac{([\mathrm{U}_{234_{total}}]\lambda_{234})_{\mathrm{water}_{total}}}{v_{total}} =&\\
&\left(\mathrm{f}_{mean}\frac{([\mathrm{U}_{238_{mean}}]\lambda_{238})_{\mathrm{bedrock}_{mean}}}{v_{mean}}\left(1-\mathrm{e}^{-\lambda_{234}\mathrm{t}_{mean}}\right)\right.\\
&+\frac{([\mathrm{U}_{234_{mean}}]\lambda_{234})_{\mathrm{dissolution}_{mean}}\mathrm{e}^{-\lambda_{234}\mathrm{t}_{mean}}}{v_{mean}}
\end{aligned}
$$

$$+ \frac{([U_{238_{mean}}]\lambda_{238})_{\text{dissolution}_{mean}} - ([U_{238_{mean}}]\lambda_{238})_{\text{dissolution}_{mean}} e^{-\lambda_{234} t_{mean}}}{v_{mean}}\Bigg) \quad (5b)$$

Assuming congruent dissolution of old material in which $[U_{238}]\lambda_{238} = [U_{234}]\lambda_{234} = [Rn_{222}]\lambda_{222}$ etc., ^{234}U and ^{238}U activities are in equilibrium during dissolution then $[U_{238}]\lambda_{238} = [U_{234}]\lambda_{234}$:

$$\frac{([Rn_{222_{mean}}]\lambda_{222})_{\text{water}_{mean}} - ([U_{238_{mean}}]\lambda_{238})_{\text{dissolution}_{mean}}}{v_{mean}} = f_{mean} \frac{([U_{238_{mean}}]\lambda_{238})_{\text{bedrock}_{mean}}}{v_{mean}} \left(1 - e^{-\lambda_{222} t_{mean}}\right) \quad (6a)$$

$$\frac{([U_{234_{mean}}]\lambda_{234})_{\text{water}_{mean}} - ([U_{238_{mean}}]\lambda_{238})_{\text{dissolution}_{mean}}}{v_{mean}} = f_{mean} \frac{([U_{238_{mean}}]\lambda_{238})_{\text{bedrock}_{mean}}}{v_{mean}} \left(1 - e^{-\lambda_{234} t_{mean}}\right) \quad (6b)$$

Dividing Equation 6a by equation 6b:

$$\frac{\frac{([Rn_{222_{mean}}]\lambda_{222})_{\text{water}_{mean}} - ([U_{238_{mean}}]\lambda_{238})_{\text{dissolution}_{mean}}}{v_{mean}}}{\frac{([U_{234_{mean}}]\lambda_{234})_{\text{water}_{mean}} - ([U_{238_{mean}}]\lambda_{238})_{\text{dissolution}_{mean}}}{v_{mean}}} = \frac{f_{mean} \frac{([U_{238_{mean}}]\lambda_{238})_{\text{bedrock}_{mean}}}{v_{mean}} \left(1 - e^{-\lambda_{222} t_{mean}}\right)}{f_{mean} \frac{([U_{238_{mean}}]\lambda_{238})_{\text{bedrock}_{mean}}}{v_{mean}} (1 - e^{-\lambda_{234} t_{mean}})} \quad (7)$$

In this case the geometric fraction, bedrock source, and water volume terms cancel, resulting in a general equation for the mean residence time of the subglacial water:

$$\frac{([\mathrm{Rn}_{222_{mean}}]\lambda_{222})_{\mathrm{water}_{mean}} - ([\mathrm{U}_{238_{mean}}]\lambda_{238})_{\mathrm{dissolution}_{mean}}}{([\mathrm{U}_{234_{mean}}]\lambda_{234})_{\mathrm{water}_{mean}} - ([\mathrm{U}_{238_{mean}}]\lambda_{238})_{\mathrm{dissolution}_{mean}}} = \frac{\left(1 - \mathrm{e}^{-\lambda_{222}\mathrm{t}_{mean}}\right)}{(1 - \mathrm{e}^{-\lambda_{234}\mathrm{t}_{mean}})} \quad (8)$$

Rearranging the right-hand side of the equation and simplifying the terms in the equation to express them as specific activities, representing ($[Rn_{222\text{-}mean}]\lambda_{222}$) as ($Rn_{222}$), ($[U_{234\text{-}mean}]\lambda_{234}$) as ($U_{234}$) and ($[U_{238\text{-}mean}]\lambda_{238}$) as ($U_{238}$), the equation becomes:

$$\frac{(Rn_{222}) - (U_{238})}{(U_{234}) - (U_{238})} = \frac{1 - exp(-\lambda_{222}t_{mean})}{1 - exp(-\lambda_{234}t_{mean})} \quad (9)$$

Equation 9 can be solved iteratively for all scenarios where t_{mean} is less than a year. However, for scenarios where t_{mean} is greater than a year, the Taylor expansion can be used where $1\text{-}exp(\lambda_{222}t_{mean})$ is approximately equal to $\lambda_{222}t_{mean}$ (Lopez and Temme, 2004). Thus, in these scenarios, t_{mean} can be solved for directly and the following equation should be used:

$$\frac{(Rn_{222}) - (U_{238})}{(U_{234}) - (U_{238})} = \frac{1}{\lambda_{234}t_{mean}} \quad (10)$$

The left-hand side of the equation can be simplified by multiplying the numerator and denominator by (U_{238}):

$$\frac{[(Rn_{222})/(U_{238})]}{[(U_{234})/(U_{238})]} = \frac{1}{\lambda_{234}t_{mean}} \quad (11a)$$

simplifying to:

$$\frac{(Rn_{222})}{(U_{234})} = \frac{1}{\lambda_{234}t_{mean}} \quad (11b)$$

Solving for t_{mean} the equation becomes:

$$t_{mean} = \frac{[U_{234}]}{(Rn_{222})} \quad (12)$$

Note the U_{234} variable reverts back to concentration from specific activity as it was divided by the U_{234} decay rate.

3.3.2. Comparison of Bulk or Average Residence Time with True Residence Time of Water

To understand the relationship between water mass mixing and average subglacial residence time, we compare modeled 'true' residence times applied to Equation 9 with calculated bulk residence times from Equation 12. Excess ^{222}Rn and ^{234}U are modeled from Equation 9 using reasonable f, $\frac{([U_{238}]\lambda_{238})_{\text{bedrock}}}{v}$, and t_{mean} values for stream orders one through four, and then the excess ratio is applied to Equation 12 to calculate bulk residence times. Empirical values of f, obtained from N_2 gas absorption measurements, are taken from literature (Maher et al., 2006; Aciego et al., 2011), ranging from 0.001 to 0.01; $\frac{([U_{238}]\lambda_{238})_{\text{bedrock}}}{v}$ values ranging from 50000 to 10000 were estimated from the area under the glacier exposed to water, average continental crust U concentrations, and estimated water volumes; and residence times, t, ranged from one day for the highest stream order, based on dye tracing studies, to an estimated 50 years for the lowest stream order (slow flow channels). Figure 3.1 compares these 'true' and bulk residence times based on varying equation parameters. In Figure 3.1d, we vary t, but f and $\frac{([U_{238}]\lambda_{238})_{\text{bedrock}}}{v}$ values are constant for all stream orders. In Figure 3.1e, we vary both t and f values for all stream orders but $\frac{([U_{238}]\lambda_{238})_{\text{bedrock}}}{v}$ values are constant. In Figure 3.1f, we vary t, f and $\frac{([U_{238}]\lambda_{238})_{\text{bedrock}}}{v}$ values for all stream orders. For Equation 9, there are too many unknown variables (t ,f, $\frac{([U_{238}]\lambda_{238})_{\text{bedrock}}}{v}$) to solve for a unique t value; but solving Equation 12 using a range in f and $\frac{([U_{238}]\lambda_{238})_{\text{bedrock}}}{v}$ demonstrates that calculated residence times yield similar results. Therefore, the f and $\frac{([U_{238}]\lambda_{238})_{\text{bedrock}}}{v}$ values of water storage may differ across stream orders but Equation 12 always results in bulk residence time values between possible extremes.

3.3.3 General U-series Behavior Based on Modeling

Daughter products ^{222}Rn and ^{234}U reach an equilibrium concentration over different timescales, proportional to their different half-lives, with ^{222}Rn reaching a steady-state concentration in circa 20 days (approximately five half-lives of ^{222}Rn; $t_{1/2}$ = 3.85 days (Picolo, 1996)) and ^{234}U reaching equilibrium in roughly 1.23 x 10^6 years (approximately five half lives of ^{234}U; $t_{1/2}$ = 245 kyr (Cheng et al., 2000)), as long as ^{234}U is not in equilibrium the ratio of ^{222}Rn to ^{234}U will continue to change with time. That ^{222}Rn reaches equilibrium so quickly does not alter the results of calculated residence times of subglacial water if the (^{222}Rn) is measured within two hours of collection therefore no correction for time was required.

Bulk subglacial water residence time values are sensitive to the parameters within Equation 7 in the following way. Bulk residence times will be closer to the residence times of water masses that have the highest recoil accumulation; highest accumulation will be obtained in water masses with high *f*, high ^{238}U exposed (either through high concentration of U in bedrock or large areal exposure to water), and low water volumes. Conversely, bulk residence times will differ the largest from residence times of water masses with low *f*, low ^{238}U exposed (either through low concentration of U in bedrock or small areal exposure to water), and high water volumes. Thus the bulk subglacial water residence times will be slightly skewed away from a true mean composition if there are large differences in these parameters between water sources (Figure 3.1).

The application of ^{238}U, ^{234}U and ^{222}Rn isotopes to water-rock interaction in the subglacial environment provides bulk residence time of the entirety of water moving through the subglacial system, including surface snow, surface ice, and englacial ice melt that infiltrates to the base and *in situ* basal ice melt. The overall composition and fractionation of U decay series isotopes of subglacial water is related to the composition and fractionation of U decay series isotopes of *in situ* basal melt water, having significant implications for larger ice masses where water is stored for much longer periods of time – such as beneath fast moving ice streams isolated from supraglacial melt (Bell, 2007; Fahnestock, 2001) and subglacial lakes (Carter, 2007; Fricker, 2007; Price, 2002; Wingham, 2006), which are inaccessible to *in situ* methods such as dye tracing. Here we apply -- for the first time -- the use of this technique to subglacial water to determine the mean residence time of water draining the Athabasca Glacier over two months of the summer melt season, 2011.

3.3.4 Caveats of Residence Time Calculations

We recognize that, while our residence time equation accounts for the majority of variables and conditions occurring in the glacial environment, there are some potentially complicating factors. First, radon gas may be lost to the atmosphere prior to measurement. Second, uranium in solution may be adsorbed onto solids during transport through the subglacial system.

If radon loss occurs, there would be no corresponding change in uranium concentrations and the only effect would be an underestimation of the ^{222}Rn activity and overestimation of residence times. The changes to the measured residence time as a function of 25% loss would increase the calculated subglacial water residence time by 33%. However, radon loss is unlikely due to the

close proximity of our sampling site to the terminus of the glacier and high solubility of noble gases at low temperature (Garde et al., 1999). Additionally, a ^{222}Rn loss sensitivity test was performed by collecting additional samples 20 m, 100 m and 250 m downstream from the glacial terminus, resulting in ^{222}Rn measurements within 2 standard deviations of each other. Thus, indicating that ^{222}Rn loss through degassing is not a significant process in our system (Table 3.1).

Table 3.1: Degassing test with ^{222}Rn activity measurements. Subglacial water ^{222}Rn activity measurements collected 20 m, 100 m and 250 m downstream from the Athabasca Glacier terminus to test the effect of exposure to the atmosphere on ^{222}Rn activity. All ^{222}Rn activity measurements were collected within ten minutes of each other on May 8th, 2013 and are within error of one another.

Distance downstream (m)	time	^{222}Rn (pCi/μS)
0 (toe)	9:30	25.5 ± 5.8
20	9:33	31.9 ± 4.2
100	9:37	29.3 ± 3.6
250	9:40	28.1 ± 6.3

If uranium re-precipitation or adsorption occurred, both the ^{238}U and ^{234}U isotopes would be adsorbed at equal rates, thus the excess (^{234}U) would remain unchanged (Esat and Yokoyama, 2006). The loss of uranium would affect the calculated subglacial water residence times by underestimating the amount of ^{238}U in the numerator of Equation 12. The changes to the measured residence time as a function of 25% uranium loss would decrease the calculated subglacial water residence time by 33%.

The model presented in this manuscript may be applicable to other U-series daughters including radium (Ra) and protactinium (Pr), but these daughter products exhibit behaviors where re-precipitation and adsorption could complicate calculated residence time values. This complication is limited in our applied system because ^{222}Rn, as a noble gas, is not susceptible to adsorption behavior. Thus, if bias exists from adsorption or re-precipitation, the incorporation of ^{222}Rn in our equation does not contribute to further offset from true residence time values. Furthermore, to reduce measurement bias the daughter isotopes chosen for this study are measured in two distinct ways: *in situ* alpha counting of (^{222}Rn) and in laboratory mass spectrometry measurements for [^{238}U] and ^{234}U /^{238}U.

3.4. FIELD LOCATION, SAMPLING AND CHEMICAL METHODS

3.4.1. The Athabasca Glacier

We focused on the well-studied land-terminating temperate Athabasca Glacier (Brugmann and Demuth, 1994; Butler, 1980; Hart, 2006; Hugenholtz, 2008; Kite and Reid, 1977; Paterson, 1964; Paterson and Savage, 1963; Reynolds and Young, 1997) in Jasper National Park, Alberta, Canada (Figure 2.1). The Athabasca Glacier extends from the Columbia Icefield in a succession of three icefalls 6 km in length (Hart, 2006) and has an area of 8.6 km^2. The area of the Athabasca Glacier in this paper (8.6 km^2) was calculated using ArcMap 10, an Arc Global Imaging System (ArcGIS) software to create a polygon outlining the of the Athabasca Glacier up to the 2600 m contour line. The polygon was traced over the Digital Elevation Model onto 12 Systeme Pour l'Observation de la Terre (SPOT) data layers (Figure 2.1) and the area was calculated using the GPS coordinates embedded in the figure to determine the area of the polygon. We recognize that the area calculated is subjective to the implemented boundaries of the glacier in this figure.

The Columbia Icefield has the largest accumulations of snow and ice south of the Arctic Circle (Paterson, 1964) with its meltwater runoff reaching the Arctic, Pacific, and the Atlantic Oceans and is therefore a significant contributor to fresh water supply in the Northern Hemisphere (Butler, 1980). Shallow ice chemistry analysis of the Athabasca Glacier indicates that the glacier accumulates atmospherically transported gases in more dilute concentrations than urban areas but is nonetheless imprinted with anthropogenic pollution during ice formation (Butler, 1980). Previous studies have also found that the surface velocity of the glacier has fluctuated over the past several decades and has been correlated to subglacial water discharge at the terminus, and thus the velocity at which the base of the Athabasca Glacier slides over bedrock (Paterson, 1964; Paterson and Savage, 1963).

The Athabasca Glacier rests on a bedrock basin with a small layer of deformable till, less than 0.5 m, between the ice and bedrock, with Middle Cambrian limestone and carbonic shale beneath (Hart, 2006). Meltwater from the greater Columbia Icefield is responsible for recharge of aquifers and formation of karst systems (Ford, 1983; Smart, 1983). The Athabasca aquifer (a confined aquifer) is approximately 50 m lower in elevation than the Athabasca glacier (Figure 2.1) and even during peak melt (which occurred during our field season), the aquifer level should not vary much more than one meter seasonally even if water depth is different in differing geographic locations (Zencich et al., 2002). Therefore, the chemical composition of the aquifer should not influence the subglacial water chemistry. Based on the predominantly carbonate/dolomite underlying geology, traditional measurements of residence time – electrical conductivity, major ions, and alkalinity -- should trend toward higher values with longer water-rock interaction time (Anderson et al., 2004; Fairchild et al., 1998; Mitchell and Brown, 2008).

The source contributions of snowmelt, ice melt, and summer rain fractions to the overall water discharged at the Athabasca Glacier terminus have been calculated for the 2011 field season using $\delta^{18}O$ and δD measurements of daily subglacial melt samples and end member components (snow, ice, summer precipitation) and a Bayesian Monte Carlo simulation model (Arendt et al., *In Revision*) to quantify the dilution effect from snowmelt throughout the melt season. For both May and July (2011), summer rain remained the smallest contributor with occasional spikes correlating with field notes of precipitation. During the onset of melt in May, the primary contributor was snowmelt ranging from 44 - 86 % of the total water discharged, followed by ice melt from 9 - 33 % (Arendt et al., *In Revision*). The melt system was established by July and the primary contributor switched to ice melt ranging from 44 – 63 % with snowmelt as the secondary contributor from 8 – 39 % (Arendt et al., *In Revision*). This reversal in melt source corroborates the evolution of the subglacial network toward more efficient drainage with higher volumes of ice melt. With the development of a more efficient subglacial network, isolated older pockets of subglacial water flowed through the subglacial system, causing the mixing of old and young melt sources.

3.4.2 Sampling

3.4.2.1 Pre-cleaning

All sample containers and tubing were pre-cleaned in an ISO 7 (class 10,000) clean laboratory prior to sample collection to minimize blanks: blanks from this study were negligible. Ultra-pure reagents were used for all cleaning and chemical separation. Super de-ionized water was purified using a super (SQ) Millipore purification system, which produces a water purity of >18.2 MΩ. The 20 L collapsible polyethylene carboys (Thermo Fisher Hedwing) and the 1 L polypropylene

bottles (Nalgene) were cleaned using the same procedure. The containers were i) rinsed three times with SQ water, ii) leached for 48 hours in 10% reagent grade HNO_3, iii) rinsed three times with SQ water, iv) leached for 48 hours in 10% double-distilled HCl, and v) and rinsed three times with SQ water. Polyethylene tubing was rinsed three times with SQ water, leached for 72 hours in 10% optima grade HCl, and rinsed three times with SQ water.

3.4.2.2. Collection of filtered subglacial water

The field season consisted of two periods of fieldwork during the melt season of 2011: 25 days in May (May 5th -29th) during the onset of melt and 24 days in July (July 2nd -27th) during the peak melt at the Athabasca Glacier subglacial system.

Daily water samples were collected mid-morning within 10 m of the glacier terminus. Suspended sediment was removed from the subglacial water to prevent further recoil and dissolution processes from occurring between the sediment and water while samples were in transport and storage prior to analysis. Subglacial water was filtered using a Masterflex modular peristaltic pump and a polycarbonate filtration unit (Geotech Environmental Equipment Inc.). Glass fiber prefilters and polytetrafluoroethylene (PTFE) filter (0.2 μm) membranes were used to remove the suspended sediment. One liter of ultra-pure SQ water was filtered through the system as a rinsing agent prior to the filtration of samples.

Subglacial water was filtered and collected directly from the main melt channel at the terminus of the Athabasca Glacier into the precleaned 20 L carboys. Samples ranged in volume from 10-40 L depending on the suspended sediment load; high-suspended sediment dramatically

increased the filtration time. In addition to carboys, 1 L of filtered water was collected and acidified (after alkalinity measurements; see below) and 25 mL of water was collected in airtight glass vials for oxygen and hydrogen isotope analysis. Filter membranes, including suspended sediment, were collected and stored for future analyses.

3.4.2.3. In-field chemical measurements

Daily electrical conductivity, temperature, pH, and alkalinity measurements were taken using a Daily Oakton Portable Waterproof Conductivity Meter. The electrical conductivity, temperature, and pH measurements were all conducted on-site in the main subglacial outlet channel by submerging the probe in the moving water at an upright position and waiting for the meter to equilibrate. These measurements took place during but downstream of the filtration and collection of the water samples to avoid any possible disturbances/contamination. Approximately 100 mL of filtered subglacial water was measured for alkalinity. For anticipated high alkalinities, the 100 mL sample was mixed with 10 mL of Total Alkalinity Reagent (FisherScientific) solution, shaken, and measured for pH. For anticipated low alkalinities, the 100 mL sample was mixed with 1 mL of Total Alkalinity Reagent solution, shaken, and measured for pH. The pH was converted to the total alkalinity using a pH-total alkalinity conversion chart (Fairchild et al., 1998).

3.4.2.4. Channel discharge

Discharge and maximum velocity measurements were taken directly after water sample collection. Manual measurements of these parameters were achieved using an Acoustic Doppler Velocimeter Flow-tracker, or ADV Flowtracker. A measuring tape was set up across the width of

the channel, perpendicular to water flow. The ADV Flowtracker's monitor was submerged at the edge of the channel parallel to water flow and calibrated prior to measurement. Following calibration, the ADV Flowtracker measured velocity and water depth at one-foot increments spanning the width of the main channel at the terminus of the glacier. Velocity and water depth measurements across the channel allowed the calculation of discharge, using the standard 0.6 rule, where velocity measurements are taken at 0.6 of the depth of each location (Morlock et al., 2002).

3.4.2.5. In-field radon measurements

The radiogenic isotope ^{222}Rn has a half-life of 3.85 days (Picolo, 1996) and thus required on site measurement. Water samples were analyzed within 3 hours of collection. Daily in-field ^{222}Rn activities in waters were determined with a Durridge RAD7 (see http:/www.durridge.com/; Lane-Smith and Sims, 2013) coupled with a RAD H_2O (see http://www.durridge.com/products_rad_h2o.shtml). For these measurements a 250 mL glass water vial was submerged in the water channel for several minutes and capped while completely submerged to prevent any atmospheric bubbles from entering the container, and consequently prevent Rn from partitioning/degassing. Prior to each analysis the Durridge RAD7 was purged to reduce water vapor; once the moisture content of the Durridge RAD7 was below 10%, the sample was analyzed in situ by energy dispersive alpha spectrometry. Analysis consisted of five cycles of aeration for five minutes and five minutes of radon detection following each aeration period. Reported results indicate uncertainty for each individual sample based on the variability between cycles; analytical uncertainties reported by Durridge for specific activity ranges are all lower than the variability reported (Durridge Company, 2009). The 2σ in ^{222}Rn activities are 2

standard deviations from the mean based on three replicate measurements; each measurement has a 2σ error of <5% based on counting statistics (Durridge Company Inc., 2009).

3.4.2.6. Iron co-precipitation

Each daily 10-40 L filtered water sample was reduced in sample size via iron co-precipitation field chemistry based on established procedures (Rickli et al., 2010). The pH of the sample was lowered to approximately 2-3 by adding 9M HCl and shaking the sample until it was homogenous. Next, a pre-cleaned $FeCl_3$ $6H_2O$ – 3M HCl mixture was added to the sample. The sample was then shaken vigorously and left to sit for approximately 10 minutes to reach chemical equilibrium. The addition and mixing of $[NH_4^+][OH^-]$ (ammonia hydroxide) to the sample raised the pH to 8-9 and initialized settling flocculates. The high pH iron precipitated out of the solution along with the uranium over a two-day period. Once the settling period had elapsed, the sample was decanted. Final pre-concentration of the iron precipitate was accomplished in a clean laboratory by centrifuging the samples, resulting in ~1 g of iron precipitate for dissolution and column chemistry.

3.4.3 Column Chemistry

Uranium isotopic analysis was performed on the subglacial water iron co-precipitation products using established anion exchange chromatography techniques to separate and concentrate uranium (Arendt et al., 2014; Hubert et al., 2006; Rickli et al., 2010).

3.4.4. Mass Spectrometry

3.4.4.1. Uranium isotope ratios

Uranium isotopic compositions and activity ratios, ($^{234}U/^{238}U$), were measured at the Wyoming High Precision Isotope Laboratory at the University of Wyoming on a Neptune PLUS ultra high-precision, high-sensitivity multi collector inductively coupled mass spectrometer (Ball et al., 2008). Each sample was loaded into a sample solution of 1M HNO_3 and diluted to 40 ng ml^{-1} uranium content(Arendt et al., 2014). Sample measurements were bracketed with measurements of standard U010 to correct for mass bias and ion counting efficiency, using the established ($^{234}U/^{238}U$) ratio of 18,074 (Richter and Goldberg, 2003). Standard NBS960 was run periodically to test the precision and accuracy of the Neptune PLUS over the entire sample run (Cheng et al., 2000). The sample intake system was rinsed sequentially with ultrapure SQ water and dilute HCl between analyses. External errors are 2 standard deviations of ($^{234}U/^{238}U$) for NBS960 and are equal to 0.001 for all calculated values based on multiple measurements (n > 60) of the standard solution (Arendt et al., 2014).

3.4.4.2. Elemental concentrations

Major element and ^{238}U concentrations were performed at the University of Michigan Keck Elemental Geochemistry Laboratory using a ThermoScientific Element2 inductively coupled mass spectrometer operating in pulse-counting mode. The filtered, acidified 1 L subglacial water samples were aliquoted and 3 mL of each sample solution was analyzed. An acid blank, a standard of known concentration, and an additional acid blank were run between every sample to measure the concentration accurately. Each sample was measured in triplicate, with the standard deviation of the measurements indicating the variability of the individual results. All standard deviations are lower than the reported errors in the standard concentration. The 2σ errors of the major ions and ^{238}U concentrations are based on a 0.7% standard error for the May samples and a

0.3% standard error for the July samples in the bracketing standard: internal counting errors are two orders of magnitude less than error in standard ^{238}U concentration values.

3.4.5. Residence Time Calculations

For the Athabasca Glacier subglacial water average residence time calculations, Equation 12 was solved directly, using the (^{222}Rn), [^{234}U], [^{238}U] and (^{234}U /^{238}U) measurements we obtained and the known decay rates of the isotopes (Cheng, 2000; Picolo, 1996).

3.5. RESULTS

3.5.1. In-Field Measurements

Table 3.2: Athabasca Glacier traditional water chemistry measurements. pH, electrical conductivity, total alkalinity, and discharge measurements during sample collection at the Athabasca Glacier in May and July of 2011. The horizontal line through the table represents the break between May and July. Only samples that had all chemical values are included (for example, samples taken during days when machine malfunction or weather did not allow for sampling are excluded).

Sample (Day of Year)	pH	conductivity (μS)	total alkalinity (ppm $CaCO_3$)	discharge (m^3/s)
AG050611CA-2 (126)	8.1	349	113	0.01
AG050711CA-3 (127)	7.7	332	124	0.01
AG050811CA-4 (128)	8.1	315	115	0.01
AG051011CA-6 (130)	8.2	284	87	0.02
AG051111CA-7 (131)	8.2	248	68	0.05
AG051211CA-8 (132)	8.4	184	36	0.06
AG051411CA-10 (134)	8.4	190	51	0.07
AG051511CA-11 (135)	8.4	171	43	0.07
AG051711CA-13 (137)	8.5	156	36	0.10
AG051811CA-14 (138)	8.4	161	27	0.11
AG051911CA-15 (139)	8.4	180	37	0.07
AG052111CA-17 (141)	8.4	156	42	0.22
AG052211CA-18 (142)	8.6	149	37	0.19
AG052311CA-19 (143)	8.6	132	28	0.35
AG070311CA-27 (184)	9.0	82	21	2.42
AG070411CA-28 (185)	8.9	120	25	1.60
AG070511CA-29 (186)	8.7	128	25	1.52
AG070611CA-30 (187)	8.9	111	25	2.32
AG070711CA-31 (188)	9.1	87	24	3.28
AG070911CA-33 (190)	8.7	131	21	1.55
AG071011CA-34 (191)	8.6	131	25	1.22
AG071111CA-35 (192)	9.6	122	15	1.24

The discharge from the primary outlet channel at the terminus of the Athabasca Glacier (Figure 2.1) increased from < 5 x 10^{-3} m^3/s in May to > 3.3 m^3/s in July. From early May to late July the pH increased from 7.7 to a 9.6, while conductivity decreased from ~350 uS/cm to ~120 uS/cm, and total alkalinity decreased ~125 to ~15 ppm $CaCO_3$. As shown in Figure 3.2 and Table 3.2, the pH and discharge of subglacial water in the main channel have an inverse relationship with the conductivity and total alkalinity of the subglacial water.

3.5.2. Chemical Measurements

3.5.2.1. Radioactive and radiogenic isotopes

The measured ^{222}Rn activities and ^{238}U concentrations and the (^{234}U/^{238}U) of the Athabasca Glacier subglacial water samples in May exhibit correlated temporal trends, but in July the chemical species diverge.

Radon-222 activities decrease from ~145 to ~9 pCi/L during May, whereas in July the ^{222}Rn activities average approximately 110 pCi/L and show temporal oscillations (Table 3.3). To ascertain the impact of Rn loss on our sampling environment we performed radon measurements 50 and 100 m downstream that were nearly identical to the measurement taken at the terminus: therefore, we propose that radon loss during water transport was negligible. The ^{238}U concentrations of the Athabasca Glacier subglacial water decreases from 840 to 20 ppt during May and fluctuates within the range of 70 to 230 ppt in July (Table 3.3). We observed a correlation between the discharge from the primary outlet channel and ^{238}U concentrations for July with an R^2 value of 0.81, and a much weaker correlation for May, with a R^2 value of 0.51 (Figure 3.3). The (^{234}U/^{238}U) values decrease from ~1.04 to ~1.00 in May and are more tightly

clustered in July with values decreasing from ~1.03 to ~1.00 (Table 3.3 and Figure 3.3). We observe stronger correlations between ($^{234}U/^{238}U$) values and the discharge from the primary outlet channel in July, with an R^2 value of 0.72, compared to May with an R^2 value of 0.43.

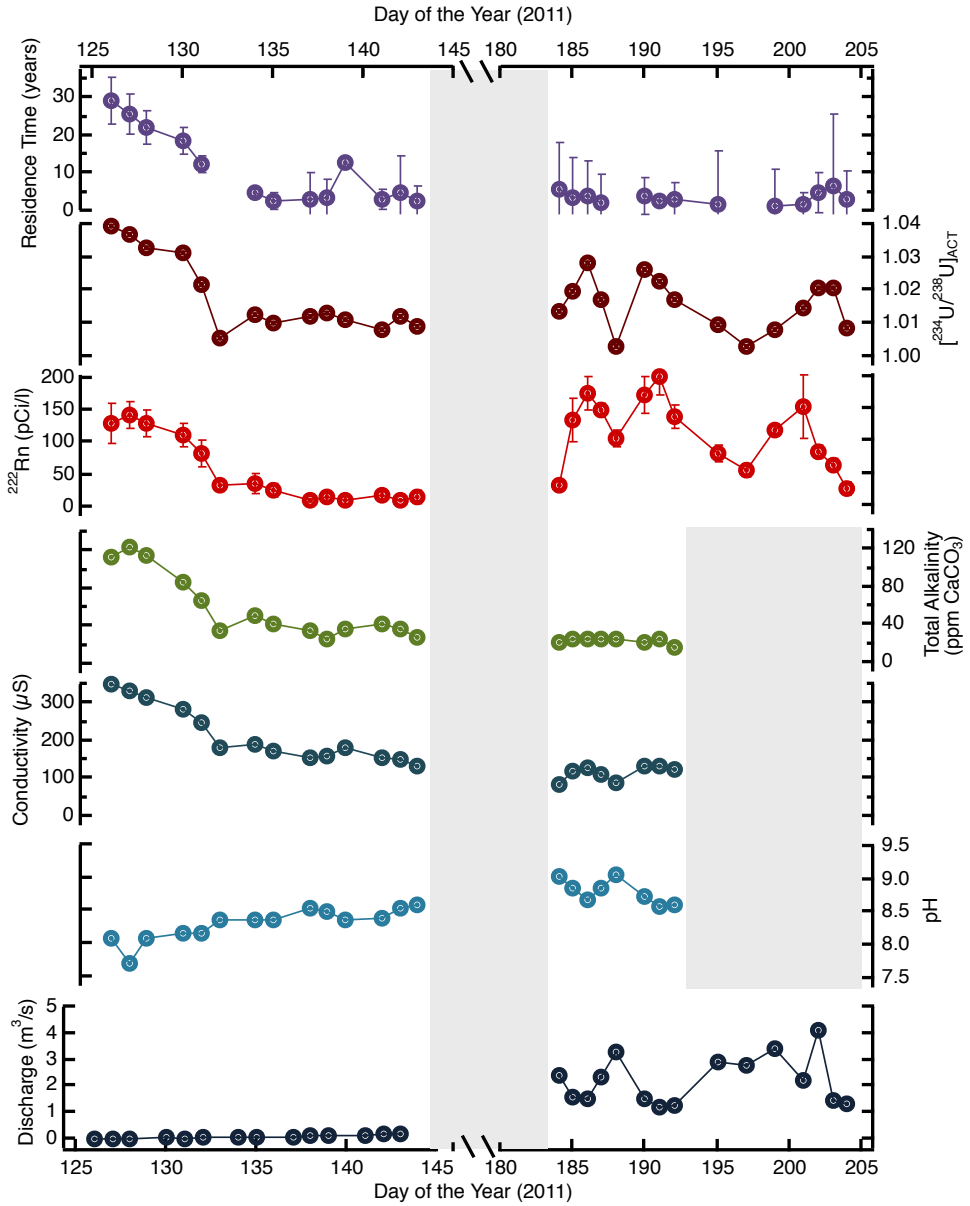

Figure 3.2: Seasonal measurements from the Athabasca Glacier. Variations in the subglacial residence time in years, ($^{234}U/^{238}U)_{activity}$, [$^{222}Rn$], total alkalinity, conductivity, pH and discharge in m^3/s of water samples at the terminus of the Athabasca Glacier over the 2011 calendar year: days 126-143 occurred in May when melt initiated and snow cover was the dominant melt source (Arendt et al., In Revision) and days 184-204 occurred in July when melt was at its peak and snow cover was no longer a significant contribution to melt (Arendt et al., In Revision) Sampling did not occur during the middle of the melt season in June, days 144-183, thus the x-axis is condensed for that period. No total alkalinity/conductivity/pH measurements were taken from days 194-205 due to instrument error. Residence times of subglacial water were calculated iteratively using Equation 9, utilizing ($^{234}U/^{238}U)_{activity}$, [$^{238}U$] and [$^{222}Rn$] measurements (Table 3.3). The residence time of the Athabasca Glacier subglacial water averaged approximately 11.2 years in May and 3.5 years in July; the average standard deviation of the mean is 8.1 in May and 4.0 in July indicating that the difference in range of residence time values between May and July are real.

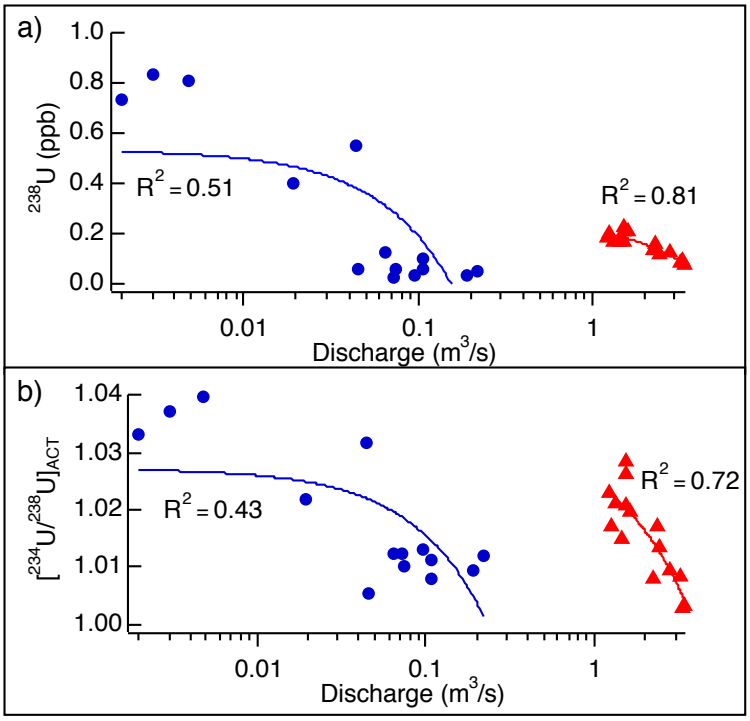

Figure 3.3: U-series isotopic measurements versus discharge. Uranium-238 (^{238}U) concentrations and uranium activity ratio measurements shown against discharge measurements of the primary melt channel located at the terminus of the Athabasca Glacier (Fig. 2) for May (blue circles) and July (red triangles), 2011. (a) ^{238}U concentrations in ppb versus discharge in m^3/s. (b) Uranium activity ratios $(^{234}U/^{238}U)_{activity}$ versus discharge in m^3/s. While the trend in ^{238}U concentrations (a) might result from dilution, the $(^{234}U/^{238}U)_{activity}$ values are ratios that are not altered from dilution.

The relationship between ^{222}Rn activities and $(^{234}U/^{238}U)$ values of Athabasca Glacier subglacial water also changes from May to July (Table 3.3 and Figure 3.4). In May the R^2 value of 0.92 for this relationship shows that the ^{222}Rn activities and $(^{234}U/^{238}U)$ values are well correlated (Figure 3.4). In July the R^2 value of 0.36 for the relationship between ^{222}Rn activities and $(^{234}U/^{238}U)$ measurements shows poor correlation. The ^{222}Rn values were less consistent and fluctuated more on a daily basis in July than in May (Table 3.3 and Figure 3.4).

Table 3.3: Isotopic measurements and 2σ of Athabasca subglacial water samples. Samples were collected at the main outlet channel at the terminus of the Athabasca Glacier in May (a) and July (b) 2011. The 2σ shown for ^{222}Rn activities are 2 standard deviations of the mean based on three replicate measurements, each measurement has a 2σ error of <5% based on counting statistics (Durridge Company Inc., 2009). For the ^{238}U concentration values, the 2σ errors are based on a 0.7% error for the May samples and a 0.3% error for the July samples in the bracketing standard: internal counting errors are 2 orders of magnitude less than error in standard ^{238}U concentration values. Internal errors are shown as the 2σ for $(^{234}U/^{238}U)_{activity}$. External errors are 2 standard deviations of $(^{234}U/^{238}U)_{activity}$ for NBS960 and are equal to 0.001 for all calculated values and are based on multiple measurements (n > 10) of the standard solution. The $(^{234}U/^{238}U)_{activity}$ values used to calculate residence time had three significant figures but is shown here with four significant figures to provide a greater overview. Residence times of subglacial water are propagated based on 2σ errors in the ^{222}Rn activities and external errors in ^{238}U and $(^{234}U/^{238}U)_{activity}$.

Sample (Day of Year)	^{222}Rn (pCi/L)	2σ	^{238}U (ppt)	2σ	$(^{234}U/^{238}U)_{activity}$	2σ	Residence Time (years)	2σ
AG050611CA-2 (126)	130	32	807	50	1.040	0.001	29.3	6.1
AG050711CA-3 (127)	143	21	832	50	1.037	0.001	25.7	5.4
AG050811CA-4 (128)	129	21	729	50	1.033	0.001	22.3	4.6
AG051011CA-6 (130)	112	18	551	26	1.032	0.001	18.5	3.7
AG051111CA-7 (131)	84	20	402	26	1.022	0.001	12.5	2.4
AG051211CA-8 (132)	33	8	59	12	1.005	0.001	–	–
AG051411CA-10 (134)	36	16	123	12	1.012	0.001	5.0	0.7
AG051511CA-11 (135)	25	12	55	12	1.010	0.001	2.7	2.3
AG051711CA-13 (137)	11	4	23	12	1.012	0.001	3.1	7.2
AG051811CA-14 (138)	16	5	35	12	1.013	0.001	3.4	4.8
AG051911CA-15 (139)	11	6	101	12	1.011	0.001	12.8	1.5
AG052111CA-17 (141)	18	5	58	12	1.008	0.001	3.2	2.5
AG052211CA-18 (142)	9	1	46	12	1.040	0.001	4.7	9.6
AG052311CA-19 (143)	15	9	33	12	1.009	0.001	2.5	3.9
AG070311CA-27 (184)	31	5	113	8	1.014	0.001	5.9	3.9
AG070411CA-28 (185)	133	33	212	8	1.020	0.001	3.7	1.3
AG070511CA-29 (186)	174	27	205	8	1.029	0.001	4.0	1.4
AG070611CA-30 (187)	147	10	159	8	1.017	0.001	2.2	1.0
AG070711CA-31 (188)	104	12	93	8	1.003	0.001	–	–
AG070911CA-33 (190)	171	30	227	8	1.026	0.001	4.1	1.3
AG071011CA-34 (191)	201	28	186	8	1.023	0.001	2.5	1.0
AG071111CA-35 (192)	138	19	203	8	1.017	0.001	3.0	1.1
AG071611CA-38 (195)	80	12	121	8	1.010	0.001	1.7	1.1
AG071811CA-40 (197)	55	9	74	8	1.003	0.001	–	–
AG072011CA-42 (199)	116	6	137	8	1.008	0.001	1.1	0.6
AG072211CA-44 (201)	154	51	156	8	1.015	0.001	1.9	0.8
AG072311CA-45 (202)	83	12	166	8	1.021	0.001	4.9	2.3
AG072411CA-46 (203)	62	10	168	8	1.021	0.001	6.7	3.0
AG072511CA-47 (204)	26	11	85	8	1.008	0.001	3.3	4.1

3.5.3. Quantitative Residence Time

Calculated residence times of Athabasca Glacier subglacial water discharged from the main outlet channel are < 30 years in May and < 7 years in July (Table 3.3). Error in the residence times of subglacial water is propagated based on 2σ errors in the ^{222}Rn, ^{238}U and $(^{234}U/^{238}U)$.

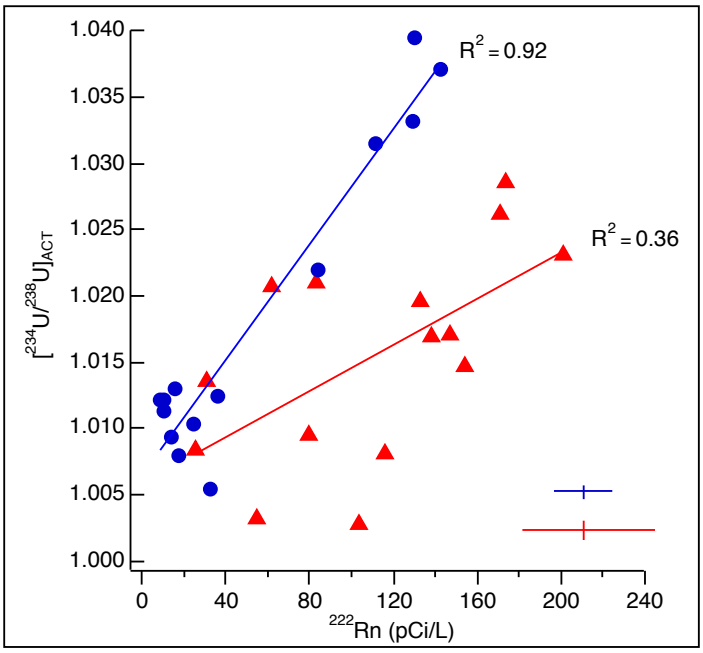

Figure 3.4: Changes in $(^{234}U/^{238}U)_{activity}$ measurements compared with ^{222}Rn activities. Athabasca Glacier subglacial water samples from May are blue circles and samples from July are red triangles, 2011. The R^2 values and error bars in the lower right hand corner for May and July show the $(^{234}U/^{238}U)_{activity}$ and ^{222}Rn are more highly correlated in May than July.

3.6. DISCUSSION

6.1 Synthesis of U-series Residence Time with Traditional Models

Our chemical measurements and interpretations of the evolving Athabasca Glacier subglacial system are in agreement with previous studies that have analyzed the switching of subglacial drainage from a distributed network to a channelized system (Walder, 1986), whose average residence time is reflective of a mixture of fast-flow and slow-flow subglacial channels (Anderson, 2003b, a).

3.6.1.1. Traditional analysis and dilution effects

Major cations including potassium (K^+), calcium (Ca^{2+}), sodium (Na^+) and magnesium (Mg^{2+}) decrease as discharge measurements increase and the melt season progresses, which is in

agreement with previous interpretations of subglacial water residence time decreasing with decreasing cation concentrations (Anderson, 2003b, a) (Table 3.2 and Fig. S1). High concentrations of major cations in subglacial water correlate with calculated high residence time values (Table 3.4, Fig. S1), which is consistent with previous interpretations of high and low ion concentrations corresponding to slow-flow and fast-flow subglacial drainage respectively (Anderson, 2003b, a).

Delayed flow water in the subglacial system - implied by high residence time calculations – experiences prolonged water-rock interaction time. In anoxic subglacial systems with predominately carbonate bedrock, meltwater is saturated in CO_2 with respect to the underlying carbonate substrate, causing the pH to decrease due to carbonate reaction kinetics (Fairchild et al., 1998; Tranter, 2005). Evolution of the subglacial network shifts the system from delayed flow waters to fast flow waters and increases the availability of atmospheric gases to the subglacial water. Hence, as the melt season progresses the subglacial drainage network becomes increasingly exposed to and interacts with atmospheric CO_2, transitioning the subglacial system to become less anoxic with time (Mitchell and Brown, 2008; Tranter, 2005). This transition results in the under-saturation of subglacial meltwater with respect to the underlying carbonate substrate, again due to carbonate dissolution kinetics (Fairchild et al., 1998; Tranter, 2005). Because of the highly reactive nature of carbonate minerals, the new under-saturation of the meltwater enables an amplified incorporation of carbonate material into the meltwater (Sharp et al., 2002), increasing meltwater pH (Figure 3.2). Therefore, the observed increase in subglacial water pH as the melt season progresses at the predominantly carbonate Athabasca Glacier, is in

agreement with our calculated residence time values, which decrease from ~ 30 years to < 6 years from May to July 2011 (Table 3.3, Figure 3.4, Table 3.4 and Figure 3.5).

Table 3.4: Measurements of Athabasca Glacier meltwater major cations: including potassium (K), calcium (Ca), sodium (Na) and magnesium (Mg) from Athabasca subglacial water samples collected at the main outlet channel at the terminus of the Athabasca Glacier in May and July 2011.

Sample (Day of Year)	K (ppm) ± 4	Ca (ppm) ± 2	Na (ppm) ± 1	Mg (ppm) ± 1
AG050611CA-2 (126)	0.550	37.3	1.20	21.7
AG050711CA-3 (127)	0.529	35.3	1.10	20.8
AG050811CA-4 (128)	0.514	33.8	1.04	19.5
AG051011CA-6 (130)	0.461	32.0	0.83	17.1
AG051111CA-7 (131)	0.398	28.6	0.71	13.7
AG051211CA-8 (132)	0.204	19.0	0.37	6.18
AG051411CA-10 (134)	0.289	21.5	0.48	8.57
AG051511CA-11 (135)	0.240	19.9	0.45	7.27
AG051711CA-13 (137)	0.202	18.4	0.37	6.60
AG051811CA-14 (138)	0.194	17.4	0.47	6.44
AG051911CA-15 (139)	0.234	20.9	0.42	8.14
AG052111CA-17 (141)	0.198	19.3	0.36	6.41
AG052211CA-18 (142)	0.192	17.9	0.32	5.97
AG052311CA-19 (143)	0.171	17.0	0.28	4.76
AG070311CA-27 (184)	0.099	10.8	0.11	2.85
AG070411CA-28 (185)	0.147	15.0	0.23	5.04
AG070511CA-29 (186)	0.178	14.6	0.27	5.01
AG070611CA-30 (187)	0.117	12.2	0.18	3.92
AG070711CA-31 (188)	0.100	9.9	0.10	2.34
AG070911CA-33 (190)	0.163	16.0	0.29	6.08
AG071011CA-34 (191)	0.121	13.8	0.20	4.71
AG071111CA-35 (192)	0.149	14.4	0.23	5.17
AG071611CA-38 (195)	0.089	10.8	0.14	3.46
AG071811CA-40 (197)	0.051	8.4	0.08	2.00
AG072011CA-42 (199)	0.105	12.0	0.14	3.50
AG072211CA-44 (201)	0.091	13.7	0.26	4.46
AG072311CA-45 (202)	0.077	13.3	0.19	4.46
AG072411CA-46 (203)	0.080	12.7	0.22	4.37
AG072511CA-47 (204)	0.054	9.1	0.08	2.17

Previous studies have suggested that high water-rock interaction times correspond to high ion concentrations in subglacial water and have used electrical conductivity measurements as a proxy for residence time (Bartholomaus et al., 2008; Mitchell and Brown, 2007). The calculated

residence times for the Athabasca Glacier subglacial water correspond to dilution trends in ion concentrations: thus, the observed decrease in ion concentrations of the subglacial water is consistent with a decrease in the calculated residence time values.

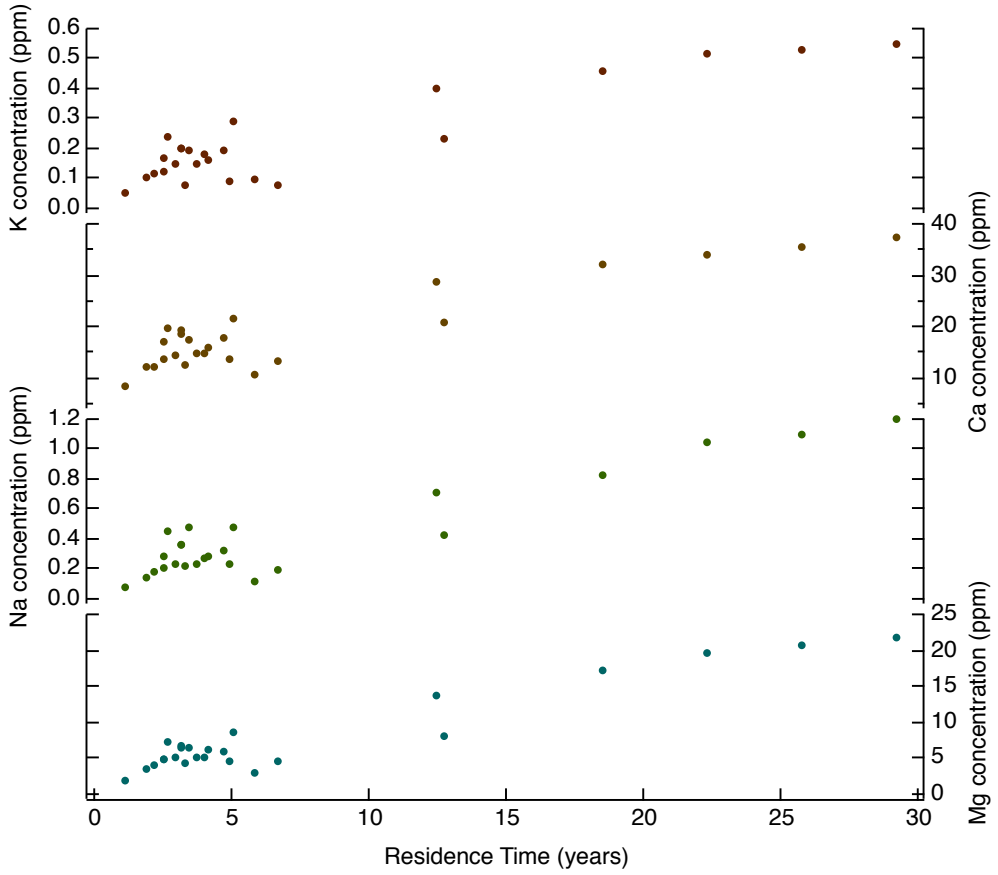

Figure 3.5. Changes in major cation concentrations (K, Ca, Na, and Mg). Cation measurements are plotted against our calculated residence time values for the Athabasca Glacier subglacial water.

3.6.1.2. Positive degree days and residence times

Evolution of the subglacial hydrology is commonly associated with seasonal melting, and our calculated residence time values compare well with regional meteorological climate data (Canada National Climate Archive, 2013) based on the simple positive degree days (PDD), temperature index we calculated for the Athabasca Glacier (Arendt et al., *In Revision*). Because PDD is associated with seasonal melt that corresponds to minimum transit time estimates

obtained from dye trace studies (Behrens, 1975; Collins, 1982), the 'low' overall average residence times calculated from the technique presented here should correspond to high PDD values as the increase in 'new' melt would dilute the age of the average meltwater. Our measurements in May and July show an inverse relationship between residence time and PDD values (Figure 3.6). We found that our residence time values in May agree with the seasonal increase of PDD greater than zero and the beginning of the subglacial melt season. During July, the temperature, PDD and the volume of melt water discharged increased, indicating that the subglacial system was dominated by fast-flow dynamics. These July observations are consistent with a lowered subglacial water residence time, which is supported by the calculations performed in this study.

3.6.1.3. Channel switching, residence times, and transit times

We acknowledge that the measured subglacial water residence times at the Athabasca Glacier are significantly longer by several orders of magnitude than model results and those measured using dye-trace techniques for similarly sized glaciers (Baker, 1982; Bartholomew et al., 2010; Burkimsher, 1983; Collins, 1982; Nienow, 1993). Only one estimate of 2.2 years for the Sermeq Avannarleq flowline in Greenland is in the same order of magnitude as our calculated values (Colgan et al., 2011). However, this method is the first to quantitatively measure the average subglacial water residence time using high precision isotopic measurements, taking into consideration the residence time value of a mixture of both slow and fast flow processes, as the (^{222}Rn) provides a mean flux rate for the entire flow path and [^{234}U] and (^{234}U/^{238}U) measurements integrate input values throughout the flow path. Slow flow subglacial water is isolated from the rest of the network, potentially in the greater Icefield, subglacial lakes or karst

systems, causing extremely elevated chemical compositions. When mixed with the fast flow component, the mean residence time of subglacial water is elevated even if the fast-flow component is on the order of hour to days, as shown by dye tracer studies. The high bulk residence times may also be an indication that the slow-flow water masses have a large areal extent (e.g., are largely distributed), low water volumes, and high *f* (see section 2.3), which would skew the bulk residence time toward the residence time of the slow-flow waters.

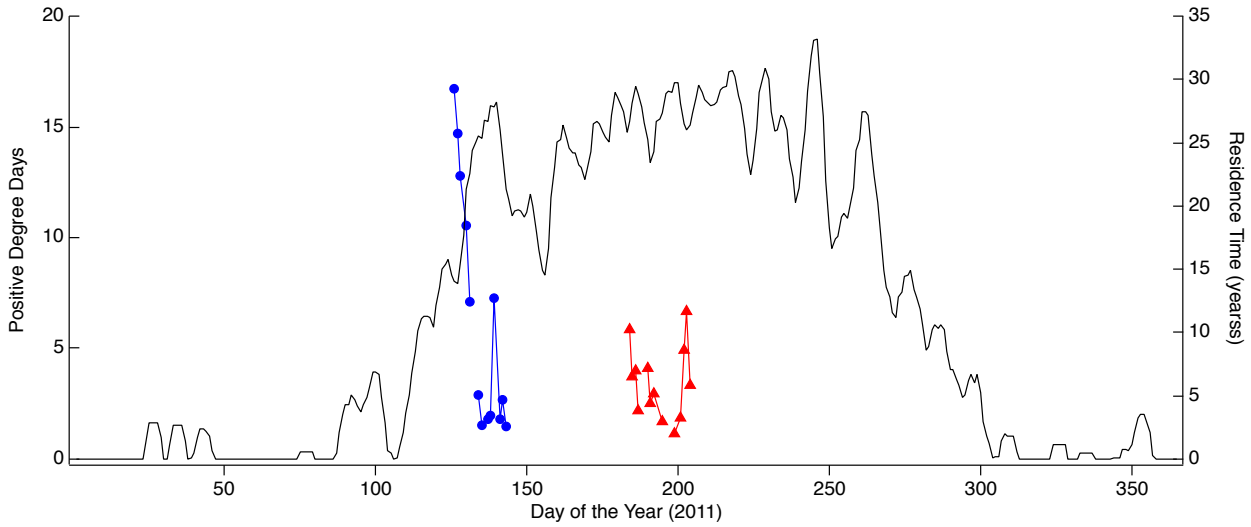

Figure 3.6: Athabasca Glacier residence times versus Positive Degree Days. Calculated residence time of discharged subglacial water from the Athabasca Glacier for May (blue circles) and July (red triangles) 2011 and positive degree days (black line) at the Athabasca Glacier. The PDD values used are 5-day averages compiled from temperature measurements taken at the Athabasca Glacier by the National Climate Data and Information Archive, Environment Canada (2013).

3.6.1.3.1. Reservoir volume

One way to assess the validity of our residence time model is to calculate the volume of water stored within the Athabasca Glacier subglacial system. In May, the glacial discharge represents delayed flow with old melt water mixed with a small amount of new snowmelt: approximately 33% ice melt, 44% snowmelt, and the remaining 23% summer precipitation in the beginning of

May as calculated in Arendt *et al.* [2015]. Because melt pathways from the supraglacial system have not yet connected to the subglacial system early in the melt season, the basal melt rate in May should represent the total ice melt discharge. Hence, the measured discharge at the beginning of May multiplied by the fraction of discharge from ice melt is a good approximation for the subglacial melt flux.

We assess the feasibility of the residence time of subglacial water in early May, equal to 29.3 years when the average discharge is low at 4.8 x 10^{-3} m^3 s^{-1}, by calculating the volume of old meltwater stored beneath the Athabasca Glacier, or reservoir size, before it is discharged using a simple box model. In these equations we assume that the Athabasca Glacier is in discharge steady-state, where the meltwater volume generated is equal to the meltwater volume discharged in each month.

$$t_{mean} = \frac{volume_{subglacial}}{flux} \quad \text{(eq. 13)}$$

and

$$volume_{subglacial} = area_{glacier} + depth_{water} \quad \text{(eq. 14)}$$

where t_{mean} represents the average subglacial water residence time, $volume_{subglacial}$ represents the average volume of water stored in the subglacial system, and flux is the average volume of water discharged from the subglacial system. In the instance where the subglacial melt is represented by only the fraction of discharge from ice melt, the average meltwater volume approximation in the subglacial system is 1.4 x 10^{-3} km^3 and an average depth of ~ 17 cm if the network is evenly distributed. In the instance where 100% of the total discharge is derived from the subglacial system, the average meltwater volume approximation in the subglacial system is 4.5 x 10^{-3} km^3 and an average depth of ~ 50 cm if the network is evenly distributed. Two possibilities can

account for the size of the reservoir beneath the Athabasca Glacier: 1) a shallow unevenly distributed system with pockets of old meltwater that are several meters deep and dispersed within the subglacial system, or 2) a shallow unevenly distributed system with the presence of a deep (~10 m) subglacial lake. Both of these scenarios are reasonable based on what is known about the subglacial hydrologic system of alpine glaciers (Anderson, 2003; Bartholomaus, 2011; Capps et al., 2010; Collins, 1979; Hubbard and Nienow, 1997). Thus, these subglacial reservoir volume estimations provide further support for the validity of our residence time model.

3.6.1.4. Transit time versus residence time

The differences between our large calculated residence times and the typical residence time estimates indicate a large disparity between surface-to-base transit time and the residence time of water in the subglacial system produced by *in situ* basal melt. The large residence times are consistent with the subglacial environment maintaining a complex structure that includes both distributed (slow-flow) and high-discharge (fast-flow) channels. Our method accounts for the length of time between when *in situ* basal water enters the subglacial system and when it exits, a parameter not measureable using external tracers, and is in agreement with recent models depicting glacial variations with seasonal forcing (Creyts and Schoof, 2009; Mitchell and Brown, 2007, 2008; Pimentel and Flowers, 2011; Schoof, 2010; Sundal et al., 2011; Tranter et al., 2005).

Transition from a slow-moving distributed drainage system to a fast-moving channelized system (Figure 3.1a, b, c) over a complete melt season has been quantitatively modeled to occur over a period of ~25 days (Creyts and Schoof, 2009; Pimentel and Flowers, 2011; Schoof, 2010), but these step-function models have not been constrained by quantitative chemical measurements.

Time-series chemical measurements have shown that the pH, total alkalinity and ion presence in bulk melt water follow trends throughout a melt season that correlate to the evolution of subglacial drainage pathways (Richter and Goldberg, 2003; Sharp, 1999). Furthermore, multi-parameter models (Richards et al., 1996) have incorporated these basic chemical measurements to place initial constraints on understanding subglacial evolution. Our study expands upon what is already known about subglacial drainage and is in agreement with the timing of the initial subglacial transitions. In accordance with our measurements and calculated residence times (Tables 3.1 and 3.3), we infer that in late July the Athabasca Glacier subglacial system had evolved to high channelization toward the terminus but still maintained a steady contribution of slow flow water up-glacier, an observation noted by other field studies (Bhatia et al., 2011; Marston et al., 1991; Moorman, 2003) and predicted in models (Creyts and Schoof, 2009; Pimentel and Flowers, 2011; Schoof, 2010), including our own independent stable isotope mixing model (Arendt et al., In Revision).

3.6.1.4.1. Comparison with dye-trace studies

The absolute values of the residence times calculated here provide additional context to results of dye-tracing experiments (Collins, 1982; Nienow, 1993; Seaberg, 1988). The time measured by dye-tracing studies is the absolute minimum time required for water to be discharged from the surface to the subglacial system. Our results indicate there are longer periods of time in which subglacial water can be stored, which is consistent with studies in which the dye is partially or never recovered (Moorman, 2003; Nienow et al., 1998; Schuler, 2002; Seaberg, 1988). Combining our method with dye-tracing studies can provide insight into both the minimum and average length of time that meltwater is stored in the subglacial system, thereby placing

additional constraints on subglacial hydrologic flow paths and the timescale of water storage. Our study newly quantifies the subglacial residence time using U-series isotopic analysis to establish the large array of potential maximum residence times. One way of placing more constraints on the range of residence times would be sampling during the end of a melt season (October-November) when the presence of snowmelt dilution is non-existent and surface melt should cease. In addition, this method should be applied to a variety of field sites to gain a better understanding of subglacial water storage in different glacial environments.

3.7. CONCLUSIONS

Our study provides a unique insight on the behavior of U-series isotopes in the subglacial system, the storage time of subglacial water and a quantitative means to estimate the average subglacial water residence times based on radioactive chemical measurements. Isolating at least two U-series daughter products with similar recoil characteristics in a subglacial system can be used to determine the average residence time of subglacial water from input to output in the subglacial drainage network. The application of both ^{234}U and ^{222}Rn daughter isotopes minimizes potential caveats of our residence time equation. Our findings from the Athabasca Glacier indicate that the residence time of subglacial water are likely many orders of magnitude larger than previously thought – years instead of days. Synthesis of our technique with existing methodologies indicates that our new method accurately reflects the mean value of all of the water being flushed through the subglacial system, including variations caused by mixing associated with the seasonal evolution of the subglacial system. Assuming similar processes are acting on larger glaciers and ice sheets, this unique technique can be applied to determine the

average residence time of subglacial water inaccessible to other methods that purely determine transit time, such as tracer techniques that depend on surface to base water transport.

3.8 REFERENCES

Aciego, S.M., Bourdon, B., Schwander, J., Baur, H., Forieri, A., 2011. Toward a Radiometric Ice Clock: U-series Ages of the Dome C Ice Core. Quaternary Science Reviews 30, 2389-2397.

Anderson, R.S., Anderson, S.P., MacGregor, K.R., Waddington, E.D., O'Neel, S., Riihimaki, C.A., Loso, M.G., 2004. Strong feedbacks between hydrology and sliding of a small alpine glacier. Journal of Geophysical Research-Earth Surface 109, F03005.

Anderson, S.P., 2007. Biogeochemistry of glacial landscape systems. Annual Review of Earth and Planetary Sciences 35, 375-399.

Anderson, S.P., Longacre, S.A., and Kraal, E.R., 2003a. Patterns of water chemistry and discharge in the glacier-fed Kennicott River, Alaska: evidence for subglacial water storage cycles. Chemical Geology 202, 297-312.

Anderson, S.P., Walder, J.S., Anderson, R.S., Kraal, E.R., Cunico, M., Fountain, A.G., and Trabant, D.C., 2003b. Integrated hydrologic and hydrochemical observations of Hidden Creek Lake jo¨kulhlaups, Kennicott Glacier, Alaska. Journal of Geophysical Research 108.

Arendt, C.A., Aciego, S.M., Hetland, E., 2015. An open source Bayesian Monte Carlo isotope mixing model with applications in earth surface systems. Geochemistry, Geophysics, Geosystems, DOI: 10.1002/2014GC005683.

Arendt, C.A., Aciego, S.M., Sims, K.W.W., Robbins, M.J., 2014. Sequential separation of radioactive U, and radiogenic Nd and Hf concentrated from natural waters. Geostandards and Geoanalytical Research, DOI: 10.1111/j.1751-1908X.2014.00322.x.

Arnold, N., Richards, K., Willis, I., Sharp, M., 1998. Initial results from a distributed, physically based model of glacier hydrology. Hydrological Processes 12, 191-219.

Baker, D., 1982. A glacier discharge model based on results from field studies of energy-balance, water storage and flow. Hydrological Sciences Journal 27, 257.

Ball, L., Sims, K.W.W., Schwieters, J., 2008. Measurement of U-234/U-238 and Th-230/Th-232 in volcanic rocks using the Neptune MC-ICP-MS. Journal of Analytical Atomic Spectrometry 23, 173-180.

Bartholomaus, T.C., Anderson, R.S., Anderson, S.P., 2008. Response of glacier basal motion to transient water storage. Nature Geoscience 1, 33-27.

Bartholomew, I., Nienow, P., Mair, D., Hubbard, A., King, M.A., Sole, A., 2010. Seasonal evolution of subglacial drainage and acceleration in a Greenland outlet glacier. Nature Geoscience 3, 408-411.

Behrens, H., Bergmann, H., Moser, H., Rauert, W., Stichler, W., Ambach, W., Eisner, H., and Pessel, P., 1975. Study of the discharge of Alpine glaciers by means of environmental isotopes and dye-tracers, Snow and Ice Symposium. IAHS-AISH, Moscow.

Bell, R.E., Studinger, M., Shuman, C.A., Fahnestock, M.A., and Joughin, I., 2007. Large subglacial lakes in East Antarctica at the onset of fast-flowing ice streams. Nature 445, 904-907.

Bhatia, M.P., Das, S.B., Kujawinski, E.B., Henderson, P., Burke, A., Charette, M.A., 2011. Seasonal evolution of water contributions to discharge from a Greenland outlet glacier: insight from a new isotope-mixing model. Journal of Glaciology 57.

Bottrell, S.H., Tranter, M., 2002. Sulphide oxidation under partially anoxic conditions at the bed of the Haut Glacier d'Arolla, Switzerland. Hydrological Processes 16, 2363-2368.

Brown, G.H., 2002. Glacier meltwater hydrochemistry. Applied Geochemistry 17, 855-883.

Brugmann, M.M., Demuth, M.N., 1994. Surface and basal topography of the Athabasca Glacier: a glaciological interpretation and recommendation for the location of near-ice interpretive facilities. National Hydrology Research Institute, Saskatoon.
Burkimsher, M., 1983. Investigations of glacier hydrological systems using dye tracer techniques: observations at Pasterzengletscher, Austria. Journal of Glaciology 29, 403-416.
Butler, D., 1980. Shallow core snow chemistry of Athabasca Glacier, Alberta. Canadian Journal of Earth Sciences 17, 278-281.
Canada National Climate Archive, 2013. National climate data and information archive. National Climate Data Center.
Carter, S.P., Blankenship, D.D., Peters, M.E., Young, D.A., Holt, J.W., and Morse, D.L., 2007. Radar-based subglacial lake classification in Antarctica. Geochemistry Geophysics Geosystems 8.
Chandler, D.M., Wadham, J.L., Lis, G.P., Cowton, T., Sole, A., Bartholomew, I., Telling, J., Nienow, P., Bagshaw, E.B., Mair, D., Vinen, S., and Hubbard, A., 2013. Evolution of the subglacial drainage system beneath the Greenland Ice Sheet revealed by tracers. Nature Geoscience 6, 195-198.
Cheng, H., Edwards, R.L., Hoff, J., Gallup, C.D., Richards, D.A., Asmerom, Y., 2000. The half-lives of uranium-234 and thorium-230. Chemical Geology 169, 17-33.
Cochran, J.K., Masque, P., 2003. Short-lived U/Th series radionuclides in the ocean: Tracers for scavenging rates, export fluxes and particle dynamics. Reviews in mineralogy and geochemistry 52, 461-492.
Colgan, A., Rajaram, H., Anderson, R., Steffen, K., Phillips, T., Joughin, I., Zwally, H.J., Abdalati, W., 2011. The annual glaciohydrology cycle in the ablation zone of the Greenland ice sheet: Part 1. Hydrology model. Journal of Glaciology 57, 697-709.
Collins, D.N., 1979. Quantitative determination of the subglacial hydrology of two Alpine glaciers. Journal of Glaciology 23, 347-369.
Collins, D.N., 1982. Flow-routing of meltwater in an alpine glacier as indicated by dye tracer tests. Beitrage zur Geologie der Schweiz-Hydrologie 28, 523-534.
Creyts, T.T., Schoof, C.G., 2009. Drainage through subglacial water sheets. Journal of Geophysical Research 114, F04008.
Cuffey, K.M., Paterson, W.S.B., 2010. Physics of Glaciers. Academic Press.
DePaolo, D.J., Maher, K., Christensen, J.N., McManus, J., 2006. Sediment transport time measured with U-series isotopes: Results from ODP North Atlantic drift site 984. Earth and Planetary Science Letters 248, 394-410.
Dosseto, A., Bourdon, B., Turner, S.P., 2008. Uranium-series isotopes in river materials: Insights into the timescales of erosion and sediment transport. Earth and Planetary Science Letters 265, 1-17.
Durridge Company, I., 2009. RAD7 Radon Detector, 7 Railroad Avenue, Suite D, Bedford, MA 01730.
Esat, T.M., Yokoyama, Y., 2006. Variability in the uranium isotopic composition of the oceans over glacial–interglacial timescales. Geochimica et Cosmochimica Acta 70, 4140-4150.
Fahnestock, M.A., Joughin, I., Scambos, T.A., Kwok, R., Krabill, W.B., and Gogineni, S., 2001. Ice-stream-related patterns of ice flow in the interior of northeast Greenland. Journal of Geophysical Research: Atmospheres 106, 34035-34045.
Fairchild, I.J., Kilawee, J.A., Hubbard, B., 1998. Interactions of calcareous suspended sediment

with glacial meltwater: a field test of dissolution behaviour. Chemical Geology 155, 243-263.
Flowers, G.E., Clarke, G.K.C., 2002a. A multicomponent coupled model of glacier hydrology - 1. Theory and synthetic examples. Journal of Geophysical Research-Solid Earth and Planets 107, 2287.
Flowers, G.E., Clarke, G.K.C., 2002b. A multicomponent coupled model of glacier hydrology - 2. Application to Trapridge Glacier, Yukon, Canada. Journal of Geophysical Research-Solid Earth and Planets 107, 2288.
Ford, D.C., Smart, P.L., and Ewers, R.O., 1983. The physiography and speleogenesis of Castleguard Cave, Columbia Icefields, Alberta, Canada. Arctic and Alpine Research 15, 437-450.
Fountain, A.G., Walder, J.S., 1998. Water flow through temperate glaciers. Reviews of Geophysics 36, 299-328.
Fricker, H.A., Scambos, T., Bindschadler, R., and Padman, L., 2007. An active subglacial water system in West Antarctica mapped from space. Science 315, 1544-1548.
Garde, S., Garcia, A.E., Pratt, L.R., Hummer, G., 1999. Temperature dependence of the solubility of non-polar gases in water. Biophysical Chemistry 78, 21-32.
Goldstein, S.J., Murrell, M.I., Nishiizumi, K., Nunn, A.J., 2004. Uranium-series chronology and cosmogenic Be-10-Cl-36 record of Antarctic ice. Chemical Geology 204, 125-143.
Hannah, D.M., Gurnell, A.M., 2001. A conceptual, linear reservoir runoff model to investigate melt season changes in cirque glacier hydrology. Journal of Hydrology 246, 123-141.
Hart, J.K., 2006. Athabasca Glacier, Canada - a field example of subglacial ice and till erosion? Earth Surface Processes and Landforms 31, 65-80.
Henderson, G., Hall, B.L., Smith, A., Robinson, L.F., 2006. Seawater ($^{234}U/^{238}U$) in lake water: A study in the Dry Valleys of Antarctica. Chemical Geology 226, 298-308.
Hooke, R.L., and Pohjola, V.A., 1994. Hydrology of a segment of a glacier situated in an overdeening, Storglaciaren, Sweden. Journal of Glaciology 40, 140-148.
Hubbard, B., Nienow, P., 1997. Alpine subglacial hydrology. Quaternary Science Reviews 16, 939-955.
Hubert, A., Bourdon, B., Pili, E., Meynadier, L., 2006. Transport of radionuclides in an unconfined chalk aquifer inferred from U-series disequilibria. Geochimica et Cosmochimica Acta 70, 5437-5454.
Hugenholtz, C., 2008. Large-scale moraine deformation at the Athabasca Glacier, Jasper National Park, Alberta, Canada. Landslides 5.
Joughin, I., Das, S.B., King, M.A., Smith, B.E., Howat, I.M., Moon, T., 2008. Seasonal speedup along the western flank of the Greenland Ice Sheet. Science 320, 781-783.
Kamb, B., Raymond, C.F., and Harrison, W.D., 1985. Glacier surge mechanism - 1982-1983 Surge of Variegated Glacier, Alaska Science 227, 460-479.
Kite, G.W., Reid, L.A., 1977. Volumetric change of the Athabasca Glacier over the last 100 years. Journal of Hydrology 32, 279-294.
Lane-Smith, D., Sims, K.W.W., 2013. The effect of CO_2 on the measurement of ^{220}Rn and ^{222}Rn, with instruments utilizing electrostatic precipitation. Acta Geophysica 61, 822-830, doi: 810.2478/s11600-11013-10107-11603.
Lopez, J.L., Temme, N.M., 2004. Multi-point Taylor expansions of analytical functions. Transactions of the American Mathematical Society 356, 4323-4342.
Maher, K., DePaolo, D.J., Christensen, J.N., 2006a. U-Sr isotopic speedometer: Fluid flow and

chemical weathering rates in aquifers. Geochimica et Cosmochimica Acta 70, 4417-4435.
Maher, K., Steefel, C.I., DePaolo, D.J., Viani, B.E., 2006b. The mineral dissolution rate conundrum: Insights from reactive transport modeling of U isotopes and pore fluid chemistry in marine sediments. Geochimica et Cosmochimica Acta 70, 337-363.
Marston, R., Pochop, L., Kerr, G., Varuska, M., Veryzer, D., 1991. Recent Glacier Changes in the Wind River Range, Wyoming. Physical Geography 12, 115-123.
Mitchell, A.C., Brown, G.H., 2007. Diurnal hydrological - physicochemical controls and sampling methods for minor and trace elements in an Alpine glacial hydrological system. Journal of Hydrology 332, 123-143.
Mitchell, A.C., Brown, G.H., 2008. Modeling geochemical and biochemical reactions in subglacial environments. Institute of Alpine and Arctic Research 40, 531-547.
Moorman, B.J., 2003. Glacier-permafrost hydrological interconnectivity: Stagnation Glacier, Bylot Island, Canada. Permafrost.
Morlock, S.E., Nguyen, H.T., Ross, J.H., 2002. Feasibility of Acoustic Doppler Velocity Meters for the Production of Discharge Records from U.S. Geological Survey Streamflow-Gaging Stations. USGS.
Murray, T., Clarke, G.K.C., 1995. Black-box modeling of the subglacial water system. Journal of Geophysical Research-Solid Earth and Planets 100, 2156-2202.
Naftz, D.L., Susong, D.D., Schuster, P.F., Cecil, L.D., Dettinger, M.D., Michel, R.L., Kendall, C., 2002. Ice core evidence of rapid air temperature increases since 1960 in alpine areas of the Wind River Range, Wyoming, United States. Journal of Geophysical Research-Atmospheres 107, 4171.
Nienow, P., Sharp, M., Willis, I., 1998. Seasonal changes in the morphology of the subglacial drainage system, Haut Glacier d'Arolla, Switzerland. Earth Surface Processes and Landforms 23, 825-843.
Nienow, P.W., 1993. Dye-tracer investigations og glacier hydrological systems. University of Cambridge, Cambridge, p. 337.
Paterson, W.S.B., 1964. Variations in velocity of Athabasca Glacier with time. Journal of Glaciology 5, 277-285.
Paterson, W.S.B., Savage, J.C., 1963. Geometry and movement of the Athabasca Glacier. Journal of Geophysical Research 68, 4513-4520.
Picolo, J.L., 1996. Absolute measurement of radon 222 activity. Nuclear Instruments & Methods in Physics Research 369, 452-457.
Pimentel, S., Flowers, G.E., 2011. A numerical study of hydrologically driven glacier dynamics and subglacial flooding. Proceedings of the Royal Society 467, 537-558.
Pogge von Strandmann, P.A.E., Burton, K.W., James, R.H., van Calsteren, P., Gialason, S.R., and Mokadem, F., 2006. Riverine behaviour of uranium and lithium isotopes in an actively glaciated basaltic terrain. Earth and Planetary Science Letters 251, 134-147.
Porcelli, D., Swarzenski, P.W., 2003. The behavior of U- and Th-series nuclides in groundwater. Uranium-Series Geochemistry 52, 317-361.
Price, S.F., Bindschadler, R.A., Hulbe, C.L. and Blankenship, D.D., 2002. Force balance along an inland tributary and onset to Ice Stream D, West Antarctica. Journal of Glaciology 48, 20-30.
Raiswell, R., 1984. Chemical Models of Solute Acquisition in Glacial Melt Waters. Journal of Glaciology 30, 49-57.
Raymond, C.F., et al., 1995. Hydrological discharges and motion of Fels and Black Rapids

Glaciers, Alaska, U.S.A.: implications for the structure of their drainage systems. Journal of Glaciology 41, 290-304.
Reynolds, J.R., Young, G.J., 1997. Changes in the areal extent, elevation, and volume of Athabasca Glacier, Alberta, Canada, as estimated from a series of maps produced between 1919 and 1979. Annals of Glaciology 24, 60-65.
Richards, K.S., Sharp, M., Arnold, N., Gurnell, A., Clark, M., Tranter, M., Nienow, P., Brown, G., Willis, I., Lawson, W., 1996. An integrated approach to modeling hydrology and water quality in glacierized catchments. Hydrological Processes 10, 479-508.
Richter, S., Goldberg, S.A., 2003. Improved techniques for high accuracy isotope ratio measurements of nuclear materials using thermal ionization mass spectrometry. International Journal of Mass Spectrometry 229, 181-197.
Rickli, J., Frank, M., Baker, A.R., Aciego, S.M., de Souza, G., Georg, R.B., Halliday, A.N., 2010. Hafnium and neodymium isotopes in surface waters of the eastern Atlantic Ocean: Implications for sources and inputs of trace metals to the ocean. Geochimica et Cosmochimica Acta 74, 540-557.
Schoof, C.G., 2010. Ice sheet acceleration driven by melt supply variability. Nature 468, 803-806.
Schuler, T., 2002. Investigation of water drainage through an alpine glacier by experiments and numerical modeling, Natural Sciences. Swiss Federal Institute of Technology Zurich, Zurich.
Seaberg, S.Z., Seaberg, J.Z., Hooke, R., Le, B., and Wiberg, D.W., 1988. Character of the englacial and subglacial drainage system in the lower part of the ablation area of Storglaciaren, Sweden as revealed by dye-trace studies. Journal of Glaciology 34, 217-227.
Semkow, T., 1991. Fractal Model of Radon Emanation from Solids. Physical Review Letters 66, 3012-3015.
Sharp, M., Brown, G.H., Tranter, M., Willis, I.C. and Hubbard, B., 1995. Comments on the use of chemically based mixing models in glacier hydrology. Journal of Glaciology 41, 241-246.
Sharp, M., Parkes, J., Cragg, B., Fairchild, I.J., Lamb, H. and Tranter, M., 1999. Wide spread bacterial populations at glacier beds and their relationship to rock weathering and carbon cycling. Geology 27, 107-110.
Skidmore, M., Anderson, S.P., Sharp, M., Foght, J., Lanoil, B.D., 2005. Comparison of microbial community compositions of two subglacial environments reveals a possible role for microbes in chemical weathering processes. Applied and Environmental Biology 71, 6986-6997.
Skwarzec, B., Borylo, A., Struminska, D., 2002. U-234 and U-238 isotopes in water and sediments of the southern Baltic. Journal of Environmental Radioactivity 61, 345-363.
Smart, C.C., 1983. The hydrology of Castleguard Karst, Columbia Icefields, Alberta, Canada. Arctic and Alpine Research 15, 471-486.
Smith, B.P.G., Hannah, D.M., Gurnell, A.M., Petts, G.E., 2001. A hydrogeomorphological context for ecological research on alpine glacial rivers. Freshwater Biology 46, 1579-1596.
Sundal, A.V., Shepherd, A., Nienow, P., Hanna, E., Palmer, S., Huybrechts, P., 2011. Melt-induced speed-up of Greenland Ice Sheet offset by efficient subglacial drainage. Nature 469, 522-U583.

Tranter, M., 2005. Geochemical weathering in glacial and proglacial environments. Surface and Groundwater, Weathering and Soils 5, 189-205.
Tranter, M., Huybrechts, P., Munhoven, G., Sharp, M.J., Brown, G.H., Jones, I.W., Hodson, A.J., Hodgkins, R., Wadham, J.L., 2002. Direct effect of ice sheets on terrestrial bicarbonate, sulphate and base cation fluxes during the last glacial cycle: minimal impact on atmospheric CO2 concentrations. Chemical Geology 190, 33-44.
Tranter, M., Skidmore, M., Wadham, J., 2005. Hydrological controls on microbial communities in subglacial environments. Hydrological Processes 19, 995-998.
Verbunt, M., Gurtz, J., Jasper, K., Lang, H., Warmerdam, P., Zappa, M., 2003. The hydrological role of snow and glaciers in alpine river basins and their distributed modeling. Journal of Hydrology 282, 36-55.
Vigier, N., Burton, K.W., Gislason, S.R., Rogers, N.W., Duchene, S., Thomas, L., Hodge, E., and Schaefer, B., 2006. The relationship between riverine U-series disequilibria and erosion rates in a basaltic terrain. Earth and Planetary Science Letters 249, 258-273.
Wadham, J.L., Bottrell, S., Tranter, M., Raiswell, R., 2004. Stable isotope evidence for microbial sulphate reduction at the bed of a polythermal high Arctic glacier. Earth and Planetary Science Letters 219, 341-355.
Wadham, J.L., Tranter, M., Dowdeswell, J.A., 2000. Hydrochemistry of meltwaters draining a polythermal-based, high-Arctic glacier, south Svalbard: II. Winter and early Spring. Hydrological Processes 14, 1767-1786.
Walder, J., 1982. Stability of sheet flow of water beneath temperate glaciers and implications for glacier sliding. Journal of Glaciology 28, 273-293.
Walder, J.S., 1986. Hydraulics of subglacial cavities. Journal of Glaciology 32, 493-445.
Wingham, D.J., Siegert, M.J., Shepard, A., and Muir, A.S., 2006. Rapid discharge connects Antarctic subglacial lakes. Nature 440, 1033-1036.
Zencich, S.J., Froend, R.H., Turner, J.V., Gailitis, V., 2002. Influence of groundwater depth on the seasonal sources of water accessed by Banksia tree species on a shallow, sandy coastal aquifer. Oecologia 131, 8-19.

CHAPTER IV

Greenland subglacial water residence times and proximal seawater U chemistry: Implications for seawater $\delta^{234}U$ on glacial-interglacial timescales

Official citation:

Arendt, C.A., Aciego, S. M., Sims, K.W.W., Das, S.B., Sheik, C., and Stevenson, E.I., 2015, Greenland subglacial water residence times and proximal seawater U chemistry: Implications for seawater $\delta^{234}U$ on glacial-interglacial timescales, *Earth and Planetary Science Letters*, *In Review*.
Reproduced within author's rights.

ABSTRACT

Climate reconstructions based on uranium-thorium (U/Th) dating techniques assume uranium (U) chemistry of seawater has remained stable over time despite notable fluctuations in major elemental compositions, concentrations, and isotopic compositions of global seawater over glacial-interglacial timescales. Here we investigate the influence of modern Greenland Ice Sheet (GrIS) meltwater on adjacent seawater U chemistry as a proxy to assess the potential influence of glacial melt on the $\delta^{234}U$ composition of global seawater on glacial-interglacial timescales. Deglaciation processes increase weathering, which subsequently increases the concentration and composition of the U flux to the world's oceans. Analysis of glacial discharge from multiple GrIS outlet glaciers reveals that meltwater runoff with long residence times (1074 years versus 12 to 266 years) have elevated U concentrations and compositions, which may increase the $\delta^{234}U$ of proximal seawater. We use a simple box model to scale these processes to periods of extreme deglaciation to examine the impact of glacial melt on global seawater $\delta^{234}U$.

To estimate seawater $\delta^{234}U$ compositions we account for U fluxes from the largest glacial catchments including the Greenland Ice Sheet, Antarctica, and large Northern Hemisphere Continental Ice Sheets and use variable (i) melt volumes, (ii) durations and (iii) U flux input rates based on modern subglacial water U concentrations and compositions. Results vary broadly due to the range of variables being considered, but all scenarios depict changes in seawater $\delta^{234}U$ compositions over glacial-interglacial timescales. These results supports the hypothesis that global seawater $\delta^{234}U$ is not constant through time and is altered by changes in U flux due to deglaciation.

4.1. INTRODUCTION

Substantial contribution of glacial melt to oceans occurs over sustained warming (interglacial) events (Esat and Yokoyama, 2006; Lambeck et al., 2002). Periods of deglaciation alter the relationship between elemental 'inputs' and 'outputs', where oceanic inputs may no longer be balanced by oceanic outputs (Henderson, 2002; Vance et al., 2009). If the radioactive elements of interest have long half-lives, this imbalance between input and output processes can cause a noticeable shift in seawater chemistry over glacial-interglacial timescales (Vance et al., 2009; Wortmann and Paytan, 2012).

The decay rates and oceanic residence times of ^{238}U and ^{234}U are longer than glacial-interglacial cycles (Cheng et al., 2000; Cochran and Masque, 2003). Thus, based on decay rates and oceanic mixing timescales, glacial melt is capable of altering seawater U chemistry over glacial-interglacial timescales (Esat and Yokoyama, 2006; Robinson et al., 2004). To influence the U

budget of the ocean, glacial melt input must have both a large flux of U and $\delta^{234}U$ distinctive from the seawater composition. For glacial meltwater to have elevated U concentrations and $\delta^{234}U$, the residence time of subglacial water must be long enough for an excess of ^{234}U relative to ^{238}U to accumulate from recoil processes (Arendt et al., 2015), and sufficient weathering must take place to establish a high baseline of ^{234}U and ^{238}U concentrations from dissolution processes. Therefore, glacial melt contributions should elevate seawater $\delta^{234}U$ if the melt volumes, weathering rates, residence times and associated $\delta^{234}U$ are heightened and the corresponding U concentrations are non-negligible. We postulate that if all these criteria are met, glacial meltwater U contributions to global seawater have the ability to alter seawater $\delta^{234}U$ over glacial-interglacial timescales.

We explicitly test the hypothesis that glacial melt influences seawater U chemistry by measuring the U chemistry of Greenland Ice Sheet glacial meltwater and the $\delta^{234}U$ of proximal seawater. To evaluate the conditions necessary (e.g. residence time) for glacial meltwater to impact seawater U chemistry, we apply a new chronometer (Arendt et al., 2015) to measure the residence time of subglacial water. Finally, to assess the influence of globally varying glacial melt water contributions on the $\delta^{234}U$ of seawater, we implement a box model to estimate the impact of significant U glacial melt contributions on seawater $\delta^{234}U$ during glacial-interglacial cycles.

4.2. BACKGROUND

4.2.1. Seawater U Chemistry

Glacial-interglacial cycles cause changes in major elemental fluxes, e.g. oxygen, within the ocean geochemical budget but cyclic changes in trace elements and metals such as strontium,

lead, osmium, iron, boron, sulfur, silicon and calcium isotopic composition of seawater remain the subject of debate (Blum and Erel, 1995; Hendry et al., 2012; Jones et al., 2002; The oceans' uranium (U) budget is generally thought to remain relatively stable over glacial-interglacial timescales: the U composition of global seawater is assumed to be uniform within 1% throughout the global oceans (Andersen et al., 2010; Gallup et al., 1994; Stirling et al., 1995). The oceans' U chemistry is presumed stable as the residence time of U in seawater is long (Chen et al., 1986; Cheng et al., 2000; Esat and Yokoyama, 2006): estimated to be in the range of 300-600 thousand years (Henderson and Anderson, 2003), relative to the mixing time of the world's oceans, estimated to be 100 thousand years (Veizer, 1989). Notable variations in seawater U chemistry in previous studies are attributed to local influences and/or diagenesis (Gallup et al., 1994; Stein et al., 1993). Previous studies have indicated the possibility of variable U flux, and $^{234}U/^{238}U$ activity ratios, to the world's oceans over time (Dunk et al., 2002; Henderson, 2002; Scholz et al., 2004; Villemant and Fleuillet, 2003), which would directly impact climate reconstructions based on U/Th dating (Esat and Yokoyama, 2006; Robinson et al., 2004). Constraints on the impact of U concentrations and compositions of glacial meltwater on seawater U chemistry and the variables that impact this influence should be explored in more detail.

The extent of seawater U chemical change depends on the chemical composition of glacial melt: U concentrations and $(^{234}U/^{238}U)_{ACT}$. If the $(^{234}U/^{238}U)_{ACT}$ composition of glacial meltwater, commonly referred to in $\delta^{234}U$ notation, is unique from seawater and the U flux is high enough, there is the possibility of eliciting a change in the $\delta^{234}U$ of seawater (Scholz et al., 2004; Villemant and Fleuillet, 2003). Here, we assess (i) U compositions of glacial meltwater from one of the largest ice sheets, the GrIS, (ii) the impact glacial melt has on proximal seawater U

chemistry, and (iii) investigate the magnitude of influence that changes in glacial melt U flux input has on seawater $\delta^{234}U$ on glacial-interglacial timescales using a seawater $(^{234}U/^{238}U)_{ACT}$ box model.

4.2.2. Subglacial U Chemistry

Subglacial meltwater residence time is the length of time meltwater is stored beneath glaciers and ice sheets while in direct contact with underlying substrate (e.g. bedrock, subglacial till). The U-series chemical signal of subglacial water is recorded purely from water-rock interaction time, which is the only source of U into the subglacial system (see Arendt et al., Submitted). The chemical method used in this manuscript to quantify the residence time of subglacial water is quantifying a different process than transit time approximations from dye-trace studies: i.e. transit time is the time it takes water/dye to be transferred from the surface to the base of the glacier and our residence time calculation accounts for the average length of time that the bulk water discharged has interacted with the underlying substrate. Subglacial meltwater can be stored for decades to tens of thousands of years before discharging from the subglacial system (Arendt et al., 2015; Bell, 2007). The residence time of subglacial water is linked to subglacial drainage processes and the corresponding hydrologic evolution of the subglacial system (Bhatia et al., 2011). These subglacial processes and consequent subglacial water residence times are the determining factors influencing the U chemistry of glacial melt (Arendt et al., 2015). Specifically, longer residence times correlate to higher elemental concentrations, excess ^{234}U and higher $\delta^{234}U$ values (Arendt et al., 2015). Depending on meltwater residence times, the large volume of glacial melt from rapid warming periods has the potential to inflate the U flux to global seawater. Therefore, in scenarios where the residence time of subglacial water is long and

the melt volume is large, the impact of this contribution to the overall composition of seawater may be significant.

Physical weathering in the subglacial system produces large quantities of small particles with high surface area to volume ratios (Anderson, 2005; Blum and Erel, 1995; Stevenson et al., In Review). These small particles with freshly exposed surfaces are easily subjected to chemical weathering (Anderson, 2005) and can enhance the U flux from glacial meltwater due to the increase in sediment surface area from which isotopes such as ^{234}U and ^{238}U can dissolve (Bonotto and Andrews, 2000). An additional increase in the U flux of glacial meltwater may come from the association of an increase in sediment surface area to an increase in recoil products (i.e. ^{234}U) (Pogge von Strandmann et al., 2006; Robinson et al., 2004). However, if the physical weathering rate is highly elevated, the baseline concentrations of ^{234}U and ^{238}U from dissolution may overwhelm the increase in ^{234}U from recoil: causing the associated increase in $\delta^{234}U$ to be negligible relative to the overall U concentrations (e.g. Arendt et al., Submitted). Further research is needed to explore the relationship between $\delta^{234}U$ and U concentrations in glacial environments, as few glacial meltwater systems have been characterized with respect to uranium chemistry.

4.3 FIELD LOCATIONS

The GrIS is the second largest ice mass in the world, containing both land and ocean terminating glaciers. Samples were collected from subglacial drainages directly at the terminus of GrIS outlet glaciers as well as from proximal seawater at varying depths ~20 km off of the Greenland coast at four distinct locations: Narsarsuaq, Ilulissat, Nuuk and Kulusuk (Figure 4.1 and Table

4.1). Additional details for each sample collection site, including specific GPS coordinates, are found in Table 4.1.

Table 4.1: Precise GPS coordinates and traditional water chemistry measurements: including percent dissolved oxygen, specific conductivity, total alkalinity, pH and salinity for each subglacial water and seawater sample collected at each field location.

Name	**Sample Type**	**Location**		**Date**	**Hydrochemistry**				
		Latitude	*Longitude*	*2013*	*%DO*	*SPC*	*pH*	*Total Alkalinity*	*Salinity (ppt)*
Narsarsuaq									
GNR-sw-230713	Seawater	61°05.401	45°25.374	7/23	148.1	22	9.60	7.6	21.9
GNR-ch-230713	Fjord	61°10.250	45°27.507	7/23	118.2	36616	8.14	84	22.9
GNR 240713	Subglacial Outflow	61°12.466	45°19.765	7/24	122.3	35066	8.14	89	0.0
Ilulissat									
GIL-072813-sw-A	Seawater	69°13.586	51°05.321	7/28	162.1	43724	8.28	81	27.6
GIL-072813-sw-B	Seawater	69°21.160	51°05.710	7/28	168.7	45527	8.30	77	28.9
GIL-072813-sw-C	Seawater	69°12.525	51°14.768	7/28	131.3	46328	8.13	72	29.0
GIL-SD-072913-surface-plume	Seawater Plume	68°53.135	50°20.980	7/29	156.7	37134	8.42	52	24.2
GIL-SD-072913-depth-plume	Seawater Plume	68°53.135	50°20.980	7/29	138.1	43530	8.16	68	27.2
GIL-SD-072813-subglacial	Subglacial Outflow	68°53.851	50°22.957	7/29	141.8	3.7	7.81	5.4	0.0
Nuuk									
GNU-080613-Toe	Subglacial Outflow	64°06.167	49°57.123	08/06	196.2	10.8	8.27	24.7	0.0
GNU-080713-Toe	Subglacial Outflow	64°06.167	49°57.123	08/07	140.3	15.9	8.11	10.6	0.0
GNU-080713-Surface	Surface Melt	64°00.367	49°18.269	08/07	119.4	1.1	5.36	12.5	0.0
GNU-080813-Toe	Subglacial Outflow	64°06.167	49°57.123	08/08	161.2	14.3	8.38	9.8	0.0
GNU-080913-Fjord-surface	Fjord Surface	64°03.599	51°23.514	08/09	119.6	46350	8.22	188	29.5
GNU-080913-Fjord-30depth	Fjord Depth	64°03.599	51°23.514	08/09	130.4	46961	8.18	196	29.9
GNU-080913-Fjord-90depth	Fjord Depth	64°03.599	51°23.514	08/09	136.7	47353	8.08	187	30.0
Kulusuk									
GKU-081113-Fjord A	Subglacial Outflow	65°42.597	38°27.524	08/11	116.7	15.2	8.51	6.2	0.0
GKU-081213-sw-35depth	Seawater	65°37.991	38°27.351	08/12	128	44091	8.21	73	27.6
GKU-081213-sw-surface	Seawater	65°37.991	38°27.351	08/12	128.6	36082	8.28	41	22.2
GKU-081213-Fjord A	Subglacial Outflow	65°42.597	38°27.524	08/12	107.7	25.2	7.82	6.2	0.0
GKU-081313-sw-35depth	Seawater	65°41.004	38°27.136	08/13	125.2	39163	8.22	61	24.0
GKU-081313-sw-surface	Seawater	65°41.004	38°27.136	08/13	122	20730	8.21	41	12.0
GKU-081313-Fjord A	Subglacial Outflow	65°42.597	38°27.524	08/13	111	10	8.50	4.8	0.0
GKU-081413-Fjord A-am	Subglacial Outflow	65°42.597	38°27.524	08/14	109.5	10.1	7.66	6.4	0.0
GKU-081413-Fjord A-pm	Subglacial Outflow	65°42.597	38°27.524	08/14	114.5	7.1	6.88	2.8	0.0
GKU-081513-sw-surface	Seawater	65°32.614	38°32.614	08/15	124.6	41387	8.22	63	25.7
GKU-081513-sw-30depth	Seawater	65°32.614	38°32.614	08/15	112.2	43439	8.20	83	27.2
GKU-081513-sw-90depth	Seawater	65°32.614	38°32.614	08/15	101.7	45468	8.19	101	28.7

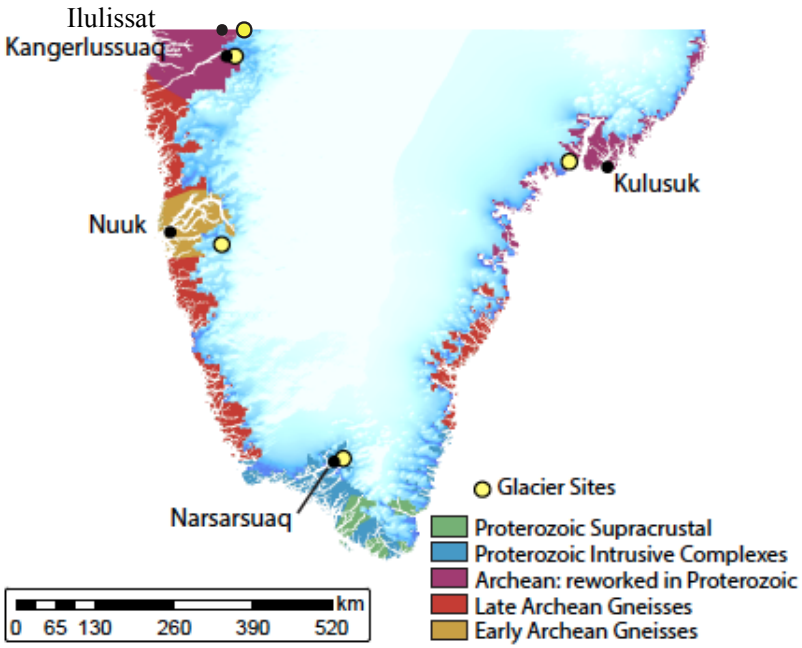

Figure 4.1: Location Map of subglacial water sampling sites in southern Greenland. Figure modified from (Aciego et al., 2015). Regional Geology of Southern Greenland with sampling sites indicated as yellow circles and the nearest towns labeled and represented as black dots.

4.3.1 Site Locations and Lithology

Outlet glaciers in this study are all located on unique bedrock of varying ages which provide distinctive chemical compositions of subglacial water draining from these locations (Aciego et al., 2015; Stevenson et al., 2015). Near Narsarsuaq, the outlet glacier subglacial water sampling site at the terminus of the Qoorqup Sermia is located at the southern tip of Greenland is located on the Proterozoic Garder Intrusive Complex while the body of the proximal ice sheet is primarily situated on top of granite/granodiorite (1.8 Ga) (Figure 4.1, Table 4.1). The sampling site for adjacent seawater is located off of the southern coast of Greenland at the intersection of the Labrador Sea and the Atlantic (Table 4.1). The Ilulissat outlet glacier subglacial water sampling site at the terminus of the 'fjord site' sampled in Bhatia *et al.* [2011] on the southwest coast of Greenland is located on Late Archean Gneiss that underwent metamorphosis in the

Proterozoic (Figure 4.1, Table 4.1). The sampling site for adjacent seawater is located off of the west coast of Greenland at the intersection of Baffin Bay and the Labrador Sea (Table 4.1). The outlet glacier subglacial water sampling site at the terminus of Kangaarsarsuup Sermia (~45 km from Nuuk) on the southwest coast of Greenland is located on a combination of Late Archean Gneiss and Proterozoic supracrustal bedrock, proximal to Amitsoq Gneiss (3.8 Ga) (Figure 4.1, Table 4.1). The sampling site for adjacent seawater is located off of the west coast of Greenland at the mouth of the Ameralik Fjord (Table 4.1). The Kulusuk outlet glacier subglacial water sampling site at the terminus of unnamed glacier – Glacier "G" (Aciego et al., 2015) - on the east coast of Greenland is located on a combination of Late Archean Gneiss and Proterozoic supracrustal bedrock, with the majority of the proximal GrIS margin situated atop Proterozoic Intrusives: mainly granite and granodiorite (Figure 4.1, Table 4.1). The sampling site for adjacent seawater is located in the open Atlantic Ocean (Table 4.1).

4.4. METHODS

4.4.1 Pre-Cleaning

All sample containers and tubing were pre-cleaned in an ISO 7 (class 10,000) clean laboratory prior to sample collection to minimize blanks: blanks from this study were negligible. Ultra-pure reagents were used for all cleaning and chemical separation (double distilled acids and >18.2 MΩ water). Ten liter collapsible polyethylene carboys (Thermo Fisher Hedwing) were cleaned using the procedure outlined in (Arendt et al., 2014).

4.4.2 Sample Collection

All subglacial water samples were collected mid-morning at the terminus of each glacier, within 10 m of the glacial terminus. All seawater samples were collected mid-afternoon approximately 30 km from each glacier at depths of 0 m, 10 m, and 25 m to ascertain homogenous values at varying mixing depths so the samples would be representative of the average seawater composition. Seawater was obtained using a PVC (RAL 7011) Niskin sampling bottle. Water samples were filtered onto Millipore Durapore® 0.22 μm GV membrane filters using a Masterflex modular peristaltic pump and a Perfluoroether (PFA) filtration unit (custom machined). One liter of >18.2 MΩ water was filtered through the system prior to filtration of samples.

4.4.3. Sample Analysis

4.4.3.1. Sample preparation

Each 10 L carboy sample underwent iron coprecipitation to reduce sample volume based on established procedures (Arendt et al., 2014; Rickli et al., 2010). Iron precipitates were transferred into a pre-cleaned 1 L LDPE Nalgene bottle for transport and storage. Final pre-concentration of the iron precipitate was accomplished in the clean laboratory by centrifuging samples, resulting in ~4 g of iron precipitate for digestion and column chemistry. Prior to column chemistry, seawater samples were rinsed 10 times with SQ water buffered with ammonia hydroxide to a pH of 9 (Auro et al., 2012) after final centrifugation to remove excess salts prior to digestion. All samples were treated twice with 1 mL of aqua regia to remove any organics that could compromise the ion exchange chromatography process. Uranium isotopic analysis was performed on the subglacial meltwater and seawater iron coprecipitation products using

established ion exchange chromatography techniques to isolate and concentrate U from samples (Aciego et al., 2009; Arendt et al., 2014).

4.4.3.2. Mass spectrometry

Uranium isotopic compositions were measured at the Wyoming High Precision Isotope Laboratory at the University of Wyoming on a Neptune PLUS ultra high-precision, high-sensitivity multi-collector inductively coupled mass spectrometer in 1 N HNO_3 (Ball *et al.* 2008, Sims *et al*. 2008). Uranium measurements were obtained in 10 cycles of 5 s integrations after 30 s of baseline measurements. Each U sample was bracketed with standard U010, diluted to a similar concentration as the samples (40 ppb) and a linear correction was applied for both mass fractionation and detector efficiency. SRM-960 U standards were run as external standards every five to ten samples. A total of 72 SRM-960 standard runs were completed alongside the $(^{234}U/^{238}U)_{ACT}$ sample measurements from August of 2011 to March of 2014, including four that underwent iron coprecipitation and column chemistry (Arendt et al., 2014). The reproducibility of these runs is presented in Arendt et al. (2014) with a long-term mean value of 0.9637± 10 compared to the accepted $(^{234}U/^{238}U)_{ACT}$ value for SRM-960 of 0.9631 ± 5 (Cheng et al., 2000). $(^{234}U/^{238}U)_{ACT}$ values were converted to the commonly referenced $\delta^{234}U$ notation using the following equation:

$$\delta^{234}U = \left((U_{234}/U_{238})_{ACT_{SW}} - 1\right) * 1000 \quad \text{(eq. 1)}$$

4.4.4. Residence Time Calculations

The subglacial water residence times were calculated using ^{222}Rn measurements and ^{234}U values derived from ^{238}U and $(^{234}U/^{238}U)_{ACT}$ measurements from each of the four GrIS outlet glacier

locations. These measurements were incorporated into the following age-relationship equation (Arendt et al., 2015):

$$t_{mean} = \frac{[U_{234}]}{(Rn_{222})}, \quad \text{(eq. 2)}$$

where $[U_{234}]$ is the concentrations of ^{234}U, (Rn_{222}) is the specific activity of ^{222}Rn using the decay rate of ^{222}Rn (-66.27 yr^{-1} using ^{222}Rn $t_{1/2}$ of 1.046 x 10^{-2} yr (Picolo, 1996)), and t_{mean} is the average residence time of the subglacial water. The equation was solved directly for t_{mean} to obtain the average length of time the meltwater discharged at the glacial terminus was in contact with underlying bedrock for each individual sample day. Additional details and the full derivation of the age-relationship equation used (eq. 1) can be found in Arendt et al. *(Submitted)*.

4.5. RESULTS

In situ measurements (including pH, and salinity), sample collection dates, and precise GPS coordinates for each sample are found in Table 4.1.

4.5.1. U-series Subglacial Water Measurements and Residence Times

The measured ^{222}Rn and ^{238}U concentrations and the $\delta^{234}U$ of the subglacial water sampled from GrIS outlet glaciers for each respective location (Narsarsuaq, Ilulissat, Nuuk, and Kulusuk) are presented in Table 4.2. Average U chemistry measurements and corresponding 2 SD for each subglacial water sample location are also presented in Table 4.2. Subglacial water $\delta^{234}U$ compositions are shown in Figure 4.2. Calculated residence times of subglacial water sampled from outlet glaciers of the GrIS for each respective location are listed below. Error in the

residence times of subglacial water is propagated based on 2 SD errors in the ^{222}Rn, ^{238}U and $\delta^{234}U$ (Table 4.2). Specific sample collection dates and locations are provided in Table 4.1.

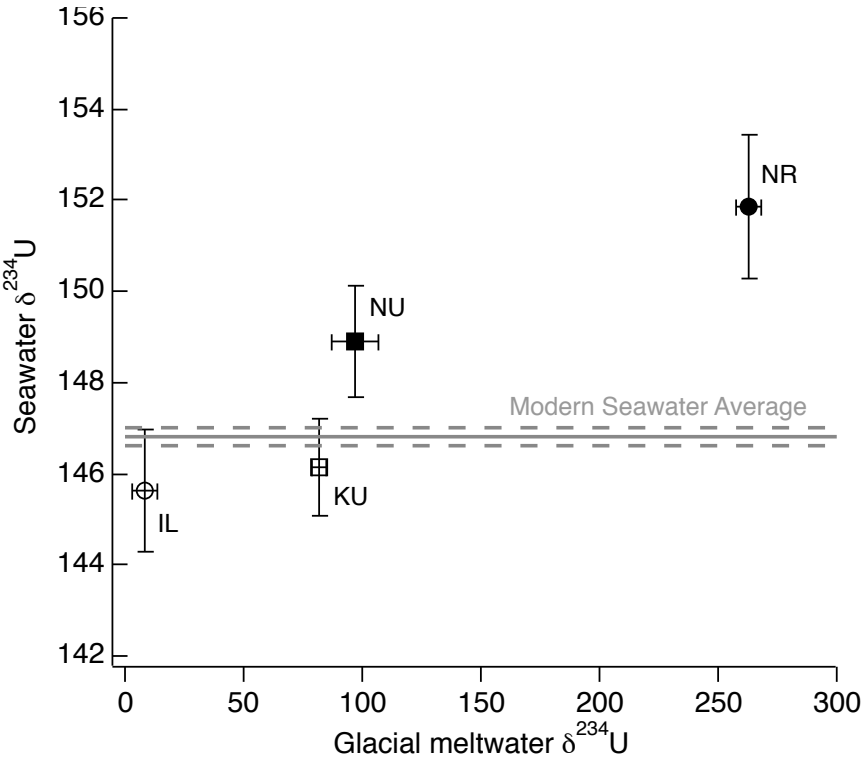

Figure 4.2: $\delta^{234}U$ measurements of glacial meltwater versus corresponding proximal seawater. Glacial meltwater samples were collected directly from each respective glacial terminus. $\delta^{234}U$ glacial meltwater and seawater measurements are plotted for Narsarsuaq (NR), Ilulissat (IL), Nuuk (NU) and Kulusuk (KU). Error bars indicate the range in measurements for multiple samples and duplicate (2-6) runs. The solid grey line is the accepted value for global seawater $\delta^{234}U$ of 146.8‰ and the dashed grey lines indicate the global seawater $\delta^{234}U \pm 2SD$ (Andersen et al., 2010).

The highest calculated subglacial water residence time was from Narsarsuaq and was ~1,074 ± 193 years. The lowest calculated subglacial water residence time was from Ilulissat and was ~12 ± 1 years. The calculated subglacial water residence times from Nuuk and Kulusuk averaged to ~266 ± 54 years over a 3-day sampling period and ~203 ± 35 years over a 4-day sampling

period, respectively. Only a singular residence time calculation was made for both Narsarsuaq and Ilulissat because of complications with the on-site filtration unit.

Table 4.2: U-series measurements from all GrIS sample locations. Sample location, sample type, average calculated residence time values, average ^{238}U concentrations and corresponding 2SD errors for subglacial water samples for each field location, and average $\delta^{234}U$ compositions and corresponding 2SD errors for subglacial water and seawater samples from each location.

Sample Location	Sample Type	Residence Time (years)	^{238}U (ppm)	2σ	$\delta^{234}U$ (‰)	2σ
Narsarssuaq	subglacial melt	1074 ± 193	0.123	0.071	263	5
Narsarssuaq	proximal seawater	–	–	–	152	2
Ilulisat	subglacial melt	12 ± 1	0.018	0.001	8	5
Ilulisat	proximal seawater	–	–	–	146	1
Nuuk	subglacial melt	266 ± 54	0.017	0.001	82	3
Nuuk	proximal seawater	–	–	–	146	1
Kulusuk	subglacial melt	203 ± 35	0.009	0.004	97	10
Kulusuk	proximal seawater	–	–	–	149	1

4.5.2. $\delta^{234}U$ Seawater Measurements

The $\delta^{234}U$ values, converted from $(^{234}U/^{238}U)_{ACT}$ as discussed in section 2.4, of the sampled subglacial water and Atlantic seawater adjacent to the GrIS outlet glaciers sampled for each respective location are presented in Figure 4.2 and Table 4.1. The $\delta^{234}U$ measurements from the Narsarsuaq coastal region were noticeably elevated compared to the other sampling locations, averaging 152‰. The $\delta^{234}U$ measurements off of the coasts of Ilulissat and Nuuk were comparable with the accepted $\delta^{234}U$ value of 146.8‰ for global seawater (Andersen et al., 2010) averaging 146‰. The $\delta^{234}U$ measurements off of the coast of Kulusuk were elevated from the accepted $\delta^{234}U$ for global seawater, averaging 149‰.

4.6. DISCUSSION

4.6.1. Spatial Subglacial Residence Time Comparisons

The calculated residence time of the southernmost drainage basin (NR) is significantly longer than the surrounding southern drainage basins. This extended subglacial water residence time (~ 1,074 years), may be indicative of the presence of established subglacial lake(s) draining very old water, or a tortuous path from the interior of the ice sheet. Samples from NR are most comparable to periods of extreme deglaciation as the highest modern mass loss in Greenland occurs in the drainage basin containing Narsarsuaq (Aciego et al., 2015). Low U concentration and U compositions correlate to locations with melting occurring closer to the ice sheet margin where residence times are lower (i.e. Nuuk), which should represent peak glacial conditions.

4.6.2. Subglacial Residence Time and Seawater Chemistry

We note that the calculated uranium residence times for these GrIS locations may be skewed if U loss occurs due to sorption onto sediments in the subglacial system (see Arendt et al., Submitted) However, an alternate dating method using helium-4 accumulation (Niu et al., In Review) was applied to samples collected from the same locations at the same time, confirms the magnitude of the timescales calculated from our U-series method.

The GrIS residence times calculated in this study appear to be linked to the U concentrations and $\delta^{234}U$ compositions of subglacial water, with elevated residence times corresponding to elevated U fluxes. The $\delta^{234}U$ of subglacial meltwater discharged into surrounding seawater has an impact on how glacial melt influences seawater $\delta^{234}U$: the seawater sampled near the Narsarsuaq outlet glacier with an elevated residence time had elevated $\delta^{234}U$. Drainage locations with longer

residence times have larger impacts on surrounding seawater chemistry. Thus, increased bed interaction time associated with longer residence times causes glacial runoff to have both elevated U concentrations and $\delta^{234}U$ compositions, which likely impact seawater U chemistry if the volumes of glacial runoff contributions are large enough relative to total seawater volume. Therefore, glaciated regions with long residence times, large melt volumes, and long melt seasons have the capacity to significantly impact seawater $\delta^{234}U$ compositions. In contrast, glaciated regions with short residence times, small melt volumes, and short melt seasons will most likely not have significant impacts seawater $\delta^{234}U$ compositions.

4.6.2.1. Seawater U chemistry and salinity

Numerous studies demonstrate the conservative relationship between uranium concentration and salinity of seawater (Andersen et al., 2007; Chen et al., 1986; Not et al., 2011; Shen and Dunbar, 1995). However, no obvious trends were visible in our seawater measurement relationships between $[^{238}U]$ and salinity, and $\delta^{234}U$ and salinity. We directly compared these relationships from our GrIS seawater measurements to measurements collected in the Arctic Ocean in Andersen et al. (2007) in Figure 4.3 to highlight the obvious deviation of our GrIS proximal seawater U chemistry and salinity relationships from expected trends. This lack of clear trends between seawater U chemistry and salinity may be attributed to advection anomalies in seawater mixing as indicated in a recent study by Owens et al., 2011.

The anticipated relationships between the U chemistry and salinity documented from previous studies (Andersen et al., 2007; Chen et al., 1986; Not et al., 2011; Schmidt and Reyss, 1991; Shen and Dunbar, 1995; Swarzenski et al., 1995) were not prominent in our GrIS proximal

seawater measurements as displayed in Figure 4.3. The Arctic Ocean samples from all locations demonstrate clear trends of increasing salinity with increasing U concentrations, and decreasing salinity with increasing δ234U compositions. Whereas, our GrIS proximal seawater samples do not follow these expected same trends (Figure 4.3).

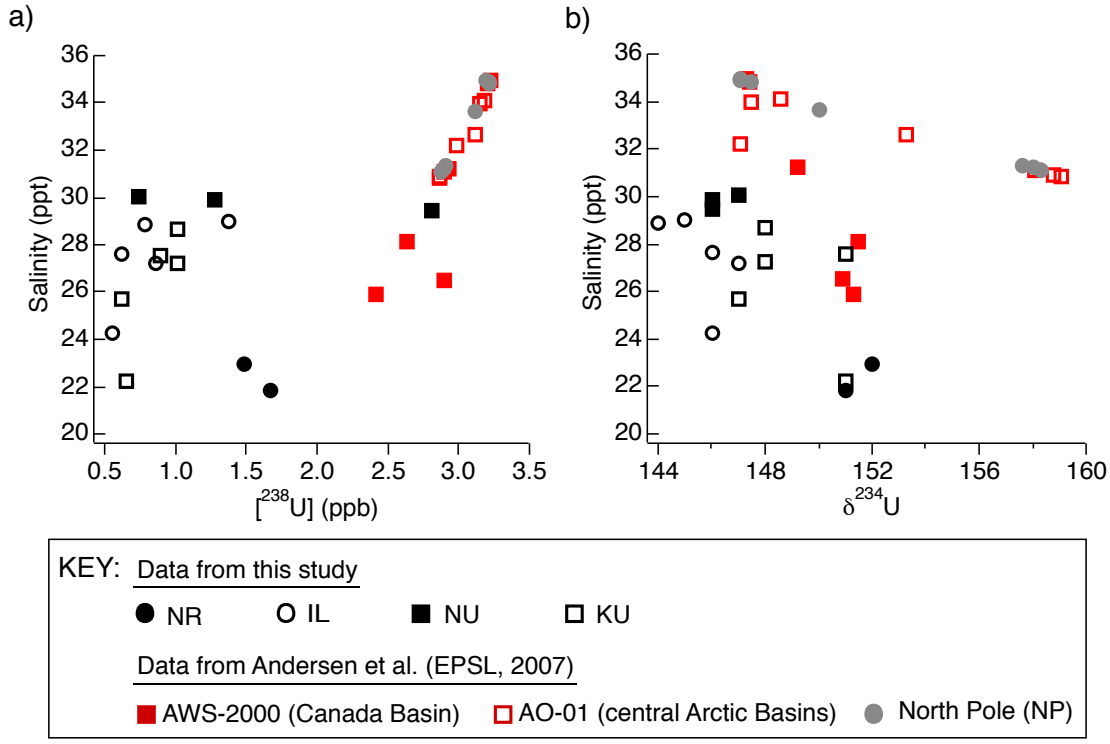

Figure 4.3: Uranium and salinity measurements of GrIS samples versus other Arctic samples. Direct comparison of the relationships between our GrIS seawater samples from Narsarsuaq (NR), Ilulissat (IL), Nuuk (NU), and Kulusuk (KU) to Arctic Ocean samples from the Canadian Basin, central Arctic Basins, and the North Pole (Andersen et al., 2007). Samples collected and measured in this study are all black: solid black circles indicate NR samples, open black circles indicate IL samples, solid black squares indicate NU samples, open black squares indicate KU samples. Samples previously published from Arctic Ocean samples (Andersen et al., 2007) are red and grey: solid red squares indicate AWS-2000 samples from the Canadian Basin, open red squares indicate AO-01 samples from central Arctic Basins, and solid grey circles indicate samples collected at the North Pole. a) Salinity versus [^{238}U] measurements. a) Salinity versus δ^{234}U measurements.

4.6.3. Seawater Box Model

To test the effects of large-scale glacial melting events on seawater U chemistry, we expand on a basic box model (Henderson, 2002) that incorporates U input (rivers, pore-water ^{234}U flux) and

U output (U removal in sediments and hydrothermal, net ^{234}U decay) values to seawater U composition. The original Henderson (2007) box model elicits an estimated constant seawater composition over the past 1000 ka (see figure 4a) with no notable fluctuations on glacial-interglacial timescales. With the addition of glacial melt as a separate excess ^{234}U activity relative to ^{238}U activity ($^{234}U_{xs}$), our model integrates glacial melt during glacial-interglacial periods based on our GIS U measurements and the Marine Isotope Stages (MIS) timescale (Figure 4.4). Because we utilize the same box model setup and parameters as Henderson (2002), all $^{234}U_{xs}$ inputs are entered in $(^{234}U/^{238}U)_{ACT}$ format and the resulting seawater U chemistry estimations are then converted to $\delta^{234}U$, using equation 1.

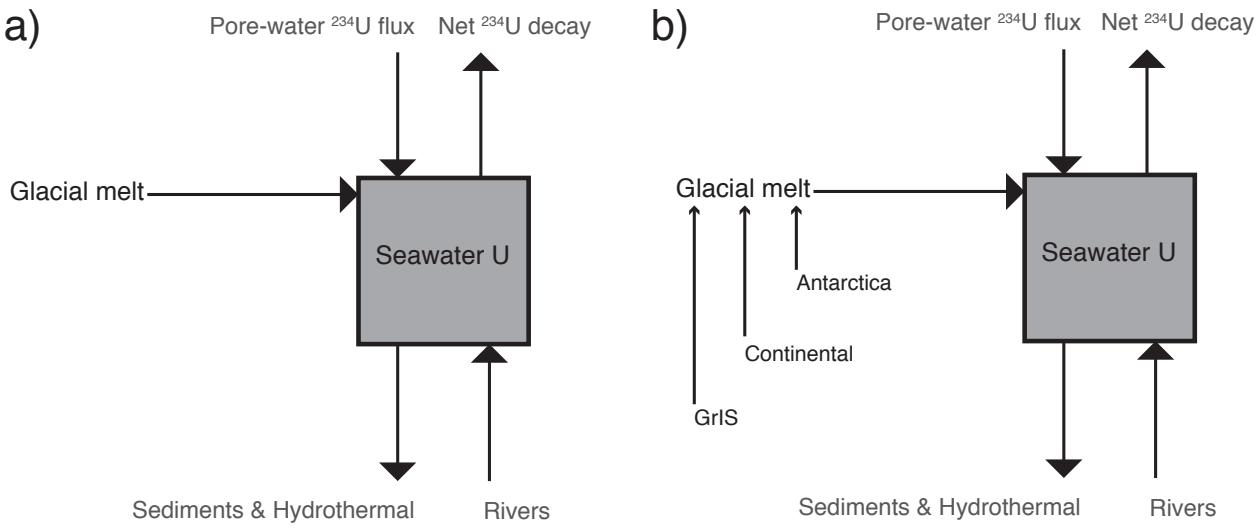

Figure 4.4: Seawater U-chemistry box model scenarios in this study. Basic box model schematic of the U budget of global seawater with U flux input (glacial melt, pore water flux, rivers) and output (U removal through sediment and hydrothermal interactions and net U decay) variables. a) Schematic of scenario that treats all glacial melt contributions as one source (e.g. scenario's 1-3). b) Schematic of scenario that identifies each glacial melt source as independent inputs of U flux (e.g. scenario's 4-10). Modified from (Henderson, 2002).

U flux values were taken directly from Henderson (2002). This model assumes a starting composition of (modern) seawater $(^{234}U/^{238}U)_{ACT}$ of 1.145 and is composed of 4.5×10^{15} g of

^{238}U. However, we update the starting (modern) seawater $(^{234}U/^{238}U)_{ACT}$ value to 1.1468, determined from a multitude of seawater samples collected from a series of oceanic locations (n = 21) representative of the global mean from Andersen et al., 2010. The net decay of ^{234}U from the world's oceans is 1.0 x 10^5 g yr^{-1} and U removal via interactions with sediments and hydrothermal processes is 1.2 x 10^{10} g yr^{-1} ^{238}U with $^{234}U_{xs}$ removal of 1.0 x 10^5 g yr^{-1}. Pore-water flux $^{234}U_{xs}$ inputs are 0.5 x 10^5 g yr^{-1} and U input from rivers is 1.2 x 10^{10} g yr^{-1} ^{238}U with a $^{234}U_{xs}$ of 1.5 x 10^5 g yr^{-1} ^{234}U. The model is run with the assumption that the residence times of ^{238}U and ^{234}U in seawater are 3.8 x 10^5 years and 1.8 x 10^5 years respectively (Henderson, 2002).

The $(^{234}U/^{238}U)_{ACT}$ composition of seawater is dependent on $^{234}U_{xs}$ activity values that are unsupported by ^{238}U activity inputs and outputs. The sum of these $^{234}U_{xs}$ activity input and output values is equal to 0 and does not alter the $(^{234}U/^{238}U)_{ACT}$ composition of seawater. To illicit change in the $(^{234}U/^{238}U)_{ACT}$ composition of seawater, we add in approximations of $^{234}U_{xs}$ activity flux values from glacial inputs using the direct subglacial melt U measurements observed at our four field locations in GrIS. The estimated reconstruction of $(^{234}U/^{238}U)_{ACT}$ compositions of seawater (calculating paleo seawater U chemistry) based on these variables is represented as the following equation.

$$(U_{234}/U_{238})_{ACT_{SW}} = \frac{\left[\left((U_{234})_{ACT_i}+\left[(U_{234})_{ACT_d}(t)\right]+\left[(U_{234})_{ACT_{ur}}(t)\right]-\left[(U_{234})_{ACT_r}(t)\right]-\left[(U_{234})_{ACT_{pw}}(t)\right]-\left[(U_{234})_{ACT_g}(t)\right]\right)+(U_{238})_{ACT_{SW}}\right]}{(U_{238})_{ACT_{SW}}}$$

(eq. 3)

Where $(U_{234}/U_{238})_{ACT_{SW}}$ is the ^{234}U-^{238}U activity ratio composition of seawater, $(U_{234})_{ACT_i}$ is the initial ^{234}U activity of seawater, $(U_{234})_{ACT_d}$ is the ^{234}U activity output from ^{234}U net decay,

$(U_{234})_{ACT_{ur}}$ is the ^{234}U activity removal output from interactions with sediment and hydrothermal vents, $(U_{234})_{ACT_r}$ is the ^{234}U activity input from river systems, $(U_{234})_{ACT_{pw}}$ is the ^{234}U activity input from pore-water flux interactions, $(U_{234})_{ACT_g}$ is the ^{234}U activity input from glacial systems, $(U_{238})_{ACT_{SW}}$ is the ^{238}U activity of seawater, and (t) is time in years. The model was used to reconstruct seawater $(^{234}U/^{238}U)_{ACT}$ compositions from the modern through marine isotope stage (MIS) 28, approximately 1,000 ka based on the timescale reconstructions of (Lisiecki and Ramo, 2005). Once$(U_{234}/U_{238})_{ACT_{SW}}$values for each scenario were obtained, they were converted to δ^{234}U using equation 1.

In this model we input differing glacial melt volume contributions to seawater during glacial-interglacial periods. Sea ice and iceberg melt volumes are not included in our glacial melt volume estimations as these melt volumes do not spend significant time interacting with underlying bedrock where glacial melt accrues both uranium concentration and enriched ^{234}U compositions and thus have negligible U input (Aciego et al., 2009). During the LGM, Jones et al. (2002) estimated total global (rivers and glacial melt) runoff of 2400 km^3 yr^{-1}, with total global glacial runoff (excluding sea ice and icebergs) of 1200 km^3 yr$^{-1,}$ establishing a 1:1 ratio for river to glacial melt input during the LGM. These global LGM volume approximations are applied for all glacial periods in this box model (MIS 2, MIS 4, MIS 6, MIS 8, etc.…). Because the box model from Henderson (2002) assumed that U flux from river contributions to the world oceans remained constant over glacial-interglacial periods, we also assume the volume contribution from rivers remained constant. However, the glacial runoff volume contributions do not remain constant on glacial-interglacial timescales, with total global glacial runoff values estimated at 10,600 km^3 yr^{-1} during interglacial periods (Jones et al., 2002). The modified box

model uses glacial meltwater to river contribution ratios of 1:1 and 8:1 for glacial and interglacial periods respectively, as estimated by Jones et al., 2002, unless otherwise noted.

The calculated seawater $\delta^{234}U$ compositions from the box model presented in this study for the past one million years are calculated using glacial melt input components with various U fluxes and timescales. The model incorporates glacial melt associated $^{234}U_{xs}$ values from both an average ice mass (Figure 4.4a) and separate Antarctic, GrIS, and Northern Hemisphere Continental Ice Sheet melt sources (Figure 4.4b).

4.6.4. Box Model Scenarios

To test an extensive range of possible scenarios that may alter seawater $\delta^{234}U$, we ran our box model using a wide variety of glacial parameters, presented in Table 4.3. We test scenarios where (i) all glacial melt is derived from one average source, (ii) glacial melt U chemistry remains constant on glacial-interglacial timescales, (iii) glacial melt U chemistry changes on glacial-interglacial timescales, (iv) differences exist in the volume contribution ratio of glacial melt to rivers, (v) glacial melt is derived from three independent ice masses, (vi) variations exist in the U chemistry of the differing glacial melt sources, (vii) variations exist in the volume contribution of the differing glacial melt sources, and finally (viii) variations exist in the duration of glacial-interglacial cycles. Detailed descriptions of the box model scenarios are available in Table 4.3. It should be noted that this box model predicts the $(^{234}U/^{238}U)_{ACT}$ values that would be measured in the modern from corals that grew in the past and not the actual seawater $(^{234}U/^{238}U)_{ACT}$ composition at the time of coral growth.

Scenarios 1a-b and 2a-b, based on the box model in Figure 4.4a, represent the simplest approach where all glacial melt is considered to be from one average global source (Figure 4.5a) and the [^{238}U] and $^{234}U_{xs}$ contribution values do not vary from glacial to interglacial timescales but remain constant with uranium chemistry values from our four GrIS sampling locations: IL, NR, NU and KU (Figure 4.5b). In these instances where glacial melt $\delta^{234}U$ estimations are left constant on glacial-interglacial timescales, the seawater $\delta^{234}U$ composition reaches equilibrium over time. However, based on observed U flux differences on even seasonal timescales (Arendt et al., In Review) the [^{238}U] and $^{234}U_{xs}$ values from glacial melt are likely to vary notably over glacial-interglacial timescales, with the different melt intensities associated with glacial versus interglacial periods. Therefore, in scenarios 1c and 2c, the meltwater contributions from the average glacial melt source has different [^{238}U] and $\delta^{234}U$ values on glacial-interglacial timescales: moderate fluctuations represented by NU-KU and extreme fluctuations in high/low values represented by IL-NR respectively (Figure 4.5c). In scenario 1c, all ice melt is represented as one average source with $^{234}U_{xs}$ values from NU and KU over glacial-interglacial cycles. In this scenario, seawater $\delta^{234}U$ decreases exponentially toward equilibrium at a seawater $\delta^{234}U$ composition of ~70‰ (Figure 4.5). In scenario 2c, all ice melt is represented as one average melt source with $^{234}U_{xs}$ values from IL and NR on glacial-interglacial cycles, in this scenario seawater $\delta^{234}U$ increases from present to the MIS 5/6 boundary where it reaches a maximum value of ~190‰ before decreasing toward equilibrium at a seawater $\delta^{234}U$ composition of ~130 (Figure 4.5).

The estimated glacial melt volume contribution to river contribution ratios on glacial-interglacial cycles in this box model were applied from Jones et al., 2002; where the glacial melt volume

contribution to river contribution ratio is 1:1 during glacial periods and 8:1 during interglacial periods (section 4.3). Because these ratios on interglacial timescales are only estimations, we

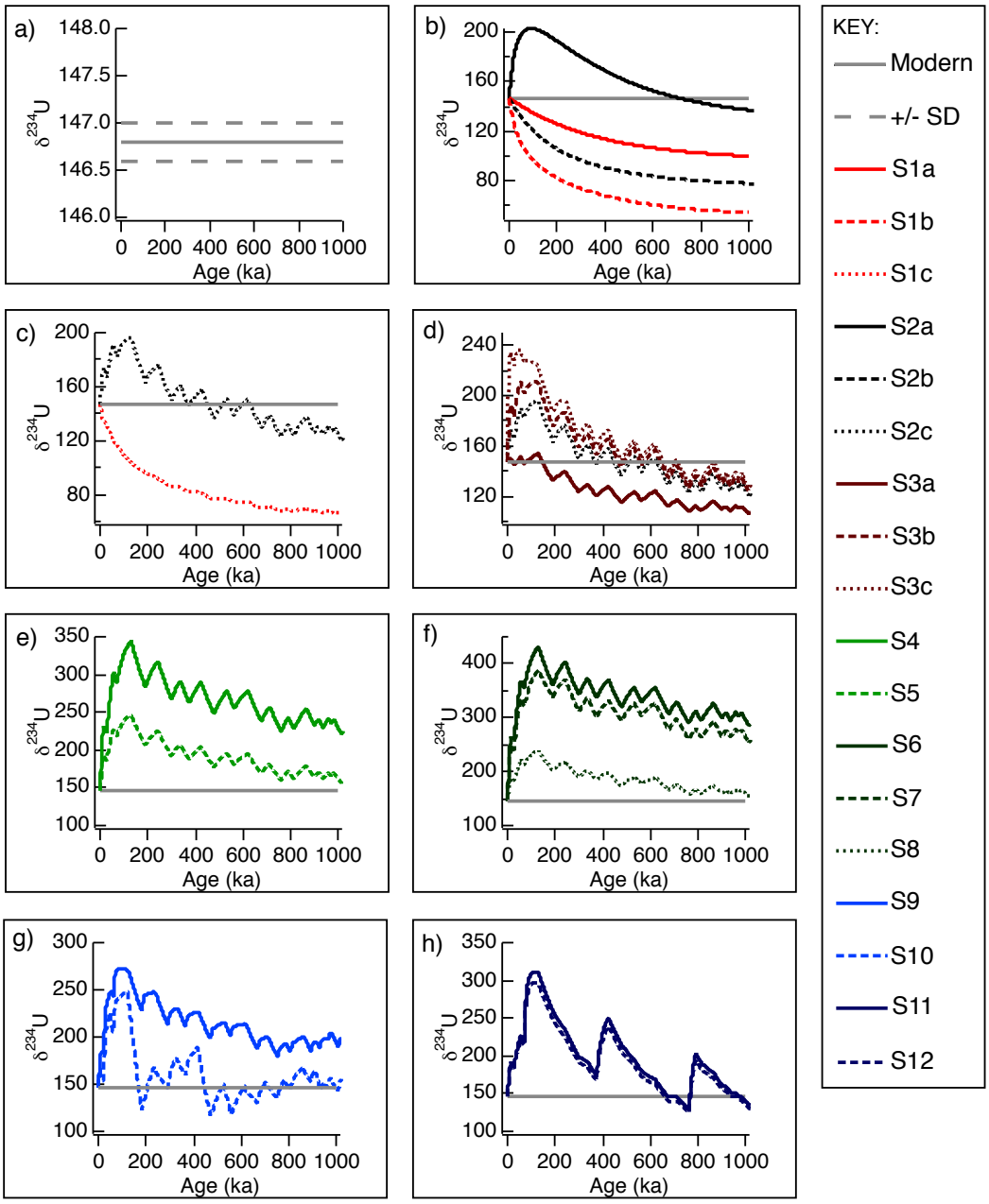

Figure 4.5: Box model seawater $\delta^{234}U$ composition estimation scenarios. Note the differing ranges in salinity on the x-axes. a) Original Henderson (2002) box model results where the solid grey line depicts the accepted constant seawater $\delta^{234}U$ composition over time, the dashed grey lines represent the accepted constant seawater $\delta^{234}U \pm 2SD$ (Andersen et al., 2007). b) Scenarios calculated from our GrIS measurements with one average glacial melt composition (Figure 4.4a) with constant glacial melt input concentrations, compositions, and volume contributions over glacial-interglacial cycles. The red lines depict scenarios 1a (NU) and 1b (KU), representing moderate estimations and the black lines depict

scenarios 2a (NR) and 2b (IL), representing extreme minimum/maximum input estimations. c) The dashed red line depicts moderate scenario 1c seawater $\delta^{234}U$ estimations with glacial melt input alternating between NU and KU input values on glacial and interglacial cycles respectively. The dashed black line depicts low/high scenario 2c seawater $\delta^{234}U$ estimations with glacial melt input alternating between IL and NR input values on glacial and interglacial cycles respectively. d) Box model seawater $\delta^{234}U$ composition estimations that incorporate glacial melt input for differing glacial melt volume input to river volume input ratios: 1:1(S3a), 20:1 (S3b), and 100:1 (S3c), along with the standard 8:1 from Jones et al. (2002) (S2c). The solid grey line depicts the accepted constant seawater $\delta^{234}U$ composition over time (Andersen et al., 2007). The maroon lines represent alternate glacial melt to river volume contribution estimations, and the black dashed line represents the standard 8:1 glacial melt to river volume contribution estimations. e) Box model seawater $(^{234}U/^{238}U)_{ACT}$ composition estimations that incorporate glacial melt for volume input ratios of three individual glacial melt contribution sources (Antarctica, GrIS, and Northern Hemisphere Continental Ice Sheets) (box model depicted in Figure 4.4b). The solid grey line depicts the accepted constant seawater $\delta^{234}U$ composition over time (Andersen et al., 2007). The solid green line depicts the scenario 5 where all glacial melt contributors have elevated $^{234}U_{xs}$ values. The dashed green line depicts the scenario 5 where all glacial melt contributors have lower $^{234}U_{xs}$ values. f) The solid dark green line depicts scenario 6 where the volume contribution from Antarctica is elevated in both glacial-interglacial period. The long-dashed dark green line depicts scenario 7 where the volume contribution from Northern Hemisphere Continental Ice Sheets is non-existent on interglacial timescales and moderate on glacial timescales. The short-dashed dark green line depicts scenario 8 where the volume contribution from Antarctica is minimized on both glacial-interglacial periods. The solid grey line depicts the accepted constant seawater $\delta^{234}U$ composition over time (Andersen et al., 2007). g) The solid blue and the dashed blue lines depicts scenarios 9 and 10, which are alterations of scenarios 5 and 8 respectively that have the glacial-interglacial timescales for the Northern Hemisphere Continental Icesheets are offset by 8 ka. The solid grey line depicts the accepted constant seawater $\delta^{234}U$ composition over time (Andersen et al., 2007). h) The solid dark blue and the dashed dark blue lines depicts scenarios 11 and 12, which are alterations of scenarios 5 and 8 respectively that have the same glacial-interglacial timescales for all ice masses but have nearly complete deglaciation occurrences during MIS 5, MIS 11, and MIS 19. The solid grey line depicts the accepted constant seawater $\delta^{234}U$ composition over time (Andersen et al., 2007).

altered the glacial melt volume contribution to river contribution ratio for interglacial periods in scenarios 3a-c, based on the box model presented in Figure 4.4a, to assess the impact these volume changes have on the magnitude of change on seawater $\delta^{234}U$ (Table 4.3, Figure 4.5). The glacial meltwater [^{238}U] and $\delta^{234}U$ contribution values for the changing river to glacial melt volume ratio scenarios are the IL and NR values used in scenario 2c. The interglacial ratios of 8:1, 20:1 and 100:1 all demonstrate an overall increasing trend from ~0-100 ka before switching to an overall decreasing trend (Figure 4.5). Yet the 1:1 interglacial ratio demonstrates an overall decreasing trend from 0-1000 ka. All volume ratio scenarios decrease toward equilibrium values

between 115‰ and 135‰, both of which are below the modern seawater $\delta^{234}U$ composition (Figure 4.5d). The magnitude of change in these estimated seawater $\delta^{234}U$ compositions is impacted by changes in source fractional contributions. However, during periods of deglaciation there are large increases in glacial melt contributions (Church et al., 2011; Gallup et al., 1994; Lambeck et al., 2002), suggesting that box model results from scenario 3a with a 1:1 ratio is an unlikely representation of past seawater $\delta^{234}U$. Furthermore, the likelihood of the volume of glacial melt compared to river input to be on the scale of 100:1 (scenario 3c) is highly improbable with river volume contributions remaining at 1200 km3 yr-1. Additionally, because the trends and magnitude of seawater $\delta^{234}U$ reconstructions from box model scenario 2c (8:1 ratio) and 3b (20:1 ratio) are quite comparable (Figure 4.5) we chose to complete all further box model seawater $\delta^{234}U$ reconstruction scenarios using the 8:1 interglacial ratio estimated by Jones et al., 2002.

Scenarios 1c, 2c and 3 are more realistic approximations than scenarios 1a-b and 2a-b as they incorporate glacial melt change on glacial-interglacial cycles, however U chemistry subglacial water measurements from Antarctica (Henderson et al., 2006) and Northern Hemisphere alpine glaciers (Arendt et al., In Review) indicate that the primary ice sheets (GrIS, Antarctica and Northern Hemisphere Continental Ice Sheets) during glacial periods likely have U chemistry unique to each ice sheet. Thus, glacial melt U flux contributions should not be treated as one average source but as distinct sources with U chemistry values and volume contributions specific to each ice mass. Therefore, in the next model scenarios we separate the GrIS, Antarctica and Northern Hemisphere Continental Ice Sheets into three separate glacial melt sources with differing U chemistry and volume contributions in the remainder of the scenarios.

In scenarios 4 and 5 we separate individual ice masses and assign varying volume contributions and glacial meltwater $\delta^{234}U$ composition estimates to each (Figure 4.4b). Scenario 4 represents extreme 'minimum-maximum' U compositions and concentrations and scenario 5 represents 'moderate' U compositions and concentrations to test the impact these U chemistry changes have on the magnitude of change on seawater $\delta^{234}U$ over time (Table 4.3, Figure 4.5e). Although there is a noticeable difference in the magnitude of change of reconstructed seawater $\delta^{234}U$ values, the overall behavior of the estimated seawater $\delta^{234}U$ remains comparable; with an overall increasing trend from ~0-100 ka before switching to an overall decreasing trend (Figure 4.5e). Here we assume that U chemistry glacial melt values during interglacial periods to be elevated in isotopic compositions, therefore we apply the [^{238}U] and $\delta^{234}U$ values from scenario 4 to the remaining scenarios (6 to 10, Figure 4.5e-h).

General fractional volume contributions of 0.15 and 0.30 for Antarctica, 0.45 and 0.65 for the GrIS and 0.40 and 0.05 for Northern Hemisphere Continental Ice Sheets were applied over glacial and interglacial cycles respectively, which are based off of meltwater volumes estimated to occur during the present (interglacial) and the LGM (glacial) (Bamber et al., 2012; Church et al., 2011; Jones et al., 2002; Raiswell et al., 2005; Statham et al., 2008; Tranter, 2006). In scenarios 6-8 we input differing volume contributions from the three primary sources of glacial melt to test the impact these volume changes have on the magnitude of change on seawater $\delta^{234}U$ over time (Table 4.3, Figure 4.5f). Specifically, scenario 6 tests the occurrence of larger melt contributions from Antarctica relative to the other ice masses, scenario 7 tests the occurrence of no melt contributions from Northern Continental Ice Sheets during interglacial periods, and

scenario 8 tests the occurrence of smaller melt contributions from Antarctica relative to the other ice masses. The magnitude of change in estimated seawater $\delta^{234}U$ is impacted by these variations in relative melt volume contributions. However, the overall trend remains similar to scenarios 5 and 6 with a continued increase during ~0-100 ka before switching to an overall decreasing trend for all four volume scenarios (Figure 4.5f). Based on these scenarios, we determine that the original glacial-interglacial melt volume contributions from the primary three glacial melt sources in scenario 4 are the best estimates for our box model seawater $\delta^{234}U$ reconstructions, as there is evidence of volumes of these proportions from previous studies (Bamber et al., 2012; Church et al., 2011; Jones et al., 2002; Raiswell et al., 2005; Statham et al., 2008; Tranter, 2006).

Scenarios 5 and 8 represent the best possible seawater $\delta^{234}U$ estimations for glacial-interglacial cycles under the condition that all ice mass melting timescales are aligned. However, these estimated seawater $\delta^{234}U$ were achieved in scenarios that had quite different fractional contributions and starting U concentrations and seawater $\delta^{234}U$ values (Table 4.3): therefore, further constraints are needed to resolve which scenario is more likely. In addition, the transitions between glacial and interglacial periods are most likely less extreme, and so the possibility of an offset in the melting timescales of the ice masses should be considered.

Because the melting timescales of all three glacial melt sources may not align exactly, we implemented two additional box model scenarios, scenario 9 and scenario 10 (Figure 4.5g), that are respective alterations of scenarios 5 and 8 with offset melting timescales. The overall impact of this timescale shift is subtle in scenario 9, consistently raising the global seawater $\delta^{234}U$ box

model estimations by 15-32, as the excess contribution of ^{234}U during glacial-interglacial boundaries from Northern Continental Ice Sheets amplifies the estimations of global seawater

Table 4.3: Differing glacial melt U-flux scenarios addressed by our model. Presented are the model run scenarios: parameters for each scenario, glacial melt contribution to river contribution ratios for glacial and interglacial periods, specific ice mass, the total melt fraction contribution of that ice mass during glacial and interglacial periods, and the glacial melt [^{238}U] concentrations and $\delta^{234}U$ for that ice mass during glacial and interglacial periods are explicitly presented. Asterisks indicate that the Antarctic glacial melt U concentrations and compositions were applied from subglacial lake and pond measurements collected in the Dry Valleys by Henderson et al. (2006). Prime number symbols on scenarios 9-10 indicate box model scenarios where glacial-interglacial transitions for the Northern Hemisphere Continental glaciers were offset by eight thousand years from the standard MIS boundaries based on melting timescale estimations (i.e. (Carlson et al., 2008; Clark, 2009; Stokes et al., 2009).

Model Run	**Volume (glacial melt:river)**		**Ice Mass**	**Melt Fraction**		**[^{238}U] (ppb)**		**$\delta^{234}U$**	
	glacial	*interglacial*		*glacial*	*interglacial*	*glacial*	*interglacial*	*glacial*	*interglacial*
Moderate Melt									
Scenario 1a	1:1	8:1	One Bulk	1.000	1.000	0.0173	0.0173	82.0	82.0
Scenario 1b	1:1	8:1	One Bulk	1.000	1.000	0.0086	0.0086	97.2	97.2
Scenario 1c	1:1	8:1	One Bulk	1.000	1.000	0.0173	0.0086	82.0	97.2
Low/High Melt									
Scenario 2a	1:1	8:1	One Bulk	1.000	1.000	0.0176	0.0176	8.0	8.0
Scenario 2b	1:1	8:1	One Bulk	1.000	1.000	0.1227	0.1227	263.0	263.0
Scenario 2c	1:1	8:1	One Bulk	1.000	1.000	0.0176	0.1227	8.0	263.0
Meltwater Volume									
Scenario 3a	1:1	1:1	One Bulk	1.000	1.000	0.0176	0.1227	8.0	263.0
Scenario 3b	1:1	20:1	One Bulk	1.000	1.000	0.0176	0.1227	8.0	263.0
Scenario 3c	1:1	100:1	One Bulk	1.000	1.000	0.0176	0.1227	8.0	263.0
Increased U Flux									
Scenario 4	1:1	8:1	Greenland	0.450	0.650	0.0176	0.1227	8.0	263.0
Scenario 4*	1:1	8:1	Antarctica	0.150	0.300	1.2000	0.0470	963.0	1189.0
Scenario 4	1:1	8:1	N.H. Continental	0.400	0.050	0.0173	0.0086	82.0	97.2
Decreased U Flux									
Scenario 5	1:1	8:1	Greenland	0.450	0.650	0.0173	0.0086	82.0	97.2
Scenario 5*	1:1	8:1	Antarctica	0.150	0.300	0.0090	1.2000	479.0	963.0
Scenario 5	1:1	8:1	N.H. Continental	0.400	0.050	0.0090	0.0040	30.0	60.0
Increased Antarctic Volume									
Scenario 6	1:1	8:1	Greenland	0.300	0.250	0.0176	0.1227	8.0	263.0
Scenario 6*	1:1	8:1	Antarctica	0.400	0.500	1.2000	0.0470	479.0	963.0
Scenario 6	1:1	8:1	N.H. Continental	0.300	0.250	0.0173	0.0086	82.0	97.2
No Interglacial N.H. Continental									
Scenario 7	1:1	8:1	Greenland	0.500	0.625	0.0176	0.1227	8.0	263.0
Scenario 7*	1:1	8:1	Antarctica	0.200	0.375	1.2000	0.0470	479.0	963.0
Scenario 7	1:1	8:1	N.H. Continental	0.300	0.000	0.0173	0.0086	82.0	97.2
Decreased Antarctic Volume									
Scenario 8	1:1	8:1	Greenland	0.450	0.625	0.0176	0.1227	8.0	263.0
Scenario 8*	1:1	8:1	Antarctica	0.150	0.125	1.2000	0.0470	479.0	963.0
Scenario 8	1:1	8:1	N.H. Continental	0.400	0.250	0.0173	0.0086	82.0	97.2
Offset Timescales: modified S5									
Scenario 9'	1:1	8:1	Greenland	0.450	0.650	0.0173	0.0086	82.0	97.2
Scenario 9*'	1:1	8:1	Antarctica	0.150	0.300	0.0090	1.2000	479.0	963.0
Scenario 9'	1:1	8:1	N.H. Continental	0.400	0.050	0.0090	0.0040	30.0	60.0
Offset Timescales: modified S8									
Scenario 10'	1:1	8:1	Greenland	0.450	0.625	0.0176	0.1227	8.0	263.0
Scenario 10*'	1:1	8:1	Antarctica	0.150	0.125	1.2000	0.0470	479.0	963.0
Scenario 10'	1:1	8:1	N.H. Continental	0.400	0.250	0.0173	0.0086	82.0	97.2

$\delta^{234}U$ during these periods. This offset deglaciation also shifts the glacial-interglacial peaks and dips toward the modern by 8 ka, when the maximum and minimum melt contributions from all three glacial melt sources overlap: thus, making transitions between glacial and interglacial cycles less severe (Figure 4.5g). Contrastingly, while scenario 10 remains within the accepted range of published seawater $\delta^{234}U$ values from corals, it presents a much more exaggerated estimated reconstruction of seawater $\delta^{234}U$ values. Scenario 10 experiences a significant transition from an overall positive trend to a negative trend at ~100 ka in which the estimated $\delta^{234}U$ dips below the accepted $\delta^{234}U$ value of modern seawater and oscillates within 50 of the modern seawater value for the duration of the estimation.

Additionally, the intensities between interglacial periods and timescales of deglaciation may vary, potentially causing the U flux intensities to also vary over time (Esat and Yokoyama, 2006; Lambeck et al., 2002; Yokoyama and Esat, 2004). As the melting intensities of all interglacial periods may not be identical, we implemented two additional box model scenarios, scenario 11 and scenario 12 (Figure 4.5h), that are respective alterations of scenarios 5 and 8 with the inclusion of interglacial cycles of extreme melt where nearly complete deglaciation was achieved during MIS 5, 11, and 19 (Carlson et al., 2008; Clark, 2009; Lambeck et al., 2002; Rabineau et al., 2006). The overall impact of these scenarios was that both scenario 11 and scenario 12 followed the same oscillating trends, with periods of extreme seawater $\delta^{234}U$ increase during the nearly complete deglaciations followed by a tapering trend (Figure 4.5h).

4.6.4.1. Likelihood of box model scenarios

We assess glacial-interglacial seawater $\delta^{234}U$ estimations obtained from our box model scenarios for feasibility. Scenarios 1a-c, 2a-c and 3a-c (Figures 4.5b-d) are excluded because these scenarios are unlikely to be representative of global glacial melt U flux input based on $\delta^{234}U$ measurements from continental alpine glacier (Arendt et al., 2015) and Antarctic subglacial water (Henderson et al., 2006). Given the range of $\delta^{234}U$ values published from corals and marine carbonates, approximately 0‰ to 250‰ (Dunk et al., 2002; Esat and Yokoyama, 2006; Henderson, 2002; Yokoyama and Esat, 2004), the likelihood of the remaining box model scenarios can be evaluated. Because the total variation in seawater $\delta^{234}U$ in scenarios 4, 6, and 7 (Figures 4.5e-f) greatly exceeds the previously published range in seawater carbonate $\delta^{234}U$ values, these scenarios can also be disregarded. Thus, scenarios 5 and 8 (Figures 4.5e-f) represent the best possible seawater $\delta^{234}U$ estimations for glacial-interglacial cycles under the condition that all ice mass melting timescales are aligned. However, these estimated seawater $\delta^{234}U$ were achieved in scenarios that had quite different fractional contributions and starting U concentrations and seawater $\delta^{234}U$ values (Table 4.3): therefore, further constraints are needed to resolve which scenario is more likely. In addition, the transitions between glacial and interglacial periods are most likely less extreme, and so the possibility of an offset in the melting timescales of the ice masses should be considered.

Records of extreme melting events in the Northern Hemisphere indicate a probable offset in peak melting timescales of Northern Hemisphere Continental Ice Sheets from the melting timescales of the two large ice sheets that existed continuously on glacial-interglacial timescales, Antarctica and the GrIS (Carlson et al., 2008; Clark, 2009). Based on estimates of Northern Hemisphere Continental deglaciation timescales, we offset the glacial-interglacial boundaries from the

standard MIS boundaries for the Northern Hemisphere Continental Ice Sheets by eight thousand years with the peak Northern Hemisphere Continental Ice Sheet melt contributions from the last glacial period at ~21 to 6 ka (Carlson et al., 2008; Clark, 2009). We project this discrepancy in ice sheet melting back 1,000 ka to test the impact that this offset would have on the magnitude of change of global seawater $\delta^{234}U$ (Table 4.3, Figure 4.5g). We therefore implemented two additional box model scenarios, scenario 9 and scenario 10 (Figure 4.5g), which are respective alterations of scenarios 5 and 8 with offset melting timescales. In these scenarios, it becomes apparent that the different starting compositional and volumetric values impact the shape of the estimated seawater $\delta^{234}U$ trends more in these scenarios than in the scenarios where all ice masses melt on concurrent timescales.

Furthermore, indications of nearly complete deglaciation of the glacial melt sources exist for MIS 5, MIS 11, MIS 19, and additional time periods based on sea level rise reconstructions (Carlson et al., 2008; Clark, 2009; Lambeck et al., 2002; Reyes et al., 2014). Thus, we implemented two additional box model scenarios, scenario 11 and scenario 12 (Figure 4.5h), that are respective alterations of scenarios 5 and 8 with nearly complete deglaciations during MIS 5, MIS 11, and MIS 19. In our box model, these deglacial periods have glacial melt volume inputs of five times the volume input during normal interglacial cycles, as indicated by previous studies (Carlson et al., 2008; Clark, 2009; Lambeck et al., 2002), which elicits an increase in U flux to global seawater.

Scenarios 9-12 are all feasible models for recreating seawater $\delta^{234}U$ over glacial-interglacial timescales because their projected values all fall within the accepted range of $\delta^{234}U$ values

published from coral records (Dunk et al., 2002; Esat and Yokoyama, 2006; Henderson, 2002; Yokoyama and Esat, 2004). However, further investigation into seawater $\delta^{234}U$ compositions over the past 1000 ka is needed to verify the conditions implemented in our various box model scenarios: specifically, the melting timescale offset between glacial melt sources and the occurrences of nearly complete deglaciations. Nevertheless, the assumption that seawater $\delta^{234}U$ has remained stable over time with random scatter is not necessarily true, as these box model estimations show definite trends that could potentially offset climate record age reconstructions from U/Th coral dating methods.

4.6.5. Box Model Caveats and Assumptions

Within our modified box model we acknowledge several complicating factors and possible sources of error. First, because we assume the volume contribution from rivers has remained constant over time, our model results may be skewed, as the glacial input to river ratio would be different if the river volume estimations changed over glacial-interglacial timescales. Thus, our model would be more accurate if there were better-constrained, higher precision estimations of river volume contributions to seawater over the past several hundred thousand years.

Second, a possible underrepresented source of glacially sourced U to seawater may be icebergs whose melt volume contributions were not taken into consideration in our model in accordance with previous models of glacially derived elemental flux (Bhatia et al., 2013). However, icebergs are likely an insignificant source of U as they have minimal water-rock interaction, required for U concentrations necessary to impact seawater chemistry.

Third, a potentially complicating issue to consider is the inherent temporal and spatial variability of glacial meltwater U chemistry. Seasonal and cyclical variations in melt rates would affect the magnitude of physical weathering occurring. Spatial differences in melting rates would occur from the terminus of the glacier to several kilometers up-glacier, affecting the rate at which U is delivered into subglacial water.

Fourth, the role permafrost melt has in influencing the U chemistry of seawater during large-scale melting events is an under-characterized parameter that should be included in seawater models. The extent of permafrost during glacial and even interglacial periods is quite large and may equate to massive volumes of meltwater with high U concentrations and $\delta^{234}U$ compositions. For example, elevated U concentrations were measured in permafrost in Siberia (Vaks et al., 2013) and $\delta^{234}U$ compositional values as high as 155‰ were measured in Alaskan permafrost (Ewing et al., 2014). Therefore, input from permafrost to seawater may have a significant impact on seawater chemistry and need to be taken into consideration but there is currently not an accurate estimation of the scale of melt from permafrost alone.

Finally, the existence of extreme deglaciation events, where nearly complete deglaciation of the three main ice masses is achieved, would be an additional complicating factor for our box model seawater $\delta^{234}U$ estimations. In these additional periods of extreme deglaciation, much larger U fluxes from glacial melt would be incorporated into global seawater, causing spikes in the seawater $\delta^{234}U$ compositions on these timescales. We suggest that in moving forward, U concentrations and $\delta^{234}U$ composition measurements from coral samples that grew during these periods of potential near-deglaciation (e.g., MIS 5, MIS 11, MIS 19) (Carlson et al., 2008; Clark,

2009; 2005; Lambeck et al., 2002; Reyes et al., 2014) are needed to verify if seawater U chemistry was notably elevated during these periods. If these samples demonstrate the potential for spikes in seawater $\delta^{234}U$ compositions during these timescales, there is the potential to impact interpretations of other weathering budgets (e.g., Sr, Nd, Ge (Jones et al., 2002; Vance et al., 2009)).

4.6.6. Significance

The glacial-interglacial variations of seawater $\delta^{234}U$ from glacial melt proposed in this study impact seawater mixing models and would influence existing timescales based on coral U/Th dating as well as other techniques (Shen and Dunbar, 1995; Stirling et al., 1995), indicating that dating proxies based on constant chemical compositions of seawater U over time may need to be reevaluated. Extrapolating from the results of this model, we would expect the glacially derived U contribution to global seawater to continue to oscillate with predicted future climate-warming scenarios. Further evidence for a changing seawater $\delta^{234}U$ composition may be obtainable through high precision U analysis of marine carbonates and corals. The $\delta^{234}U$ noise observed in previous coral and marine carbonate records may in fact not be an error in measurement but rather a reflection of changing seawater $\delta^{234}U$ composition due to fluctuations in glacial melt input (Dutton et al., 2009; Esat and Yokoyama, 2006; Henderson, 2002; Robinson et al., 2004). Thus, there is a strong possibility that notable fluctuations in seawater U chemistry occurred on glacial-interglacial timescales from significant variations in $^{234}U_{xs}$ input values to global seawater from extreme melting events.

4.7. CONCLUSIONS

Uranium analyses from both GrIS outlet glacier subglacial drainage and proximal seawater demonstrate that glacial melt contributions have the capacity to alter the $\delta^{234}U$ of proximal seawater in response to varying U chemistry (both composition and concentration) of glacial meltwater. At locations where subglacial waters have long residence time values, subglacial water $\delta^{234}U$ values are elevated and may potentially contribute to large changes in the oceans' U budget and in the $\delta^{234}U$ composition of seawater.

Using these subglacial U chemistry values as representative compositions of glacial and interglacial meltwater runoff, our model results show how $\delta^{234}U$ seawater compositions, vary over glacial-interglacial timescales in response to differing scenarios of: glacial meltwater volume contributions; U flux intensities; $\delta^{234}U$ values; and melting timescales. Notably, we show that in all our possible scenarios, changes in meltwater U fluxes invoke deviations in seawater $\delta^{234}U$ compositions. The most realistic scenarios (9-12) present the most realistic seawater $\delta^{234}U$ estimations with values within the range of 130‰ and 350‰ over the past 1,000 ka: however, additional research is needed to place further constraints on the parameters influencing U fluxes from glacial melt on these timescales.

Overall, these box model scenarios predict that seawater $\delta^{234}U$ has not behaved as a constant over glacial-interglacial timescales, contradicting the widespread belief that the U composition of seawater has remained stable through time. Therefore, the assumption that glacial meltwater cannot influence the trace chemistry, specifically the $\delta^{234}U$, of global seawater on glacial-interglacial cycles should be re-visited.

4.8 REFERENCES

Aciego, S.M., Bourdon, B., Lupker, M., Rickli, J., 2009. A new procedure for separating and measuring radiogenic isotopes (U, Th, Pa, Ra, Sr, Nd, Hf) in ice cores. Chemical Geology 266, 194-204.

Aciego, S.M., Stevenson, E.I., Arendt, C.A., 2015. Climate versus geological controls on glacial meltwater micronutrient production in southern Greenland. Earth and Planetary Science Letters In Press.

Andersen, M.B., Stirling, C.H., Porcelli, D., Halliday, A.N., Andersson, P.S., Baskaran, M., 2007. The tracing of riverine U in Arctic seawater with very precise $^{234}U/^{238}U$ measurements. Earth and Planetary Science Letters 259, 171-185.

Andersen, M.B., Stirling, C.H., Zimmermann, B., Halliday, A.N., 2010. Precise determination of the open ocean (234)U/(238)U composition. Geochemistry, Geophysics, Geosystems 11, Q12003.

Anderson, S.P., 2005. Glaciers show direct linkage between erosion rate and chemical weathering fluxes. Geomorphology 67, 147-157.

Arendt, C.A., Aciego, S.M., Sims, K.W.W., Aarons, S.M., 2015. Models underestimate glacial meltwater storage time, evidence from U-series. Geochimica et Cosmochimica Acta, Submitted.

Arendt, C.A., Aciego, S.M., Sims, K.W.W., Robins, M.J., 2014. Sequential separation of radioactive U, and radiogenic Nd and Hf concentrated from natural waters. Geostandards and Geoanalytical Research, In Press.

Auro, M.E., Robinson, L.F., Burke, A., Bradtmiller, L.I., Fleisher, M.Q., Anderson, R.F., 2012. Improvements to 232-thorium, 230-thorium, and 231-protactinium analysis in seawater arising from GEOTRACES intercallibration. Limnology and Oceanography: Methods 10, 464-474.

Bell, R.E., Studinger, M., Shuman, C.A., Fahnestock, M.A., and Joughin, I., 2007. Large subglacial lakes in East Antarctica at the onset of fast-flowing ice streams. Nature 445, 904-907.

Bhatia, M.P., Das, S.B., Kujawinski, E.B., Henderson, P., Burke, A., Charette, M.A., 2011. Seasonal evolution of water contributions to discharge from a Greenland outlet glacier: insight from a new isotope-mixing model. Journal of Glaciology 57.

Bhatia, M.P., Kujawinski, E.B., Das, S.B., Breier, C.F., Henderson, P.B., Charette, M.A., 2013. Greenland meltwater as a significant and potentially bioavailable source of iron to the ocean. Nature Geoscience 6, 274-278.

Blum, J.D., Erel, Y., 1995. A silicate weathering mechanism linking increases in marine Sr-87/Sr-86 with global glaciation Nature 373, 415-418.

Bonotto, D.M., Andrews, J.N., 2000. The transfer of uranium isotopes U-234 and U-238 to the waters interacting with carbonates from Mendip Hills area (England). Applied Radiation and Isotopes 52, 965-983.

Carlson, A.E., N., L.A., Oppo, D.W., Came, R.E., Schmidt, G.A., Anslow, F.S., Licciardi, J.M., Obbink, E.A., 2008. Rapid early Holocene deglaciation of the Laurentide Ice Sheet. Nature Geoscience 620-624.

Chen, J.H., Edwards, R.L., Wasserburg, G.J., 1986. 238U, 234U and 232Th in seawater. Earth and Planetary Science Letters 80, 241-251.

Cheng, H., Edwards, R.L., Hoff, J., Gallup, C.D., Richards, D.A., Asmerom, Y., 2000. The half-lives of uranium-234 and thorium-230. Chemical Geology 169, 17-33.

Clark, P.U., 2009. Ice sheet retreat and sea level rise during the last deglaciation. PAGES News 17, 64-66.
Cochran, J.K., Masque, P., 2003. Short-lived U/Th series radionuclides in the ocean: tracers for scavenging rates, export fluxes and particle dynamics. Mineralogical Society of America, Reviews in Minerology and Geochemistry.
Dunk, R.M., Mills, R.A., Jenkins, W.J., 2002. A reevaluation of the oceanic uranium budget for the Holocene. Chemical Geology 190, 45-67.
Dutton, A., Bard, E., Antoniolli, F., Esat. T.M., Lambeck, K.,McCulloch, M.T., 2009. Phasing and amplitude of sea-level and climate change during the penultimate interglacial. Nature Geoscience 2(5), 355-359.
Esat, T.M., Yokoyama, Y., 2006. Variability in the uranium isotopic composition of the oceans over glacial–interglacial timescales. Geochimica et Cosmochimica Acta 70, 4140-4150.
Ewing, S.A., Paces, J.B., O'Donnell, J.A., Jorgenson, M.T., Kanevsky, M.Z., Aiken, G.R., Shur, Y., Harden, J.W., Striegl, R., 2014. Uranium isotopes and dissolved organic carbon in loess permafrost: modeling the age of ancient ice. Geochimica et Cosmochimica Acta In Press, GCA 9047.
Gallup, C.D., Edwards, R.L., Johnson, R.G., 1994. The timing of high sea levels over the past 200,000 years. Science 263, 796-800.
Henderson, G., Hall, B.L., Smith, A., Robinson, L.F., 2006. Seawater ($^{234}U/^{238}U$) in lake water: A study in the Dry Valleys of Antarctica. Chemical Geology 226, 298-308.
Henderson, G.M., 2002. Seawater ($^{234}U/^{238}U$) during the last 800 thousand years. Earth and Planetary Science Letters 199, 97-110.
Henderson, G.M., Anderson, R.F., 2003. The U-series toolbox for paleoceanography. Reviews in Minerology and Geochemistry 52, 493-591.
Hendry, K.R., Robinson, L.F., Meredith, M.P., Mulitza, S., Chiessi, C.M., Arz, H., 2012. Abrupt changes in high-latitude nutrient supply to the Atlantic during the last glacial cycle. Geology 40, 123-126.
Jones, I.W., Munhoven, G., Tranter, M., Huybrechts, P., Shharp, M.J., 2002. Modelled glacial and non glacial HCO3-, Si and Ge fluxes since the LGM: little potential for impact on atmospheric CO2 concentrations and a potential proxy of continental chemical erosion, the marine Ge/Si. Global and Planetary Change 33, 139-153.
Lambeck, K., Esat, T.M., Potter, E.K., 2002. Links between climate and sea levels for the past three million years. Nature 419, 199-206.
Lisiecki, L.E., Ramo, M.E., 2005. A Pliocene-Pleistocene stack of 57 globally distributed benthic D18O records. Paleoceanography 20, 1-17.
Niu, Y., Castro, C., Aciego, S.M., Hall, C.M., Stevenson, E.I., Arendt, C.A., In Review. Noble gas signatures in Greenland - Tracing glacial meltwater sources. Geophysical Research Letters, Submitted.
Not, C., Brown, K., Ghaleb, B., Hillaire-Marcel, C., 2011. Conservative behavior of uranium vs. salinity in Arctic sea ice and brine. Marine Chemistry 130, 33-39.
Owens, S.A., Buesseler, K.O., Sims, K.W.W., 2011. Re-evaluating the 238U-salinity relationship in seawater: Implications for the 238U-234Th disequilibrium method. Marine Chemistry 127, 31-39.
Picolo, J.L., 1996. Absolute measurement of radon 222 activity. Nuclear Instruments & Methods in Physics Research 369, 452-457.
Pogge von Strandmann, P.A.E., Burton, K.W., James, R.H., van Calsteren, P., Gilason, S.R.,

Mokadem, F., 2006. Riverine behaviour of uranium and lithium isotopes in an actively glaciated basaltic terrain. Earth and Planetary Science Letters 251, 134-147.
Reyes, A.V., Carlson, A.E., Beard, B.L., Hatfield, R.G., Stoner, J.S., Windsor, K., Welke, B., Ullman, D.J., 2014. South Greenland ice-sheet collapse during Marine Isotope Stage 11. Nature 510, 525-530.
Rickli, J., Frank, M., Baker, A.R., Aciego, S.M., de Souza, G., Georg, R.B., Halliday, A.N., 2010. Hafnium and neodymium isotopes in surface waters of the eastern Atlantic Ocean: Implications for sources and inputs of trace metals to the ocean. Geochimica et Cosmochimica Acta 74, 540-557.
Robinson, L.F., Henderson, G.M., Hall, L., Matthews, I., 2004. Climatic control of riverine and Seawater uranium-isotope ratios. Science 305, 851-854.
Scholz, D., Mangini, A., Felis, T., 2004. U-series dating of diagenetically altered fossil reef corals. Earth and Planetary Science Letters 218, 163-178.
Shen, G.T., Dunbar, R.B., 1995. Environmental controls on uranium in reef corals Geochimica et Cosmochimica Acta 59, 2009-2024.
Stein, M., Wasserburg, G.J., Aharon, P., Chen, J.H., Zhu, Z.R., Bloom, A., Chappell, J., 1993. TIMS U-series dating and stable isotopes of the last interglacial event in Papua-New-Guinea Geochimica et Cosmochimica Acta 57, 2541-2554.
Stevenson, E.I., Aciego, S.M., Arendt, C.A., Das, S.B., Kenny, D.V., Sheik, C., Submitted. Systematic variation of 87Sr/86Sr isotope compositions of dissolved and suspended load from Northern Hemisphere glaciers and ice sheets. Earth and Planetarty Science Letters, Submitted.
Stirling, C.H., Esat, T.M., McCulloch, M.T., Lambeck, K., 1995. ￼High-precision U-series dating of corals from Western Australia and implications for the timing and duration of the Last Interglacial. Earth and Planetary Science Letters 135, 115-130.
Vaks, A., Guatareva, O.S., Breitenbach, F.M., Avirmed, E., Mason, A.J., Thomas, A.L., Osinev, A.V., Kononov, A.M., Henderson, G.M., 2013. Speleothems reveal 500,000-Year History of Siberian Permafrost. Science 340, 183-186.
Vance, D., Teagle, D.A.H., Foster, G.L., 2009. Variable Quaternary chemical weathering fluxes and imbalances in marine geochemical budgets. Nature 458, 493-496.
Veizer, J., 1989. Strontium isotopes in seawater through time. Annual Review of Earth and Planetary Sciences 17, 141-167.
Villemant, B., Fleuillet, N., 2003. Dating open systems by the 238U–234U–230Th method: application to Quaternary reef terraces. Earth and Planetary Science Letters 210, 105-118.
Wortmann, U.G., Paytan, A., 2012. Rapid variability of seawater chemistry over the past 130 million years. Science 337.
Yokoyama, Y., Esat, T.M., 2004. Long Term Variations of Uranium Isotopes and Radiocarbon in the Surface Seawater Recorded in Corals. TERRAPUB, 279-305.
Yu, J.M., Anderson, R.F., Rohling, E.J., 2014. Deep ocean carbonate chemistry and glacial-interglacial atmospheric CO2 changes. Oceanography 27, 16-25.

Chapter V

Conclusion: Geochemical Constraints on Glacial Hydrology

Chapter five summarizes the fundamental conclusions of the previous research chapters in this thesis (Chapters 2-4) and discusses my potential future research goals in glacial chemistry and glacial hydrology. My thesis is centered around gaining insight on source fraction contributions from isotopic analyses of bulk samples with a Bayesian Monte Carlo (BMC) multiple-isotope mixing model, meltwater storage timescales using uranium-series (U-series) isotopic measurements coupled with age-relationship equations, and assessing the impact of glacial meltwater chemistry on seawater U chemistry on glacial-interglacial timescales through the analysis of direct isotopic meltwater and seawater measurements combined with seawater U chemistry scenario predictions from a straightforward box model. All of these processes are critical in placing further constraints on climate change by honing in on the actual glacial hydrology processes occurring as climate change progresses so we can be better prepared inevitable outcome. With these new tools for determining fraction source contributions and associated uncertainties of glacial meltwater, quantifying the residence time of meltwater in the subglacial environment, and assessing the impact of glacial meltwater U fluxes on seawater U chemistry on glacial-interglacial timescales, a much more robust understanding of the importance of subglacial hydrology and glacial meltwater chemistry is gained. Importantly, the new chemical proxies and computational models resulting from my research offer new approaches to quantifying glacial hydrology processes.

This dissertation represents a substantial advancement in understanding glacial hydrological systems and associated processes through the application of novel chemical proxies in a number of key ways, including: 1) accurate source partitioning of end-member contributors of bulk samples and associated uncertainties via my Bayesian Monte Carlo multi-component isotope mixing model (Chapter 2); 2) quantified average residence times of glacial meltwater in alpine subglacial systems obtained through U-series isotopic analysis of bulk discharged meltwater, specifically isotopic measurements of ^{222}Rn, ^{234}U, and $(^{234}U/^{238}U)_{ACT}$ applied to an age-relationship equation (Chapter 3); 3) quantified average residence times of glacial meltwater beneath large ice masses (i.e. the Greenland Ice Sheet) and the accompanying impact on proximal seawater U chemistry (Chapter 4); and 4) predictions of feasible global seawater U chemistry fluctuation scenarios dependent on deglaciation processes over glacial-interglacial timescales (Chapter 4).

5.1. SUMMARY OF CONCLUSIONS

5.1.1. Chapter 2: Fraction Contributions to Meltwater

This research chapter presents an open source multiple isotope Monte Carlo linear mixing model to determine source fraction contribution and associated uncertainties of the possible end member contributors to a bulk sample. This BMC model was first applied to an original case study from a 2011 field season at the Athabasca Glacier in Jasper National Park, Alberta, Canada. Bulk drainage water samples from the primary meltwater discharge channel at the glacial terminus were analyzed for $\delta^{18}O$ and δD compositions and compared to end-member $\delta^{18}O$ and δD compositions for snowmelt, ice melt and summer precipitation in order to estimate fractional contributions. Results showed that the discharged bulk water from the Athabasca

Glacier transitioned from predominantly snow melt in May to predominantly ice melt in July, with a summer precipitation component representing a minimal contribution throughout both months. Determining source contributions of glacial melt provides insight into glacial hydrology and can help quantify fast versus slow melt volumes and ultimately, the longevity of a glacial system.

The BMC mixing model was next applied to a similar Earth surface environment, utilizing $\delta^{18}O$, δD and ^{222}Rn measurements from Greenland Ice Sheet bulk meltwater previously published by Bhatia *et al.* [2011]. My model estimations based on these data were comparable to the source fraction contribution predictions from the original study, which used a simple linear mixing model based on invariant end-member composition [Bhatia *et al.,* 2011]. Furthermore, the introduction of a third isotope into the mixing model led to decreases in the uncertainty associated with the fraction contribution estimations, increasing the precision of the source fraction contribution estimations. To test the relevance of my model to differing Earth surface systems and radiogenic isotopes, I also apply my BMC model to $^{87}Sr/^{86}Sr$ and ε_{Nd} isotopic data previously published from four sediment cores in Hawaii [Chadwick *et al.,* 1999; Kurtz *et al.*, 2001]. My model estimations from this dataset were logical in the context of Hawaiian soil sources (i.e. seaspray, Asian dust, Hawaiian volcanic rocks), as the regions closest to the coast showed the highest presence of seaspray at the surface, and agreed with the fraction contribution predictions for sources in Chadwick *et al.* [1999]. Thus, the additional case studies from previously published data and from the original Athabasca Glacier case study demonstrate the versatility and broad application of my multiple isotope BMC mixing model to Earth surface processes.

5.1.2. Chapter 3: Subglacial Meltwater Residence Time

This research chapter presents a new chemical method used to determine the first quantitative measurements of subglacial meltwater residence time through U-series isotopic analysis. A pilot study of this method was tested during a 2011 field season at the Athabasca Glacier in Jasper National Park, Alberta Canada in conjunction with the field work performed for Chapter 2. The application of time-series ^{222}Rn, ^{234}U, and $(^{234}U/^{238}U)_{ACT}$ measurements to a new age-relationship equation allowed the derivation of average residence time of subglacial meltwater. Utilizing this novel equation in conjunction with radioisotope measurements from collected subglacial meltwater, the calculated residence time for the Athabasca Glacier subglacial water in May 2011 was approximately 30 years, and the calculated residence time for the Athabasca Glacier subglacial water in July 2011 was approximately 1-5 years.

The magnitude of average subglacial meltwater residence time derived from my new U-series based quantitative method is several orders of magnitude larger than previous estimations from linear models and dye-trace studies. However, it is important to note that this method measures a different process than dye-trace studies, as this new chemical proxy for residence time quantifies the average water-rock interaction time of the bulk discharge, or the time water is stored in contact with the underlying substrate (e.g., bedrock, till) in the subglacial system, rather than the transit time of meltwater from the surface of the glacier to the time it is discharged at the subglacial terminus, which is the value quantified by dye-trace studies. Therefore, this finding provides new insight to the processes existing in subglacial hydrologic systems and has implications for freshwater resource sustainability, as it provides a better understanding of the

size of reservoirs that are able to exist in the subglacial environment and the length of time that water is stored before being discharged.

5.1.3. Chapter 4: Impact of Glacial Meltwater on Seawater U Chemistry

This research chapter assesses the scale of my quantitative subglacial meltwater residence time method at four outlet glaciers of the Greenland Ice Sheet, including sites neighboring Narsarsauq in the South, Ilulissat and Nuuk in the West, and Kulusuk in the East. This chapter also assesses the impact meltwater residence time and the corresponding meltwater U chemistry have on surrounding seawater U chemistry. The residence times from these four locations spanned a broad range from approximately 12 years at Ilulissat, roughly 200-270 years at Kulusuk and Nuuk, and the maximum residence time of approximately 1,074 years at Narsarsuaq. The locations with longer residence times had higher U concentrations and compositions, and the associated proximal seawater locations exhibited U chemistry that was related to that of the glaciers

Based on direct observations of the impact that meltwater residence times have on seawater proximal to the outlet glaciers sampled in Greenland, this chapter also incorporates U fluxes from deglaciation processes into a seawater U chemistry mixing model originally published by Henderson [2002] in order to assess the potential impact of subglacial meltwater residence time on global seawater U chemistry during extreme deglaciation events over glacial-interglacial timescales. In the box model, I assess the outcome of numerous glacial meltwater U flux scenarios by varying conditions such as meltwater volume, $\delta^{234}U$ composition, variability between the primary meltwater sources (e.g., Antarctica, the Greenland Ice Sheet, and Northern

Hemisphere Continental Ice Sheets), and multiple extreme deglaciation events. A variety of scenarios resulted from my box model seawater U chemistry estimations, but scenarios all indicate that the $\delta^{234}U$ composition of seawater was likely not constant on glacial-interglacial timescales as previously believed. The feasibility of fluctuations in seawater U chemistry on glacial-interglacial timescales from significant glacial meltwater U flux contributions is discussed in detail in this chapter along with the implications of these fluctuations for U/Th based timeline reconstructions from corals that are dependent on a constant seawater U chemistry over time.

5.2. FUTURE WORK

Beyond the initial objectives of my research, this thesis has also urged the investigation of new research questions that focus on expanding my methods to larger glacial systems and incorporating the original insight provided by my methods with other existing techniques to gain a more interdisciplinary perspective that will hopefully provide a better overall assessment of current and anticipated glacier and ice sheet responses to climate change. These research questions and potential future research directions include:

1) *What are the magnitudes of subglacial water residence times in Antarctica?*

   Due to the importance of glaciers and ice sheets as freshwater reservoirs, additional work needs to be done to assess the storage length of subglacial meltwater, especially in locations with large subglacial lakes (e.g., Lake Vostok beneath Antarctica). I intend on expanding upon my thesis research by applying the quantitative residence time chemical proxy resulting from Chapter 3 of this thesis to locations with sizable

subglacial reservoirs. One specific project I am hoping to undertake involves processing the U-series isotopes in Taylor Glacier subglacial meltwater samples that were collected in the winter of 2013, following the ion exchange chromatography methods outlined Arendt et al. (2014). The U concentrations and the $(^{234}U/^{238}U)_{ACT}$ compositions of glacial melt are correlated to the residence time of subglacial water and can be used to quantify the average storage time of the bulk meltwater discharged from a glacial terminus (Arendt et al., Geochimica et Cosmochimica Acta, In Review). Thus, the analyses of these samples will allow for better constraints on the role of subglacial hydrology and subglacial melt on deglaciation processes in a region of the largest concern for modern global warming: Antarctica.

2) *How will the synthesis of terrestrial cosmogenic measurements in glacial systems with geochemical meltwater analysis better inform the understanding of glacial periods of advance and retreat?*

Cosmogenic isotopes in subglacial bedrock are being developed as a new method to establish past extents of ice sheets during interglacial periods (e.g. Sugden et al., 2005). Cosmogenic isotopic compositions are dependent on direct exposure to the sun, so they actively record the timing of glacier advance/retreat at glacial margins. Subglacial till and bedrock samples will be selected to place controls on glacial and interglacial periods over the past 0.5-1 million years. The addition to this proposed cosmogenic dataset of residence time data from subglacial water collected on the proximal Antarctic Icesheet can provide insight as to the storage capacity of icesheets

even while experiencing periods of glacial retreat by combining the subglacial reservoir residence time records with the timescales of glacial advance/retreat.

3) *What additional constraints can be placed on subglacial systems if information from my geochemical proxies is combined with geophysical data from the same system?*
The synthesis of geochemical data and geophysical models will need to be explored in the near future to gain a more robust picture of the subglacial system and subglacial processes. To begin with, I will take advantage of existing data to link geophysical models with geochemical data. Specifically, I intend on undertaking a multiple-component investigation of Antarctica's climate record, including a comprehensive isotopic analysis of terrestrial and marine paleo-records to investigate Antarctic glacial-interglacial processes over the past ~0.5 - 1 Myr.

4) *Can my Bayesian Monte Carlo isotope mixing model be applied in glaciated areas to understand the longevity of these freshwater resources?*
In theory, my BMC isotope mixing model should be applicable in glacial hydrological systems to assess and predict the overall stability of these large freshwater sources that many aquifers rely on for seasonal recharge. If the melt fraction contribution is consistently dominated by ice melt, the glacier reservoir is losing mass at a rate that exceeds replacement by snowfall, and will eventually cause it to completely melt if the trend continues. The magnitude of seasonal reversals and the volumes of ice melt discharged will be crucial in predicting freshwater sustainability in regions dependent on snow and ice melt for aquifer recharge (e.g., in

regions where the discharge is dominated by icemelt, the glacier freshwater reservoir is shrinking and will continue to decrease until the glacier disappears).

In conclusion, the combined application of the glacial hydrology chemical proxies outlined in my thesis is important in terms of providing insight to subglacial systems, associated processes, and the implications of these processes on global scales. It is important to note that additional research needs to be completed in order to have a more thorough understanding of glacial hydrology as a whole and the role of subglacial systems in climate change. However, the research composing my thesis provides me with a diverse skillset in which to base my future work, including: the planning and orchestrating of field work, the development of field and laboratory methods, computational analyses, and both stable and radiogenic geochemical applications. Thus, I will continue planning field campaigns, collecting and processing my own glacial meltwater samples, assessing their chemical concentrations and compositions, and evaluating the implications of my research outcomes on global climate change. Ideally, U-series isotopes in glacial meltwater will be the major focus of my future research endeavors, but I am also interested in and excited about expanding into new isotope systems including techniques such as using cosmogenic isotopes to determine the extent of glacial advance and retreat on specific timescales.

- Carli A. Arendt

5.3. REFERENCES

Arendt, C.A., Aciego, S.M., Hetland, E., In Press. An open source Bayesian Monte Carlo isotope mixing model with applications in Earth surface systems. Geochemistry, Geophysics, Geosystems, DOI: 10.1002/2014GC005683.

Arendt, C.A., Aciego, S.M., Sims, K.W.W., Robbins, M.J., 2014. Sequential separation of radioactive U, and radiogenic Nd and Hf concentrated from natural waters. Geostandards and Geoanalytical Research, DOI: 10.1111/j.1751-1908X.2014.00322.x.

Arendt, C. A., Aciego, S.M., Sims, K.W.W., Aarons, S.M., (2015), Uranium-series isotopes confirm prolonged residence time of subglacial water, *Geochimica et Cosmochimica Acta*.

Bhatia, M.P., Das, S.B., Kujawinski, E.B., Henderson, P., Burke, A., Charette, M.A., 2011. Seasonal evolution of water contributions to discharge from a Greenland outlet glacier: insight from a new isotope-mixing model. Journal of Glaciology 57.

Chadwick, O. A., *et al.,* (1999), Changing sources of nutrients during four million years of ecosystem development, *Nature*, *397*, 491–497, doi: 10.1038/17,276.

Henderson, G., 2002. Control on ($^234U/^238U$) during the last 800 thousand years. Earth and Planetary Science Letters 199, 97-110.

Kurtz, A. C., *et al*., (2001), Accretion of Asian dust to Hawaiian soils: Isotopic, elemental, and mineral mass balances, *Geochimica et Cosmochimica Acta.*, *65* (12), 1971–1983, doi: 10.1016/S0016–7037(01)00,575–0.

APPENDIX A: SUPPLEMENTARY MATLAB CODE

```
clear

% An exterior '.csv' file may be used to call data instead of entering
% data vectors directly into the code. An example of the '.csv' format we
% used is:
%      Line 1 (day, discharge, DO, DH, DO_ice, DH_ice DO_surface,...
%      DH_surface, DO_rain, DH_rain)
%      Line 2 (125, 0, -20.8, -160.8, -20, -140, -25.5, -205, -13, -104)
%      Line 3 (126, 0.171, -20.9, -161.8, , , , , , )
%      etc…
% inputs measured bulk water delta O-18 and delta D snowmelt values and
% delta O-18 and delta D for the three designated end members: ice melt,
%  snowmelt, and summerprecipitation
%      DO_surface = delta O-18 of snow
%      DO_ice = delta O-18 of glacial ice
%      DO_rain = delta O-18 of rain
%      DH_surface = delta H-2 of snow
%      DH_ice = delta H-2 of glacial ice
%      DH_rain = delta H-2 of rain
vals=csvread('AG_OH_paper_data.csv',1,0);
Day = vals(:,1);
Discharge = vals(:,2);
DO = vals(:,3);
DH = vals(:,4);
DO_ice = vals(1,5);
DH_ice = vals(1,6);
DO_surface = vals(1,7);
DH_surface = vals(1,8);
DO_rain = vals(1,9); DH_rain
= vals(1,10);

% designated errors for delta O-18 and delta D bulk water measurements
sigmaO = 0.05;
sigmaH = 0.65;
```

```
% N is the number of model trials run
% Choice of N is dependent on the uncertainty of the problem being solved
% Size of N is the main determining factor in length of model run (time)
% Suggest starting with a small N (i.e. N = 1e5) before increasing N
% N should be large enough to produce a solution with smooth curves
% i.e. hist(fs_trial(accept), 40) should be smooth
N = 2e7;
sample_number=[1:size(vals,1)];

%Fraction of source definitions
%fs = fraction of snow input
%fi = fraction of glacial ice input
%fr = fraction of rain input

% designated errors for delta O-18 and delta D snowmelt values
sigma_fs_O = 0.7;
sigma_fs_H = 4.0;

% designated errors for delta O-18 and delta D ice melt values
sigma_fi_O = 0.5;
sigma_fi_H = 2.0;

% designated errors for delta O-18 and delta D summer precipitation values
sigma_fr_O = 2.0;
sigma_fr_H = 10.0;

% arrays to keep the best outcomes or values with the highest likelihood
% of being true for fraction contribution from end members
fs_best=zeros(size(Discharge));
fi_best=zeros(size(Discharge));
fr_best=zeros(size(Discharge));

% arrays to keep the mean of the posterior, or the average fraction
% contribution from end members
fs_mean     =     zeros(size(Discharge));
fi_mean     =     zeros(size(Discharge));
fr_mean=zeros(size(Discharge));

% arrays to keep the standard deviations of the posteriors
fs_std = zeros(size(Discharge));  fi_std
=   zeros(size(Discharge));   fr_std   =
```

```
zeros(size(Discharge));

% arrays to keep the 2D correlation coefficients of the posteriors
fsfr_corr = zeros(size(Discharge)); fsfi_corr =
zeros(size(Discharge)); frfi_corr =
zeros(size(Discharge));

% Determines best outcomes or values with the highest likelihood of
% being true for delta O-18 and delta D
DOp_best=zeros(size(Discharge));
DHp_best=zeros(size(Discharge));

for n=sample_number
  %choose f so that sum(f)=1 -> use fs & fi to find fr fs_trial=
  unifrnd(0,1,N,1);
  fi_trial=unifrnd(0,1,N,1);

  pos=find((fs_trial+fi_trial)<=1); fs_trial
  =fs_trial(pos); fi_trial=fi_trial(pos);
  fr_trial = 1 - (fs_trial + fi_trial);

  % generate random samples of D[O]_*
  DO_surface_trial=normrnd(DO_surface,sigma_fs_O,length(pos),1);
  DO_ice_trial=normrnd(DO_ice,sigma_fi_O,length(pos),1); DO_rain_trial
  =normrnd(DO_rain,sigma_fr_O,length(pos),1);

  %Delta O-18
  DOp=(fs_trial.*DO_surface_trial)+(fi_trial.*DO_ice_trial)+...
      (fr_trial.*DO_rain_trial);


  % generate random samples of D[H]_*
  DH_surface_trial=normrnd(DH_surface,sigma_fs_H,length(pos),1);
  DH_ice_trial=normrnd(DH_ice,sigma_fi_H,length(pos),1); DH_rain_trial
  =normrnd(DH_rain,sigma_fr_H,length(pos),1);

  %Delta H-2
  DHp=(fs_trial.*DH_surface_trial)+(fi_trial.*DH_ice_trial)+...
      (fr_trial.*DH_rain_trial);

  % L2^2 norm
  phi=(DOp - DO(n)).^2./sigmaO.^2 + (DHp - DH(n)).^2./sigmaH.^2;
```

```
% Determines best outcomes or values with the highest likelihood of being
% true
   [best_phi,pos]=min(phi); fs_best(n)
   =fs_trial(pos); fi_best(n)=
   fi_trial(pos); fr_best(n)=
   fr_trial(pos); DOp_best(n)=
   DOp(pos); DHp_best(n)=DHp(pos);

   %%%%Gaussian Data Error%%%%%%%%
   L=exp((-1/2).*phi); L=L./max(L);

   %REJECT or ACCEPT models and proportions
   %L->likelihood of observed predictions
   %where rand is a unit distribution between 0 and 1
   %if L=1 always accept
   %if L=0.5 accept 50%
   %if L=0 never accept
   accept=find(L>=rand(size(L)));

   fprintf(1,['day %d: tried %d samples of the prior, accepted %d ',...  'samples of the
                  posterior; %6.2f%s acceptance rate\n'],... n,length(fs_trial),length(accept),...
                  100*length(accept)/length(fs_trial),char(37));

% Isolates and determines accepted posterior values for fraction
%  contributions from snowmelt, ice melt, and summer precipitation
  phi_post=phi(accept);
   fs_post=fs_trial(accept);
   fi_post=fi_trial(accept); fr_post=
   fr_trial(accept);

% Isolates and determines accepted posterior values of delta D and
%  delta O-18 for snowmelt, ice melt, and summer precipitation
   DO_surface_post=DO_surface_trial(accept);
   DH_surface_post=DH_surface_trial(accept);
   DO_ice_post=DO_ice_trial(accept); DH_ice_post=
   DH_ice_trial(accept); DO_rain_post=
   DO_rain_trial(accept); DH_rain_post=
   DH_rain_trial(accept);



% Saves accepted values to folder
```

```
   save(sprintf('Post_%02d.mat',n),... 'phi_post',...
           'fs_post','fi_post','fr_post',...
           'DO_surface_post','DH_surface_post',...
           'DO_ice_post','DH_ice_post',...
           'DO_rain_post','DH_rain_post');

   fs_mean(n)      =      mean(fs_trial(accept));
   fi_mean(n)      =      mean(fi_trial(accept));
   fr_mean(n)=mean(fr_trial(accept));
   Cmat=cov([fs_trial(accept) fi_trial(accept) fr_trial(accept)]);

% calculates the first two moments (mean and standard deviation) of the
% posterior of fraction contribution values from snowmelt, ice melt, and
%  summer precipitation
   fs_std(n)=sqrt(Cmat(1,1));
   fi_std(n)=sqrt(Cmat(2,2));
   fr_std(n)=sqrt(Cmat(3,3));

% Determines covariance relationships between the posterior fraction
% contribution values from snowmelt, ice melt, and summer precipitation
   fsfi_corr(n)=Cmat(1,2)/(fs_std(n)*fi_std(n)); fsfr_corr(n)=
   Cmat(1,3)/(fs_std(n)*fr_std(n));
   frfi_corr(n)=Cmat(2,3)/(fr_std(n)*fi_std(n));

end

% Clears values that take up extra memory and are no longer needed
clear fs_trial fi_trial fr_trial;
clear DO_surface_trial DH_surface_trial;
clear DO_ice_trial DH_ice_trial;
clear DO_rain_trial DH_rain_trial; clear L
accept phi;
clear phi_post fs_post fi_post fr_post; clear
DO_surface_post DH_surface_post; clear
DO_ice_post DH_ice_post;
clear DO_rain_post DH_rain_post;

% Calculates mass contribution/discharge volume for each end member from
%  total  discharge and the accepted fraction contribution values from
% snowmelt, ice melt,  and summer precipitation
Discharge_s = fs_best .* Discharge; Discharge_i =
fi_best .* Discharge; Discharge_r  =  fr_best  .*
```

```
Discharge;

% saves posteriors and associated values  return
saveOH_soln.mat

Return
```

APPENDIX B: FIELD AND LABORATORY METHODS

The research chapters in this thesis provide only brief descriptions of the field and laboratory methods used to obtain and analyze samples. Field sample collection occurred at multiple locations including: the terminus of the alpine glacier, Athabasca Glacier located in Jasper National Park, Alberta Canada; the terminus of the Greenland Ice Sheet (GrIS) outlet glacier, Qoorqup Sermia in Narsarsuaq and proximal seawater at the intersection of the Labrador Sea and the Atlantic Ocean; the terminus of the GrIS outlet glacier, Saqqarilup Sermia in Ilulissat and proximal seawater at the intersection of the Labrador Sea and Baffin Bay; the terminus of the GrIS outlet glacier, Kangaarsarsuup Sermia in Nuuk and proximal seawater at the mouth of the Ameralik Fjord; and the terminus of the GrIS outlet glacier, unnamed Glacier 'G' north of Kulusuk and proximal seawater in the open Atlantic Ocean. GPS coordinates for these sampling locations are presented in Figure # and Table #. Laboratory chemical preparation and analyses were performed in two separate locations: the Glaciochemistry and Isotope Geochemistry Laboratory at the University of Michigan and the Wyoming High Precision Isotope Laboratory at the University of Wyoming.

B.1 PRE-CLEANING

To minimize potential blanks during the sampling process, all sampling containers and tubing that came into direct contact with our samples were stringently cleaned prior to the collection of meltwater samples. The pre-cleaning occurred in an ISO 7 (class 10,000) clean laboratory to ensure blanks from these studies were negligible. Ultra-pure reagents were used for all cleaning and chemical separation: either Seastar optima acid or distilled reagent grade acid. Super de-ionized water was purified using a super (SQ) Millipore purification system, which produced a water purity of >18.2 MΩ. Both the 20 L and 10 L collapsible polyethylene carboys (Thermo Fisher Hedwing) and the 1 L polypropylene bottles (Nalgene) were cleaned using the same procedure. The containers were i) rinsed three times with SQ water, ii) leached for 48 hours in 10% reagent grade HNO_3, iii) rinsed three times with SQ water, iv) leached for 48 hours in 10% double-distilled HCl, and v) and rinsed three times with SQ water. Polyethylene tubing was rinsed three times with SQ water, leached for 72 hours in 10% optima grade HCl, and rinsed three times with SQ water.

B.2 SAMPLE COLLECTION

Daily water samples were consistently collected mid-morning within 10 m of the glacier terminus and suspended sediments were removed from the subglacial water to prevent further recoil and dissolution processes from occurring between the sediment and water at all sample collection sites. However, meltwater sample filtration methods varied from the Athabasca Glacier, which was our pilot study, and the GrIS outlet glaciers.

B.2.1 Athabasca Glacier Meltwater

Subglacial water was filtered using a Masterflex modular peristaltic pump and a polycarbonate filtration unit (Geotech Environmental Equipment Inc.). Glass fiber prefilters and polytetrafluoroethylene (PTFE) filter (0.2 μm) membranes were used to remove the suspended sediment. One liter of ultra-pure SQ water was filtered through the system as a rinsing agent prior to the filtration of samples. Subglacial water was filtered and collected directly from the main melt channel at the toe of the Athabasca Glacier into the precleaned 20 L carboys. Samples ranged in volume from 10-40 L depending on the suspended sediment load; high-suspended sediment dramatically increased the filtration time.

Samples collected for oxygen and hydrogen isotopic analysis were collected onsite directly into Kimble^{TM} 20 mL glass screw-thread scintillation vials (No. 74516 20) with conical caps. Vials were filled to the brim to minimize atmospheric head space and immediately sealed tightly until measured.

B.2.2 GrIS Outlet Glacier Meltwater

Subglacial water was filtered using a Masterflex modular peristaltic pump and a Perfluoroether (PFA) filtration unit (custom machined) and Millipore Durapore® 0.22 μm GV membrane filters were used to remove the suspended sediment. One liter of ultra-pure SQ water was filtered through the system as a rinsing agent prior to the filtration of samples. Subglacial water was filtered and collected directly from the main melt channel at the toe of the Athabasca Glacier into the precleaned 10 L carboys.

B.2.3 Seawater Adjacent to GrIS Outlet Glaciers

All seawater samples were collected mid-afternoon approximately 30 km offshore from each outlet glacier sampled at depths of 0 m, 10 m, and 25 m to ascertain homogenous values at varying mixing depths so the samples would be representative of the average seawater composition. Seawater was obtained using a PVC (RAL 7011) Niskin sampling bottle which was lowered to the predetermined depths before sending down a weight to seal the bottle and bring samples from depth to the surface to be filtered. These seawater samples were filtered onto Millipore Durapore® 0.22 μm GV membrane filters using a Masterflex modular peristaltic pump and a Perfluoroether (PFA) filtration unit (custom machined). One liter of >18.2 MΩ water was filtered through the system prior to filtration of samples.

B.3 IN FIELD CHEMISTRY

In field chemistry was consistent between our sample collection locations. Each daily 10-40 L filtered water sample was reduced in sample size via iron co-precipitation field chemistry based on established procedures (Rickli et al., 2010; Arendt et al., 2014). The pH of the sample was lowered to approximately 2-3 by adding 9M HCl and shaking the sample until it was homogenous. Next, a pre-cleaned $FeCl_3$ $6H_2O$ – 3M HCl mixture was added to the sample. The sample was then shaken vigorously and left to sit for approximately 10 minutes to reach chemical equilibrium. The addition and mixing of $[NH_4^+][OH^-]$ (ammonia hydroxide) to the sample raised the pH to 8-9 and initialized settling flocculates. The high pH iron precipitated out of the solution along with the uranium over a two-day period. Once the settling period had elapsed, the sample was decanted. Final pre-concentration of the iron precipitate was

accomplished in a clean laboratory by centrifuging the samples, resulting in ~1 g of iron precipitate for dissolution and column chemistry.

B.4 IN FIELD ^{222}Rn MEASUREMENTS

The radiogenic isotope ^{222}Rn has a half-life of 3.85 days (Picolo, 1996) and thus required on site measurement. Water samples were analyzed within 3 hours of collection. Daily in-field ^{222}Rn concentrations in waters were determined with a Durridge RAD7 (see http:/www.durridge.com/; Lane-Smith and Sims, 2013) coupled with a RAD H_2O (see http://www.durridge.com/products_rad_h2o.shtml). For these measurements a 250 mL glass water vial was submerged in the water channel for several minutes and capped while completely submerged to prevent any atmospheric bubbles from entering the container, and consequently prevent Rn from partitioning/degassing. Prior to each analysis the Durridge RAD7 was purged to reduce water vapor; once the moisture content of the Durridge RAD7 was below 10%, the sample was analyzed in situ by energy dispersive alpha spectrometry. Analysis consisted of five cycles of aeration for five minutes and five minutes of radon detection following each aeration period. Reported results indicate uncertainty for each individual sample based on the variability between cycles; analytical uncertainties reported by Durridge for specific concentration ranges are all lower than the variability reported (Durridge Company, 2009). The 2σ in ^{222}Rn concentrations are 2 standard deviations from the mean based on three replicate measurements; each measurement has a 2σ error of $<5\%$ based on counting statistics (Durridge Company Inc., 2009).

B.5 *IN SITU* CHEMICAL MEASUREMENTS

In situ traditional water chemistry measurement instrumentation varied from the Athabasca Glacier, which was our pilot study, and the GrIS outlet glaciers.

B.5.1 Athabasca Glacier

Electrical conductivity, temperature, pH, and alkalinity measurements were obtained using a Daily Oakton Portable Waterproof Conductivity Meter. The electrical conductivity, temperature, and pH measurements were all conducted on-site in the main subglacial outlet channel by submerging the probe in the moving water at an upright position and waiting for the meter to equilibrate. These measurements took place during but downstream of the filtration and collection of the water samples to avoid any possible disturbances/contamination. Approximately 100 mL of filtered subglacial water was measured for alkalinity. For anticipated high alkalinities, the 100 mL sample was mixed with 10 mL of Total Alkalinity Reagent (FisherScientific) solution, shaken, and measured for pH. For anticipated low alkalinities, the 100 mL sample was mixed with 1 mL of Total Alkalinity Reagent solution, shaken, and measured for pH. The pH was converted to the total alkalinity using a pH-total alkalinity conversion chart (e.g. Hedin et al., 1994, Fujita et al., 2008).

Discharge and maximum velocity measurements were taken directly after water sample collection. Manual measurements of these parameters were achieved using an Acoustic Doppler Velocimeter Flow-tracker, or ADV Flowtracker. A measuring tape was set up across the width of the channel, perpendicular to water flow. The ADV Flowtracker's monitor was submerged at the edge of the channel parallel to water flow and calibrated prior to measurement. Following

calibration, the ADV Flowtracker measured velocity and water depth at one-foot increments spanning the width of the main channel at the toe of the glacier. Velocity and water depth measurements across the channel allowed the calculation of discharge, using the standard 0.6 rule, where velocity measurements are taken at 0.6 of the depth of each location (Morlock et al., 2001).

B.5.2 GrIS Outlet Glaciers

Daily electrical conductivity, temperature, pH, and alkalinity measurements were taken using a YSI Handheld Multiparameter Instrument (Pro Plus Multiparameter). The pH, conductivity, and temperature measurements were obtained *in situ* in the primary subglacial outlet discharge channels by submerging the probe into the moving water and waiting for the meter to equilibrate. Approximately 100 mL of filtered subglacial water was used for total alkalinity measurements. For anticipated high alkalinities, the 100 mL sample was mixed with 10 mL of Total Alkalinity Reagent (FisherScientific) solution, shaken, and the pH was measured. For anticipated low alkalinities, the 100 mL sample was shaken with 1 mL of Total Alkalinity Reagent solution and the resulting pH was measured with the YSI probe. The pH was converted to total alkalinity values via a pH-total alkalinity conversion (e.g. Hedin et al., 1994; Fujita et al., 2008).

B.6 SAMPLE PREPARATION

Labware, including Teflon beakers and columns, was stringently cleaned via a multi-step acid cleaning regiment. The labware was wiped with clean methanol to remove organic residue, rinsed three times in SQ water before being submerged in a capped 2 L beaker filled with

distilled 7M HNO_3 and left on a hotplate overnight. The labware was then rinsed another three times in SQ water and submerged in a capped 2 L beaker filled with distilled 6M HCl and left on a hotplate overnight. Again the labware was rinsed three times with SQ water and then each individual beaker was filled one third of the way with concentrated HNO_3 and trace HF, capped, and left on the hotplate for a minimum three days as a final step in the cleaning process before being rinsed an additional three times with SQ water and dried in a ProPlastic Technology Mojave-Single N_2 Dry Storage Cabinet: an enclosed metal-free drying rack system with internal ULPA air filtration that is over-pressurized with respect to laboratory air.

Final pre-concentration of the glacial meltwater and seawater iron precipitate was accomplished in the GIGLclean laboratory by centrifuging the samples, resulting in ~4 g of iron precipitate for digestion and column chemistry. Prior to column chemistry, water samples were rinsed 10 times with SQ water that had been buffered with ammonia hydroxide to a pH of 9 (Auro *et al.* 2012) after final centrifugation to remove excess salts prior to digestion. All samples were treated twice with 1 mL of aqua regia to remove any organics that could compromise the ion exchange chromatography process.

B.7 ION EXCHANGE CHROMATOGRAPHY

To isolate uranium from the iron precipitate samples underwent a new two-column ion-exchange chromatography method (Arendt et al., 2014). The first column is dedicated to the clean separation of most of the HFSEs from the Fe and U. The first column had a 10 mL reservoir with a 13 cm long column with a diameter of approximately 1.25 cm and was filled with 0.5 mL

of Eichrom Anion pre-filter 100-150 mesh resin and 5 mL of Eichrom Anion 1x8 100-200 mesh resin. This column was cleaned twice with 5 mL of 12M HCl – 0.13M HF and twice with 10 mL of MΩ water, and then pre-conditioned twice with 5 mL 12M HCl. The co-precipitate samples were dried down and digested in 10 mL of 12M HCl, which was then loaded onto the pre-conditioned columns and collected along with two rinses of 2 mL 12M HCl and 5 mL 12M HCl. This eluted volume contains cleanly separated HFSEs (including Hf, Nd, Th). The remaining sample was then rinsed off the column and collected in four 2 mL 0.5M HCl eluted volumes. This U-Fe containing portion was then dried and re-dissolved in the loading solution for the next set of columns (5 mL 7.5M HNO_3).

The second column is dedicated to the removal of iron from the remaining elements and the clean isolation of U. The second column had a 10 mL reservoir with a 13 cm long column with a diameter of approximately 1.25 cm and was filled with 5 mL of Eichrom Anion 1x4 200-400 mesh resin. This column was pre-conditioned with 3 mL 0.25M HNO_3, twice with 5 mL 7.5M HNO_3, and again with 3 mL 0.25M HNO_3. The U-Fe eluted volume from the previous column in 5 mL 7.5M HNO_3 was then loaded onto the second column. After rinsing the iron off with two additional 5 mL and one 1 mL volume of 7.5M HNO_3, the clean uranium cut was eluted and collected in three 2 mL and one 1 mL volume of 0.25M HNO_3. These uranium-containing portions were dried and re-dissolved in the analyzing solution.

B.8 MASS SPECTROMETRY

B.8.1 Uranium Activity Measurements

Uranium isotopic compositions and activity ratios, ($^{234}U/^{238}U$), were measured at the Wyoming High Precision Isotope Laboratory at the University of Wyoming on a Neptune PLUS ultra high-precision, high-sensitivity multi collector inductively coupled mass spectrometer (Ball et al., 2008; Sims et al., 2008). Each sample was loaded into a sample solution of 0.01M HCl and diluted to 10 ppb uranium content. Sample measurements were bracketed with measurements of standard U010 to correct for mass bias and ion counting efficiency, using the established ($^{234}U/^{238}U$) ratio of 18,074 (Richter and Goldberg, 2003). Standard NBS960 was run periodically to test the precision and accuracy of the Neptune PLUS over the entire sample run (Cheng et al., 2000). The sample intake system was rinsed sequentially with ultrapure SQ water and dilute HCl between analyses. External errors are 2 standard deviations of ($^{234}U/^{238}U$) for NBS960 and are equal to 0.001 for all calculated values based on multiple measurements ($n > 60$) of the standard solution (Arendt et al., 2014).

B.8.2 Elemental Concentration Measurements

Major element and ^{238}U concentrations were performed at the University of Michigan Keck Elemental Geochemistry Laboratory using a ThermoScientific Element2 inductively coupled mass spectrometer operating in pulse-counting mode. The filtered, acidified 1 L subglacial water samples were aliquoted and 3 mL of each sample solution was analyzed. An acid blank, a standard of known concentration, and an additional acid blank were run between every sample to measure the concentration accurately. Each sample was measured in triplicate, with the standard deviation of the measurements indicating the variability of the individual results. All standard

deviations are lower than the reported errors in the standard concentration. The 2σ errors of the major ions and ^{238}U concentrations are based on a 0.7% standard error for the May samples and a 0.3% standard error for the July samples in the bracketing standard: internal counting errors are two orders of magnitude less than error in standard ^{238}U concentration values.

B.8.3 Oxygen and Hydrogen Measurements

Water stable isotope measurements were performed at the University of Michigan Stable Isotope Laboratory.

Deuterium measurements were made using a Finnigan H-Device coupled to a dual inlet gas source Thermo Finnigan Delta V Plus mass spectrometer. The analysis process entailed use of an A CTC Analytics Pal Autosampler to inject 1 mL of water per sample into a chromium reactor set at 800°C, where the sample reacts for approximately 2 minutes. Next, the samples were equilibrated in the dual inlet for 1 minute (allowing the H_2O and CO_2 in the system to reach isotopic equilibrium) and run at 8V against a reference gas of known composition [Socki , et al., 1992]. The samples were run in duplicate to account for memory effects and bracketed against known standards (VSMOW/VSLAP, in-house standards) to ensure accuracy in the machine's measurements. Sample measurements were then normalized relative to the VSMOW/VSLAP scale and expressed relative to VSMOW. Accuracy and precision is better than ±1 ‰ on replicate analyses, and analytical error on standards over time is better than ±1.3 ‰.

Oxygen isotopes ($^{18}O/^{16}O$) were measured by continuous flow on a Thermo Finnigan Gas Bench

II coupled to the inlet of a Thermo Finnigan Delta V Plus mass spectrometer. The analysis process entailed use of an A CTC Analytics Pal Autosampler to inject 0.5 mL of water per sample into a pre-evacuated Labco exetainer. Next, the samples were loaded into the Finnigan Gas Bench II sample tray. The A CTC Analytics Pal Autosampler was used to flush the samples with 0.3% CO_2 in a helium (He) mixture for 8 minutes. The samples were then allowed to equilibrate over a two-day period at 30°C. Pure He (UHP grade) was then used to flush each sample for 8 minutes. The sample gas was then transported via He flow, cleaned of any remaining water with the Gas Bench water traps, and pushed through a GC column set at 70°C. The CO_2 was then admitted through a capillary to the inlet of the mass spectrometer where multiple sample peaks were measured against the CO_2 reference gas peaks. The data was normalized and reported relative to the VSMOW/VSLAP scale. Accuracy and precision for these samples is ±0.1‰.